Molecular Perspective of Static Wetting: Simulation and Theory

TECHNISCHE UNIVERSITÄT DARMSTADT

Vom Fachbereich Chemie
der Technischen Universität Darmstadt

zur Erlangung des akademischen Grades eines
Doktor rerum naturalium (Dr. rer. nat.)

genehmigte
Dissertation

vorgelegt von

Fereshte Taherian
Master of Science (M. Sc.)

aus Tehran, Iran

Referent::	Prof. Dr. Nico van der Vegt
Korreferent:	Prof. Dr. Markus Biesalski
Tag der Einreichung:	12. Dezember 2013
Tag der mündlichen Prüfung:	24. Februar 2014

Darmstadt 2014
D 17

Summary

In our daily life and many of industrial applications, we usually find fluids which interact with solid substrates. Although a lot of researches have been carried out and new developments have been made to understand the wetting phenomena at the macroscopic scale, little is known at the nanoscale due the limitation of the experimental methods. Molecular dynamics (MD) simulations have been used as a powerful tool during the last years to perform a detailed and comprehensive study of wetting problems, in addition to what has been done experimentally. One could use MD simulations to indirectly describe the macroscopic behavior of the system, while at the microscopic scale very details of the system can be revealed by MD simulations. In this thesis, understanding of the wetting phenomena at the molecular scale is developed by means of MD simulations and statistical thermodynamics. The dissertation is organized as follows.

In the first chapter an overview on several concepts of wetting phenomena, which will be the base of the discussion in the next chapters is given. In this chapter, we explain how it is possible to study wetting with nanometer size droplets and compare with macroscopic experiments. Open questions that we are addressing in this thesis are explained, and the contribution of this work to answer these questions is described.

The technical issues regarding the MD simulations of wetting is explained in Chapter 2.

In Chapter 3 with the support of classical MD simulations, an argumentation to clarify the wetting properties of a monolayer of graphene is developed, which experimentally were unknown. While in the literature for the contact angle of water on graphite values in the range of 90–95° have been reported, it has been suggested that the contact angle on graphene may either be as high as 127° or moderately enhanced in comparison with graphite. Our results show that the value of 127° is an unrealistic estimate and that a value of the order of 95–100° should be expected. This result was confirmed by recent experiment.

After bringing a liquid in contact with a solid surface, enthalpy is gained because of the attractive interaction between the liquid and the surface, and entropy is lost since the configurational space of the liquid molecules is biased. We have emphasized for the first time that entropy plays an important role in wetting behavior of surfaces, and is connected to the fluctuations in the water–substrate interaction energy.

Chapter 4 explores further the role of interfacial entropy and develops a theoretical model to predict the interfacial entropy of water at rigid hydrophobic surfaces. The interfacial entropy, which is not considered in mean field models of static wettability, is evaluated from the fluctuations of the water-surface dispersion energy at the single particle level and represents the configurational bias imposed on the fluid molecules by the attractive external potential of a solid wall. A comparison with results obtained from molecular dynamics simulations shows that the model quantitatively describes the entropy loss of water when a water-vapor interface turns to water in contact with hydrophobic surfaces such as graphene, graphite and diamond, while it overestimates this quantity on hydrophilic surfaces.

Chapter 5 gives a review of MD simulations that have been done to investigate influencing factor on the interfacial structure and dynamic properties of ionic liquids (ILs) at the solid-liquid interface. It was shown that properties of the solid–IL interface depend on (i) characteristic of the surface (ii) type of the IL and (iii) and on the thermodynamic conditions of the interface. At the end, different aspects of wetting and electrowetting of ILs are also given.

Electrowetting of [BMIM][BF_4] ionic liquid (IL) on graphene surface has been studied in Chapter 6 by MD simulation. By measuring the contact angle on positively and the negatively charged surfaces, an asymmetry in the electrowetting behavior of the IL was observed. The surface with negative charges showed more spreading (lower contact angle) of the droplet compared to positively charged surfaces on which competing orientational preferences of the cations in the three-phase contact-line are in inflicted by the solid-liquid and the liquid-vapor interface. The simulation however showed that this asymmetry disappears at high surface charge densities before a complete wetting of the droplet happens; i.e. the effect of “frustrated” cation orientations in the three phase contact line, which impedes further spreading, is overcome at a threshold value of the surface charge density where electrostatic stabilization takes over.

The last chapter gives conclusion of the different topics discussed in this dissertation, and some ideas to extend the current work are introduced.

Investigations performed in this dissertation show that MD simulation can be used as a powerful tool, beside the experimental methods, to understand different aspects of wetting in many details. With MD simulation, we have the possibility to obtain complete information about the structure and dynamic properties of different phases in contact and to explain experimental results.

Zusammenfassung

Sowohl im Alltag als auch in vielen industriellen Anwendungen finden Wechselwirkungen zwischen Fluiden und Festkörpern statt. Obwohl umfangreiche wissenschaftliche Untersuchungen betrieben und neue Entdeckungen bei Benetzungsphänomenen auf makroskopischer Ebene gemacht wurden, ist aufgrund der begrenzten experimentellen Durchführung wenig auf nanoskopischer Ebene bekannt. Molekulardynamik-Simulationen (MD-Simulationen) wurden in den letzten Jahren als wirkungsvolle Methode verwendet, um detaillierte und umfangreiche Studien von Benetzungsproblemen als Ergänzung der experimentellen Untersuchung zu erstellen. MD-Simulationen sind meist für die Beschreibung des makroskopischen Verhaltens indirekt anwendbar, während auf der mikroskopischen Ebene wenig Details des Systems einsehbar sind. In dieser Arbeit wurde mittels MD-Simulationen und statistischer Thermodynamik ein Verständnis des Benetzungsvorganges auf molekularer Ebene entwickelt. Die Dissertation ist wie im Folgenden gegliedert:

Im ersten Kapitel befindet sich eine Übersicht über mehrere Konzepte des Benetzungsphänomens, welche die Grundlage der Diskussion in den darauf folgenden Kapiteln bilden. In diesem Kapitel wird erklärt, warum es möglich ist Benetzungsprozesse anhand von einigen Nanometer großen Tropfen zu untersuchen und den Vergleich mit makroskopischen Experimenten anzustellen. Offene Fragen, die in dieser Arbeit behandelt werden, werden erläutert und der Beitrag, den diese Arbeit zur Beantwortung dieser Fragen leistet, wird beschrieben.

Die technischen Fragestellungen im Zusammenhang mit MD Simulationen von Benetzungsprozessen werden in Kapitel 2 behandelt.

In Kapitel 3 wird versucht mithilfe von klassischen MD Simulationen die Benetzungseigenschaften von Graphen-Monolagen, welche experimentell unbekannt waren, zu bestimmen.

Während neuerliche experimentelle Erkenntnisse in der Literatur darauf hinweisen, dass der Kontaktwinkel von Wasser auf Graphen zwischen 90° und 95° liegt, wurde vermutet, dass der Kontaktwinkel von Graphen entweder einen Wert bis zu 127° oder aber nur einen gegenüber dem Kontaktwinkel von Graphit leicht erhöhten Wert besitzen könnte. Die Ergebnisse dieser Arbeit zeigen, dass ein Wert von 127° eine unrealistische Schätzung ist und das ein Wert der Größenordnung 95-100° erwartet werden sollte. Diese Annahme wurde inzwischen

experimentell bestätigt. Wenn eine Flüssigkeit mit einer Oberfläche in Kontakt gebracht wird, führen die attraktiven Wechselwirkungen zwischen Flüssigkeit und Oberfläche zu einem Enthalpiegewinn, die Verzerrung des Konfigurationsraums der Flüssigkeitsmoleküle führt hierbei zu einem Entropieverlust. Es wird vermutet, dass die Entropie eine wichtige Rolle im Benetzungsverhalten von Oberflächen spielt und dass diese mit Fluktuationen der Wechselwirkungsenergie zwischen Wasser und dem Substrat zusammenhängt.

In Kapitel 4 wird die Rolle der Grenzflächenentropie weiter untersucht und ein theoretisches Modell zur Berechnung der Grenzflächenentropie von Wasser an rigiden hydrophoben Oberflächen wird entwickelt. Die Grenzflächenentropie, die in "Mean-Field"-Modellen der statischen Benetzbarkeit nicht berücksichtigt wird, wird aus den Fluktuationen der Wasser-Oberflächen-Dispersionsenergie für einzelne Teilchen bestimmt. Die Grenzflächenentropie stellt hierbei den Beitrag durch die Verzerrung des Konfigurationsraums dar, die die Fluidmoleküle durch das attraktive externe Potential einer festen Wand erfahren. Ein Vergleich mit Ergebnissen, die mittels MD Simulationen erhalten wurden zeigt, dass das Modell den Entropieverlust quantitativ beschreibt, wenn eine Wasser-Dampf-Grenzfläche zu einer Grenzfläche zwischen Wasser und hydrophoben Oberflächen, wie Graphen, Graphit oder Diamant, wird. Allerdings wird der Entropieverlust auf hydrophilen Oberflächen überschätzt.

Kapitel 5 bietet einen Überblick über MD Simulationen, die durchgeführt wurden, um die Faktoren, die Einfluss auf die Grenzflächenstruktur und die dynamischen Eigenschaften ionischer Flüssigkeiten (engl. "Ionic Liquids", IL) an Fest-Flüssig-Grenzflächen ausüben, zu untersuchen. Es wurde gezeigt, dass die Eigenschaften der Festphasen-IL-Grenzfläche von (i) dem Charakter der Oberfläche, (ii) der Art der IL und (iii) den thermodynamischen Bedingungen an der Oberfläche abhängen. Weiterhin werden verschiedene Aspekte der Benetzungs- und Elektrobenetzungseigenschaften ionischer Flüssigkeiten behandelt.

Die Elektrobenetzung einer Graphenoberfläche mit einer [BMIM][BF_4] ionischen Flüssigkeit wird in Kapitel 6 mittels MD Simulationen untersucht. Durch Messung der Kontaktwinkel auf positiv und negativ geladenen Oberflächen wurde eine Asymmetrie im Verhalten der Elektrobenetzung der ionischen Flüssigkeiten beobachtet. Die negativ geladene Oberfläche zeigte eine größere Verteilung (also einen kleineren Kontaktwinkel) des Tropfens im Vergleich zu positiv geladenen Oberflächen, auf denen konkurrierende Vorzugsorientierungen der Kationen an der Drei-Phasen-Kontaktline durch die fest-flüssig- und Gas-flüssig-Grenzflächen verursacht werden.

Die Simulation zeigte allerdings, dass diese Asymmetrie bei höheren Ladungsdichten auf der Oberfläche verschwindet, bevor die Oberfläche komplett benetzt wird; d.h. der Effekt der „frustrierten“ Kationen an der Drei-Phasen-Kontaktlinie, der weitere Ausbreitung der Flüssigkeit verhindert, wird an einem Schwellenwert der Ladungsdichte der Oberfläche überwunden, ab dem elektrostatische Stabilisierung dominiert.

Das letzte Kapitel enthält Schlussfolgerungen zu den verschiedenen, in dieser Arbeit diskutierten, Themen und behandelt einige Perspektiven für die weitere Forschung.

Die in dieser Dissertation angestellten Untersuchungen zeigen, dass MD Simulationen, zusätzlich zu experimentellen Methoden, als leistungsfähiges Instrument zur detaillierten und umfassenden Erforschung von Benetzungsprozessen verwendet werden können. Mit MD Simulationen lassen sich vollständige Informationen über strukturelle und dynamische Eigenschaften verschiedener, in Kontakt stehender, Phasen gewinnen und experimentelle Ergebnisse erklären.

Acknowledgements

I would like to thank the following people for their support in completing the project:
Firstly and most importantly, my deepest gratitude to my research advisor, Prof. Dr. Nico van der Vegt, for being wonderful friend, mentor and teacher throughout my years at the institute of Center of Smart Interfaces. His intelligence, supervision and patience have helped me mature in my research and I attribute all my accomplishments largely to him. Nico, thank you very much for everything you have done for me.
I would like to thank Dr. Frédéric Leroy for his valuable insight and comments. I have enormously benefited from scientific discussion with him.
Special thanks go to Prof. Michael C. Böhm for his priceless advices and for accepting to be part of my PhD examiners. I would like specially to thank Prof. Dr. Biesalski, Prof. Dr. Schneider and Prof. Dr. Rolf Schäfer for reading my dissertation and that accepted to be in the final discussion of my PhD studies. I express to Dr. Elmar Bonaccurso here my gratitude for his valuable discussions, and I am also very much indebted to Dr. Lars-Oliver Heim for his help and spending so much time to provide me experimental data.
I wish to express my warm thanks to all of my colleagues and friends who made the past three years successful, enjoyable and supported me in any respect during the completion of my PhD studies. First of all, thanks to Valentina for her guidance and support in understanding of the subject. I would like also to mention Pim, Martin, Samira, Emiliano, Francisco and David. I am thankful for having Timir and Pritam as my office-mate. It was great to talk and laugh with them. Many thanks also to Gregor for translating the German summary of my thesis.
I would like specially to thank Imke for her support and helping me in all administrative issues in the university.
I close this list with the most important people in my life. I would like to thank my parents for their unconditional support, trust and love during these years. Last but not the least; Ali, I absolutely thank you for continuous and constant support during many difficult times. No words can depict how grateful I am.

Publications

This dissertation is based on the following publications:

1. Taherian, F.; Marcon, V.; van der Vegt, N. F. A.; Leroy, F., "What is the Contact Angle of Water on Graphene?", *Langmuir* **2013,** *29*, 1457-1465.

2. Taherian, F.; Leroy, F.; van der Vegt, N. F. A., "Interfacial Entropy of Water on Rigid Hydrophobic Surfaces". *Langmuir* **2013,** 29, 9807- 9813.

3. Taherian, F.; Leroy, F.; Heim, L-O.; Bonaccurso, E.; van der Vegt, N. F. A., "Asymmetric Wetting Behavior of an Ionic Liquid on Electrically Charged Graphene Surfaces", (submitted).

4. Taherian, F.; van der Vegt, N. F. A., "Molecular Simulation of Ionic Liquids at Solid-Liquid Interfaces and Aspects of Electrowetting: a Review", (submitted)

1. Introduction

1.1. Wetting

Wetting in general can be defined as the process where three phases which at least two of them are fluids are brought together. In most of the situations, a solid surface is wetted by a liquid in the saturated vapor of the liquid. The vapor interface can be also replaced with an immiscible liquid. The interactions between the solid, liquid and the gas phases at the molecular scale determine how the liquid wet the surface.

We can see wetting phenomena in our daily life for example the rain droplets on the window of car or dispersing the powders in milk for breakfast, and also in different industrial and biological applications. We can name some of the industrial applications such as reducing friction between moving surfaces by using different liquids, lab-on-a-chip systems,[1] coating by polymers to protect surfaces,[2] printing applications[3] and penetration of liquids into porous environments.[4] In different applications where properties of a surface are important, very often it is needed to characterize and control the wetting properties of the surface by a liquid. One way to influence the wetting properties of a surface is by changing the surface chemistry, and substantial research has been carried out to control the wetting characteristics of a surface by functionalizing the surface with different chemical groups.[5] The interaction energy of the surface with the liquid and the vapor can be modified with different polar and non-polar groups.

The structure and dynamic properties of liquids at solid surfaces have been extensively studied by experimental and theoretical investigations due to their high interest in different applications. The wetting and drying properties of solid surfaces are controlled by the molecular interfacial properties, which in turn are governed by the interfacial intermolecular interactions. The range of the intermolecular interactions is in the order of few nanometers. Such length scales can now be studied with different experimental methods like atomic force microscopy.[6] However, experimental research of interfacial properties has always been a difficult and challenging task. Beside the experimental techniques, molecular dynamics (MD) simulations can be used to get new insights into the topic of wetting phenomena.

In the last decade, MD simulations have been used to understand different properties of pure liquids, mixture of different liquids and also liquid interfaces. With the development of molecular simulation techniques, it is possible to obtain information at the molecular scale like the

orientation of molecules where the solid, liquid and gas phases meet. Such information is impossible or hard to obtain from experiments. During the last years, MD simulations have also used to study different aspects of wetting.[7-11] One can use MD simulation to understand the contribution of different atomistic details of the system, also at the macroscopic scale with acceptable accuracy.

In defining the wetting characteristics of a solid surface by a liquid, there are several interaction terms (like the solid-liquid and the liquid-liquid interactions) that are contributing. The contribution of different terms, however, cannot be separated in experiments. Changing one of these parameters will lead to change some other parameters. MD simulations can be used as a tools to investigate the effect of different parameters separately. Depending on the question that is to be addressed by the simulations, all-atom or coarse-grained models can be used. In all-atom models, all detailed material-specific information about the chemical composition of the system are necessary for the simulation, while in the coarse-grained models the number of degrees of freedom is reduced by merging groups of atoms into superatoms, It is thus possible to simulate larger systems for longer simulation times. In this dissertation, both models are used to address some wetting phenomena.

The behavior of a liquid near a surface depends upon the strength and the range of the intermolecular (liquid-liquid and liquid-substrate) interactions and on the structural properties of the substrate. The main goal of this thesis is to understand the wetting behavior of a system in terms of the molecular interactions, and indentify the contribution of different interactions to the wetting properties by using a combination of the computer simulation and theory.

1.2. Theoretical background

Wetting can be classified into two different categories: (i) equilibrium or static, when different parameters characterizing the wetting behavior (described in the following section) are at stationary state, and (ii) dynamic, when different parameters are changing with the time. In this thesis, we mainly focus on problems related to static wetting. In the present section, we give a molecular description of the main parameters which drive the static wetting phenomena. Some open questions regarding dynamic wetting are discussed in Chapter 7.

1.2.2. Surface tension

Molecular understanding of interfacial tension: In liquids compared to gases, the attractive intermolecular forces (cohesive forces) act at short distances between the molecules (on the order of 0.1 nm). This will lead to lower compressibility and higher density of liquid compared to gas. However, the molecules are still moving and are not at a fixed position as solid. Therefore, the liquid follows the shape of the container. The molecules interact with their neighbor molecules through the attractive van der Waals interactions or by making hydrogen bonds in the case of polar molecules like water.[12] In the bulk of the liquid and far from the liquid-vapor interface, molecules are feeling attracting forces equally in all the directions, while at the interface the number of neighbors are reduced (Figure. 1.1). One should keep in mind that since the density of gas is very low compared to liquid the attraction felt by the molecules at the interface from the gas will be less than that from the liquid. This leads to puling the molecules inward the liquid, and consequently bringing the molecules stronger at the interface. Such enhancement of the attractive interactions between the molecules at the interface is call surface tension. The surface is usually expressed in unit of J/m^2 or N/m (in most cases mN/m is used as a unit).

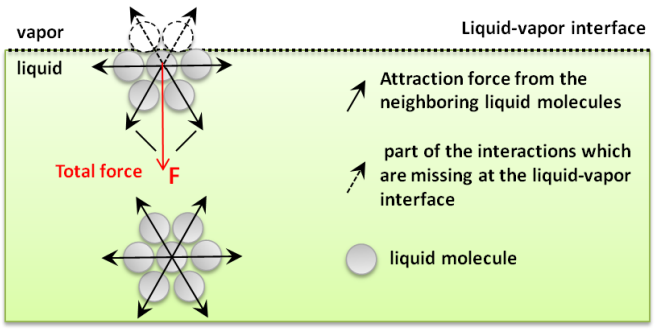

Figure 1.1. The scheme shows how a liquid molecule interacting with its neighbor in the bulk and at the liquid-vapor interface.

Thermodynamic description: Surface tension contributes to the Gibbs free energy in the following way: By using the differential change of the Gibbs free energy (G) in thermodynamics:

$$dG = -SdT + VdP + \sum \mu_i dN_i + \gamma dA \qquad (1\text{-}1)$$

where S, T, V, P, γ, A, μ_i, and N_i, are the entropy, temperature, volume, pressure, surface tension, interface area, chemical potential and number of molecules of the ith phase, respectively, the

surface tension is defined as change in the Gibbs free energy of the system by changing the interface area at the constant temperature, pressure and number of molecules. The quantity $A\gamma$ is the excess interfacial Gibbs free energy (G^s) of the interface.

Having the molecules at the liquid-vapor interface increases the surface free energy of the system, therefore the molecules at the interface try to minimize the liquid-vapor surface area. Since a sphere has a smallest surface area compared to others, final shape of a isolated droplet will be a sphere.

When two immiscible liquids are brought together, even the interaction between the molecules from one liquid with the other one at the interface is stronger than between a liquids and its gas, system try to minimize the interface area. In the case of water for example, the liquid-vapor surface tension is 72 mN/m, while the interfacial tension decreases to 50 mN/m by replacing the air with oil. For miscible liquids where there will be no defined interface between the liquids the surface tension is zero. This means that fresh and salty water have same surface tension since there are miscible. In the case of a liquid in contact with a solid surface, an attractive van der Waals interaction absorbs the liquid molecules to the surface, however because of their thermal motion they are not immobilized.

Surface tension becomes important at small scales since at such scales, the total number of atoms at the interface is comparable to the number of atoms in the bulk. Commonly, the capillary length, defined as[12]

$$\kappa^{-1} = \sqrt{\gamma_{lv}/\rho g} \qquad (1\text{-}2)$$

where γ_{lv}, ρ *and* g are the liquid-vapor surface tension, the density of the liquid and the gravitational acceleration, respectively, is used as a measure to determine whether surface forces (capillary forces) are important compared to other forces such as gravity. The capillary length is the length where the Laplace pressure is equal to the hydrostatic pressure. According to the eq. (1-2), for water ($\rho = 10^3$ kg/m^3, γ_{lv} =72 mN/m and g = 9.8 m/s^2) a typical length scale for the capillary length is of the order of a few mm. For the droplet sizes bigger than the capillary length gravity becomes important and the droplet will not have a spherical shape any more.[13]

1.2.3. Wetting—Partial or Complete Wetting

Compared to the description of a two-phase system, three interacting phases will be more complicated. In the following, we will limit our discussion to conditions where a liquid and its

vapor are in contact with a smooth solid surface. One way to measure the surface wettability is the spreading coefficient (S) defined by[14]

$$S = \gamma_{sv} - (\gamma_{sl} + \gamma_{lv}) \qquad (1\text{-}3)$$

S is change in the free energy of the surface at contact angles 0° and 180°, γ_{sv} is the solid-vapor interfacial tension, γ_{lv} is the surface tension of the liquid, and γ_{sl} is the solid-liquid interfacial tension. For a positive value of *S* the contact angle of droplet on the surface will be zero, while in the case of negative values of S the droplet will rest on the surface with angle between 0° and 180°. In this case, the liquid-vapor interface meets the solid with a contact angle (CA) θ_E. The line where the three phases (solid, liquid and gas) are coming together is called *contact-line* or the *triple line*.

In this dissertation we are dealing with water and the [BMIM][BF_4] ionic liquid which partially wet carbon based surfaces like graphite or graphene.

1.2.4. Contact angle

Wetting at the macroscopic scales can be quantified by the equilibrium CA, θ_E. Knowing the CA of a liquid on a surface will give an information on how the solid and the liquid are interacting. The CA, as seen in Figure 1.2, is the angle between the liquid-vapor and the solid-liquid interfaces. The complete wetting and drying can be identified by angles θ = 0° and θ = 180°, respectively.

The contact angle of a liquid at the equilibrium state depends on the solid-liquid interaction. One can use the CA to categorize the surfaces to *hydrophilic* and *hydrophobic* ones. The border to define the hydrophobicity will be θ = 90°, where surfaces with θ > 90° are called hydrophobic and the surface is hydrophilic when θ < 90°.

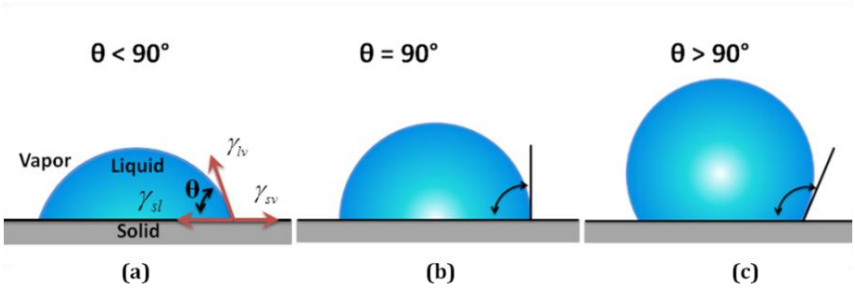

Figure 1.2. Different wetting situations for a droplet on a solid surface.

One could also define the *super-hydrophobic* and *super-hydrophilic* surfaces by the value the contact angle. For surfaces where the droplet is not willing to spread and the contact is above 150°, the surface considered to be *super-hydrophobic,* while surfaces with the contact angle around 0° are defined as *super-hydrophilic* surfaces. The partially wetted surfaces are defined with the contact angle values between 0 to 150°. One could imagine great applications for the super-hydrophobic materials for example in water-proof surfaces and also for the super-hydrophilic surface in building the self-cleaning glasses.

In the case of rigid and flat surfaces which there is no chemical heterogeneity on the surface, Young's equation is used to define the contact angle at the equilibrium:

$$\gamma_{lv}\cos\theta = \gamma_{sv} - \gamma_{sl} \qquad (1\text{-}4)$$

where the liquid-vapor, the solid-vapor and the solid-liquid interfacial tensions are denoted as γ_{lv}, γ_{sv} and γ_{sl}, respectively. Since the droplet is at the equilibrium stat, the forces on the contact line along the surface are canceled out each other, which lead to the Young's equation (Figure 1.2a). The Young's equation can be also derived from free energy minimization in the following way: suppose a liquid is in contact with a solid wall with the equilibrium contact angle of θ, as it is shown in Figure 1.3. The point at the 3-phase contact is a line perpendicular to the plane of the paper. The changes in the solid-vapor, solid-liquid and liquid vapor areas by moving up the contact-line by amount *dz* are:

$$\begin{aligned} dA_{sv} &= -ldz \\ dA_{sl} &= ldz \\ dA_{lv} &= ldz\cos(\theta - d\theta) = ldz[\cos\theta\cos d\theta - \sin\theta\sin d\theta] = ldz\cos\theta \qquad (\text{for } d\theta \to 0) \end{aligned} \qquad (1\text{-}5)$$

Where *l* is length of the contact line, and A_{sv}, A_{sl} and A_{lv} are the solid-vapor, solid-liquid and liquid vapor surface areas, respectively. The change of free energy due to a change in position of the contact-line (at constant temperature, pressure and number of molecules) can be written as:

$$dG = (\frac{\partial G}{\partial A_{sv}})dA_{sv} + (\frac{\partial G}{\partial A_{sl}})dA_{sl} + (\frac{\partial G}{\partial A_{sv}})dA_{sv} = \gamma_{sv}dA_{sv} + \gamma_{sl}dA_{sl} + \gamma_{lv}dA_{lv} \qquad (1\text{-}6)$$

Using eqs. (1-5) and (1-6) the free energy change is equal to:

$$dG = [-\gamma_{sv} + \gamma_{sl} + \gamma_{lv}\cos\theta]ldz \qquad (1\text{-}7)$$

At equilibrium condition *dG*=0 with respect to a small variation *dz*, and the Young's equation can be derived.

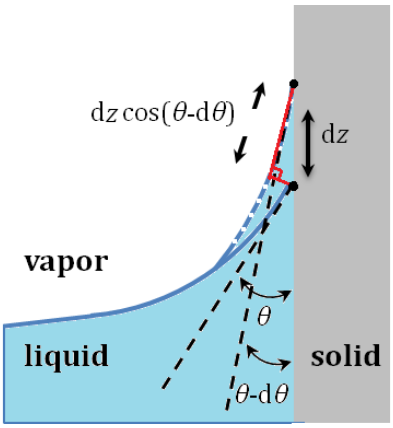

Figure 1.3. A liquid in contact with a solid wall with the equilibrium contact angle of θ. The figure shows the change in the contact angle by moving up the contact-line by amount of *dz*.

As it is mentioned above Young's equation could be only used in an ideal condition, which means the solid surface must be uniform, smooth, non-deformable and isotropic. But in reality and in most of the cases, the effect of roughness must be taken into account when characterizing the wetting properties of the surface. Two different models have been used to describe the wetting on rough surfaces. Wenzel model[15] assumed when liquid is in contact with the solid it will fill all the valleys on the surface, while Cassie model[16] assumes that the droplet is seating on a solid-vapor interface. In addition to the surface roughness,[17] chemical heterogeneities,[18] liquid penetration[19], and surface deformation[20] were also shown influencing the equilibrium contact angle. Nevertheless, since in this thesis simulations are done on a smooth and uniform graphene or graphite surface, the effect of roughness and surface heterogeneity will not be our topics of concern, and interesting readers on these topics are referred to Ref.[21] for more details.

Depending on how strong are the surface tension and the gravity forces a droplet may have different shapes. For small droplet sizes (below the capillary length of the liquid) since the gravity force is very small, it effect compared to the surface tension can be ignored, and droplet will have a spherical shape. However, at such small scales since the number of atoms at the contact-line is comparable to the total number of atoms in the droplet, line tension may change the value of the contact angle. Line tension is the work done to create a unit length of the contact line. Since the molecules at the contact-line are in contact with the three phases, they will be at different energetic state than those at the interfaces or those in the center of the droplet. Such a differences will lead to having the effect of the line tension. By considering the effect of the line tension, the Young equation will be in the following way:

$$\cos\theta = \frac{\gamma_{sv} - \gamma_{sl}}{\gamma_{lv}} - \frac{\tau}{\gamma_{lv} r_B} \quad (1\text{-}8)$$

where r_B is the base radius of the drop and τ is the line tension. Simulation results of Werder et al.[22] showed that for water on graphite the line tension is on the order of 10^{-11} J/m, and it increases the contact angle by approximately 8° for a droplet with r_B =3.0 nm.

1.2.5. Work of adhesion

Suppose a liquid is in contact with a solid surface (Figure 1.4), the surface energy of the system can be written as following:

$$G_1^s = \gamma_{sl} A \quad (1\text{-}9)$$

where A is surface area of the interface. The work which is needed to separate an unit area of the contact between the liquid and the solid phases is defined as the work of adhesion. The surface energy of the system after separating the two phases will be:

$$G_2^s = (\gamma_{sv} + \gamma_{lv}) A \quad (1\text{-}10)$$

The work of adhesion will then be the difference between the surface energies in eqs (1-9) and (1-10):

$$W_a = \gamma_{sv} + \gamma_{lv} - \gamma_{sl} \quad (1\text{-}11)$$

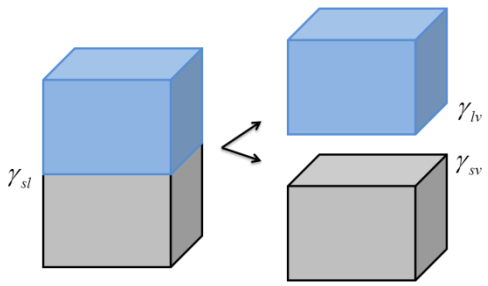

Figure 1.4. The energy needed to separate the solid and the liquid phases and form the solid-vapor and liquid-vapor interfaces is defined as the work of adhesion.

By subsisting eq. (1-4) in eq. (1-11), one can derive the Young–Dupré equation

$$W_a = \gamma_{lv}(1 + \cos\theta) \quad (1\text{-}12)$$

For a super-hydrophobic surface the contact angle is approximately 180°, and in this case no work is needed to separate the solid and the liquid phases. According to the Young–Dupré

equation by increasing the solid-liquid interaction and decreasing the contact angle the work require to separate the phases getting higher.

We can evaluate the work of adhesion by using the mean-field approaches, where only the contribution of the solid-liquid interaction is considered, and no entropy contribution is taken into account.[23-26] In these approaches, the sharp-kink approximation (SKA) is used. In the SKA, no thickness is considered for the interface and density of the liquid changes from zero to the bulk value at a specific distance from the surface.[27-30] The van der Waals interaction between the solid and the liquid can be calculated by using the Hamaker approach.[31]

Our scientific aim is to understand the static wettability of the hydrophobic systems in terms of the single molecule-substrate interaction, and we will try to obtain this understanding by combining the computer simulation and the theory. To make the link from molecular- substrate interaction to the contact angle behavior, we need to realize the contact angle as a thermodynamic quantity. To do so, we need to evaluate the contribution of the energy and entropy in the wetting. The contribution of the energy, as it was mentioned before, is considered by using SKA, while the entropy contribution is usually ignored. However, we cannot make predictions on contact angle behavior as long as we do not understand change in the liquid entropy at the solid interface. In the following section, a molecular level description of the interfacial enthalpy and entropy is given that has been developed for the first time in this dissertation, and will be used in Chapter 4 to evaluate the interfacial enthalpy and entropy of water on different surfaces by MD simulation.

1.2.6. Interfacial enthalpy and entropy

Interpretation of the work of adhesion at the molecular level: In the case of low vapor density fluids and poorly wettable substrates, where the solid-vapor interfacial tension compared to the solid-liquid and the liquid-vapor interfacial tensions can be neglected, the work of adhesion using eqs. (1-11) and (1-12) can be written as following:

$$W_a = \Delta\gamma = \gamma_{lv} - \gamma_{sl} = \gamma_{lv}(1+\cos\theta) \qquad (1\text{-}13)$$

To give a physical meaning of eq. (1-13), we consider a hypothetical thick film of water interacting with an attractive solid surface at a given temperature and a given cross sectional area *A* of the surface. If we now imagine a thermodynamic process where the attractive surface is

turned into a purely repulsive surface, provided that the number of water molecules, the number of particles in the substrate, the temperature T, the cross-sectional area A and the pressure normal to the interfaces are maintained constant, the Gibbs free energy change of the transformation is equal to the change in the excess interfacial Gibbs free energy (eq. (1-1)). It was shown by MD simulations[9, 32-33] that the interfacial excess free energy per unit area of a system in which water interacts with a purely repulsive surface is in fact the liquid-vapor surface tension of water γ_{lv}, since water tends to form a liquid-vapor like interface in the vicinity of such a surface. Therefore, the quantity $A\Delta\gamma=A(\gamma_{lv}-\gamma_{sl})$ can be understood as the change in the Gibbs free energy of the thermodynamic process of turning an attractive surface in a repulsive wall. Therefore, under assumption that γ_{sv} is a negligible quantity, the work of adhesion can be understood as sum of an enthalpy (ΔH) and entropy ($-T\Delta S$) change from an attractive to a repulsive surface i.e.:

$$W_a = \gamma_{lv}(1+\cos\theta) = \frac{1}{A}(\Delta \mathrm{H} - T\Delta S) \qquad (1\text{-}14)$$

Since the structure of the liquid is different at the attractive and the repulsive surfaces, and subsequent changes of the solid-liquid and the liquid-liquid interactions, the change in the enthalpy and entropy can be divided into the solid-liquid (ΔH_{ws} and ΔS_{ws}) and the liquid-liquid (ΔH_{ww} and ΔS_{ww}) contributions. Note that there is no contribution from the atoms within the solid, since the structure and the internal inter-atomic interactions of the solid are kept unchanged upon the transformation. It was shown on the base of studies on the hydrophobic hydration and solvation thermodynamics that the changes in the liquid-liquid interactions is exactly equal to the changes in the liquid-liquid entropy ($\Delta H_{ww}=T\Delta S_{ww}$; enthalpy-entropy compensation),[34-37] therefore these changes do not appear directly in the work of adhesion. Nevertheless, this is an indirect role played by the liquid-liquid interactions, which appear in all the ensemble averages.

The Gibbs free energy change (the work of adhesion) from the attractive (denoted as state A) to the repulsive wall (denoted as state R) can also be calculated using the *free-energy perturbation* (FEP) theory: [38]

$$W_a = -\frac{\beta^{-1}}{A}\ln\left\langle \exp\left[-\beta(V_R - V_A)\right]\right\rangle_A \qquad (1\text{-}15)$$

where $\beta^{-1} = k_B T$ with k_B the Boltzmann constant and T the absolute temperature, V_R and V_A denote the interaction potential of the liquid with the repulsive surface and the attractive

surface, respectively and notation $\langle \cdots \rangle_A$ indicates that an average is taken over the configurational distribution of the liquid molecules in the state *A* at temperature *T*. By defining $V_{disp} = V_A - V_R$ as the total solid-liquid dispersion energy, eq. (1-15) can be written as:

$$\begin{aligned} W_a &= -\frac{\beta^{-1}}{A} \ln\left\langle \exp\left[\beta V_{disp}\right]\right\rangle_A \\ &= \frac{1}{A}\left[-\left\langle V_{disp}\right\rangle_A - \beta^{-1} \ln\left\langle \exp\left[\beta \delta V_{disp}\right]\right\rangle_A\right] \equiv \frac{1}{A}(\Delta H_{WS} - T\Delta S_{WS}) \end{aligned} \tag{1-16}$$

where $\delta V_{disp} = V_{disp} - \left\langle V_{disp}\right\rangle_A$ denotes the fluctuation of the solid-liquid dispersion energy. $\Delta H_{WS} \equiv -\left\langle V_{disp}\right\rangle_A$ represents the energy contribution to the work of adhesion while $\Delta S_{WS} \equiv k_B \ln\left\langle \exp[\beta \delta V_{disp}]\right\rangle_A \geq 0$ represents the entropy contribution due the configurational bias imposed on the fluid molecules by the attractive external potential of a solid wall, and it is equal to the mean fluctuation of the solid-liquid interaction energy. [35-36, 39] Therefore, the work of adhesion can be understood as arising from the solid-liquid interaction strength and the fluctuation of these interactions. This interpretation of the work of adhesion was developed for the first time in this thesis.

In the mean field approximation, where the interaction energy is equal to the mean value, entropy has no contribution to the work of adhesion, and we will only have the contribution of the solid-liquid interaction. In this approximation, interaction of a liquid molecule with the surface is not dependent on distance to the surface, and it is always equal to the average value. Now, if the interaction potential varies with the distance to the surface, the interaction potential biases the molecules to be preferentially somewhere close to the interface. Obviously, this gives rise to the fluctuation in the energy, because the potential energy changes depending on the position of the molecules, and this fluctuation yields the entropy (see Figure (1-5)). In Section 1.3.2 a short overview of the work done in Chapter 4 to calculate interfacial entropy (ΔS_{ws}) of water on rigid hydrophobic surfaces is given. Note that ΔS_{ws} does not represent the thermodynamic entropy ΔS, which features another contribution ΔS_{ww} corresponds to the changes in the configurational degrees of freedom of the liquid molecules. As it is mentioned above, the liquid-liquid contribution of the entropy to the work of adhesion is exactly canceled by the liquid-liquid interaction contribution.

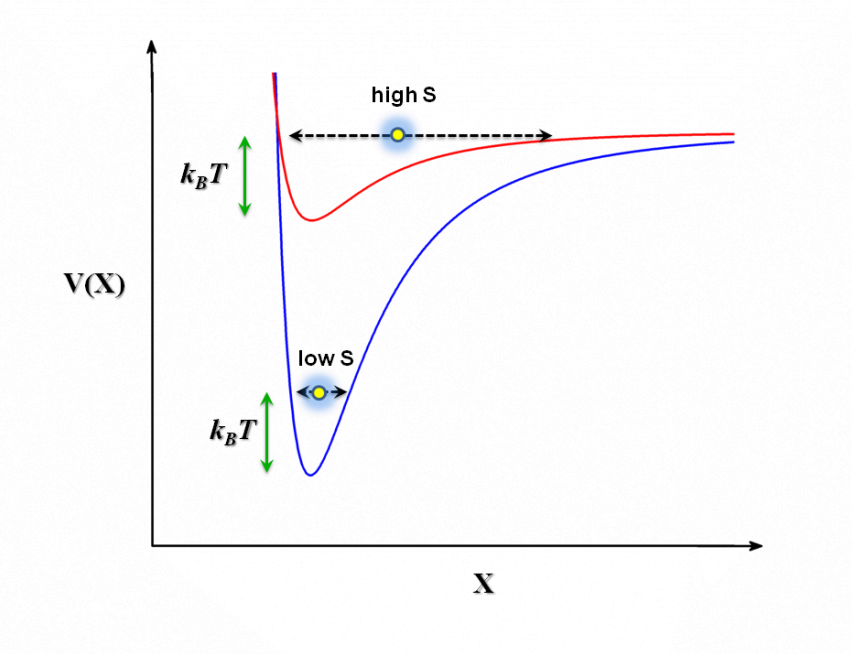

Figure 1.5. Interaction energy of a single particle of the liquid with the solid surface.

As we already mentioned, our goal is to understand wetting in terms of molecule-substrate interaction, and along the same line we would like to continue with complex fluids like ionic liquids (ILs) where the liquid is composed of asymmetric ions. The aim here is also to understand how the wettability depends on the ion-substrate interaction. Due to very low vapor pressure and very high stability of ILs at different temperatures, and also the possibility to control their interfacial properties, ILs became valuable candidates to be used as electrolytes in the electrowetting. In the following section a short introduction on the theory of electrowetting is given.

1.2.7. Electrowetting

Tuning the contact angle of a liquid on a solid by applying an external voltage between the liquid and the solid is called electrowetting (EW). During the last two decades, EW has been used extensively in different electrochemical systems where change in the wettability of the surface was needed.[40] In the original setup of electrowetting, the electrolyte droplet was in direct contact with the electrode. This configuration is not very efficient since water at voltages above a few hundred millivolts is decomposed. [41] But one could apply high voltages if a thin dielectric layer is placed between the liquid and the electrode, because in this case the voltage difference

will drop mainly in the dielectric layer and the liquid is still electrically stable. EW in presence of the dielectric is called electrowetting-on-dielectric (EWOD), and corresponding configuration is shown in Figure 1.6. The droplet before and after applying the voltage are distinguished by the dashed and the solid lines, respectively.

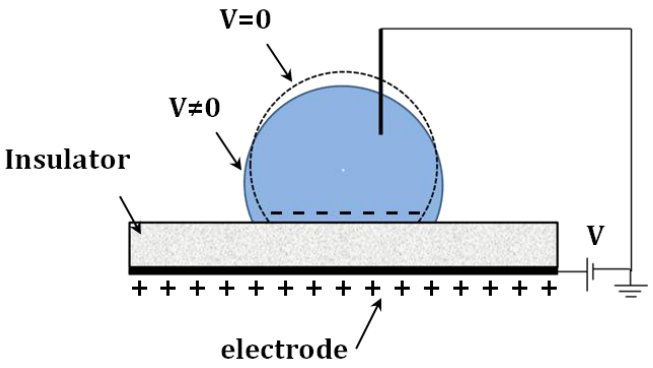

Figure 1.6. Change in the contact angle by applying voltage. The dashed line shows the droplet profile at zero voltage and the solid line corresponds to the droplet profile at voltage V.

Several approaches have been developed in the past to describe the change in the contact angle by applying the voltage like thermodynamic approach,[41] energy minimization approach,[44] or electromechanical approach.[45] Here we give the derivation using the thermodynamic approach.
According to the Helmholtz model, all the countercharges in the liquid will stand at a distance d_H from the surface, and together with the charges on the surface will form an electrical double layer (EDL) at the interface.
Since the value of d_H is in the order of a few nanometers, which is much smaller than the thickness of the dielectric layer, the drop of the potential at the EDL can be neglected and the change in the effective interfacial tension γ_{sl}^{eff} can be written as following:

$$d\gamma_{sl}^{eff} = -\delta_{sl} dV \qquad (1\text{-}17)$$

where V and δ_{sl} are the applied voltage and the charge density of the surface, respectively. The charge density on the surface is expressed in terms of the applied voltage and the capacitance of the dielectric per unit area ($\overline{C}$) as following:

$$\delta_{sl} = \overline{C} V \qquad (1\text{-}18)$$

From eqs. (1-17) and (1-18), the effective interfacial tension can be obtained

$$\gamma_{sl}^{eff} = \gamma_{sl} - \frac{1}{2}\bar{C}V^2 \quad (1\text{-}19)$$

By substituting eq. (1-19) in eq. (1-4) the Lippmann–Young equation can be derived as following:

$$\cos\theta_e = \cos\theta_0 + \frac{1}{2\gamma_{lv}}\bar{C}V^2 \quad (1\text{-}20)$$

where θ_0 and θ_e are the contact angles at zero voltage and V voltages, respectively. By using eq. (1-20) one can see that the droplet will spread more at higher voltages. Experimental results of electrowetting at different voltages showed that the Lippmann–Young equation is only able to explain the wetting behavior at low voltages. At high voltages, the contact angle saturation is happening, and the Lippmann–Young equation is not valid any longer. Several hypothesis like charging of the dielectric due to a failure,[46] charging of the insulating fluid around the droplet,[47] separation of the small droplets[48] or the solid-liquid interfacial tension of zero at the saturation[49] are proposed in the literature to explain the saturation, but none of them are confirmed to be the main reason for the saturation. MD simulations can be used as a powerful tool in order to understand the molecular sources of the saturation.

The Lippmann–Young equation predicts that the change in the contact angle is proportional to the square of the voltage, therefore it is independent of the sign of the voltage. In Section 1.3.3 and Chapter 6, we will discuss how the molecular details of the liquid can influence the symmetric change of the contact angle.

1.3. Open questions and scope of thesis

In the following section, open questions that we are investigating in this thesis are explained, and the contribution of this work to answer these questions is described.

1.3.1. Contact angle of water on graphene

Recently, graphene due to its interesting properties became very popular in both research community and industry. Graphene can be obtained by exfoliating bulk graphite into individual sheets with a technique called Scotch-tape method or the micromechanical cleavage. Graphene is expected to find applications in numerous domains of nanotechnology as optoelectronics[51] and water desalination[52] among others. The dispersion of graphene flakes in polymers[53] or the interaction of graphene sheets with aqueous solutions of salts strongly depends on the wetting

properties of graphene. In the last few years, a few papers started addressing different interfacial properties of water at graphene surface, and how the structural properties at the interface changes compared to graphite. Density functional theory calculations[54-55] and recent experimental results[56] showed that due to the adsorption of water on graphene the electronic properties of surface changes. The magnitude of the change in the electronic properties was found to be dependent on the solid-liquid interaction energy. Gordillo and Marti[57] by use of MD simulation investigate the changes in the structure of water on graphite with different number of graphene layers. Results show that the water structure (density profile) and interaction energy between the surface and water molecules is not changing that much from one layer (graphene) to two layers (graphite, according to the Werder's results) surfaces.

Graphene has already been recognized as a hydrophobic material. However, a quantitative knowledge of its wetting properties is still missing. Therefore, the precise characterization of these properties is of crucial importance and became a topic of investigation very recently. A simple way to address the wetting properties of graphene with respect to water is to measure the contact angle of a water droplet deposited on an isolated graphene surface. Although preparing a large enough monolayer of carbon atoms in the lab that is free of roughness may be a challenge, several experimental works have addressed the question of the wetting properties of graphene. In the recent experimental work by Wang et al.[58] have found that water on isolated graphene layers, and on graphite substrate have different contact angles. Results showed that water has a contact angle of 98.3° on graphite, while its value increases to 127.0° on graphene. The influence of the supporting substrate in the case of graphene was removed by stacking several flakes on top of each other. Yang et al.[59] showed instead that the contact angle of water on a SiC substrate coated with different number of graphene layers does not change with the number of layers., and they referred the high difference in the contact angle reported by Wang et al.[58] to the roughness of their graphene substrate. Recently, the effect of supporting substrate on the wetting behavior of a single layer of graphene has been investigated by Rafiee et al.[11] Results show that changes in the contact angle from graphene to graphite are strongly depends on the type of the supporting substrate used in the experimental setups. The question we will address in Chapter 3 is whether a value of the contact angle on a monolayer of graphene of the order of 127° is compatible with a value of the contact angle of approximately 90-95° on graphite. To do so, a theoretical model that connects the variations of the work of adhesion on graphene-based substrates to the change in the interaction potential between water and these substrates is

developed. We employ MD simulations to probe the assumptions we formulate, and compute interfacial tensions, contact angles, total solid-liquid interaction and interaction potentials of a single water molecule with the surfaces.

In Chapter 3, we reproduce the result previously obtained both analytically and by molecular simulations which shows that the contact angle of a water droplet on graphite is insensitive to the number of carbon atoms layers as long as this number is larger than or equal to three.[11, 60-61] We show that a value of 127° for the contact angle of water on graphene is obtained by means of an interaction potential between water and graphene that is incompatible with the accepted value of the contact angle of approximately 90° on graphite.

1.3.2. Interfacial entropy

Introducing an attractive interaction between a solid and a liquid has two effects: in one hand there will be some favorable energetic stabilization due to the attractive surface, but in other hand since the molecules are attracted to the minimum of the potential the configuration space of the liquid molecules is biased (i.e. positions and orientations of the liquid molecules at the interface change due to interaction with the solid surface), therefore entropy is lost. It have been already shown that as the surface become more hydrophobic the fluctuation in the density of the liquid at the interface increases. At such surface the weak water-substrate interactions enhance molecular scale flexibility and increase entropy. The density fluctuations are gradually decreased with increasing surface hydrophilicity where strong water-substrate interactions promote larger rigidity of interfacial water and reduces entropy.[62-64]

In Chapter 4, we show that interfacial entropy can be estimated from the knowledge of the interaction potential between water and hydrophobic surfaces. To that end, a simple theoretical model is developed to calculate the entropy change of water on a rigid hydrophobic solid surface, relative to water at the liquid-vapor interface. It will be shown that the corresponding estimates of the interfacial entropy of water on graphene, graphite and diamond are in a good agreement with the values calculated by MD simulation.

1.3.3. Electrowetting of ionic liquids

The interfacial properties of ILs with the aim of understanding their wetting behavior in terms of single molecule-substrate interaction are discussed in Chapters 5 and 6. ILs due to their

interesting properties became very popular in both research community and industry. The physical and chemical properties of ILs can be adjusted by choosing different combination of cations and anions.[65] For some of the applications like lubricants,[66-67] separations,[68-69] catalysis,[70-71] electrochemistry[72] or batteries,[73-75] the solid-liquid interfacial properties of ILs become very important, and several theoretical and experimental works have been done to investigate interface properties of ILs. Since ILs are composed of molecules with net charges which can form hydrogen-bonds, interaction between a solid surface and ILs can be completely different than the common liquids used as electrolyte.[78-81]

In addition to experimental techniques that have been used to characterize the structure of IL-solid interfaces[82-83] People have used MD simulation very frequently to study the interfacial structure of ILs at the molecular scales. Before discussing the electrowetting of ILs, in Chapter 5 we are reviewing the recent simulation results, where the different factors influencing the interfacial properties of ILs at the solid-liquid interface are discussed.

Several tries have been made recently to use ILs as electrolyte in electrowetting experiments.[88-89] Since ILs are made of cations and anions with controllable molecular structure, they can be used to understand different molecular aspects of electrowetting. Since experimental characterization of electrowetting at the molecular level is very limited, one can use MD simulations for further analysis at the nanoscales.

In the case of water, several authors[90-92] have reported asymmetric behavior of contact angles with the applied electric field polarity and direction by using MD simulations. The dependence of the contact angle of water to the polarity of the electric field was explained by changing orientations of water molecules and consequently the average number of hydrogen bonds of molecules at the interfaces with the field direction. This will lead to difference in the interfacial tensions of the liquid.[90] An asymmetry in the leading and the trailing contact angle of water was also found when the droplet was placed in an electric field parallel to the surface. The asymmetry was found to be dependent on the field strength. With an increase in the field strength, the asymmetry continuously increases, and then it disappears at high field strength.[92]

Raj et al.[93] have investigated experimentally how the size of ions affects the dielectric failure (charge penetration) which frequently occurs in electrowetting of aqueous salt solutions. Results indicated that using larger ion sizes leads to less dielectric failure by applying voltage. Therefore, in the case of ILs, since the size of cations and anions are different, one could expect asymmetry in different interfacial properties of the liquid with the polarity of the surface in the

electrowetting setup. MD simulations have already shown asymmetric changes of the number density of the ions, the volume charge density, the electric potential and the double layer capacitance with the surface polarity.[94-96] It is very interesting to see how these asymmetries influence the contact angle.

Paneru et al.[97] reported an experimental electrowetting study of a droplet of [BMIM][BF_4] IL at different DC voltages (±50, ±100, ±150 and ±200 V). Results showed that at low voltages (±50 and ±100 V) the base area of the droplet is independent of the sign of the voltage, while an asymmetry was observed at high voltages (±150 and ±200 V): the droplet spreads more (larger base area) for negative DC voltages where the cations are attracted to the polymer surface.[97]

In Chapter 6, we study the change in the contact angle of [BMIM][BF_4] IL on graphene on positive and negative surface charges by MD simulations to understand the contact angle behavior in terms of single molecule-substrate interaction. Simulation results show the droplet spreads more on negatively charged surfaces than the positively charged ones, where competing orientational preferences of the cations in the three-phase contact-line are induced by the solid-liquid and the liquid-vapor interface. At high surface charge densities before a complete wetting of the droplet happens; the effect of *frustrated* cation orientations in the three phase contact line, is overcome at a threshold value of the surface charge density, and the asymmetry will be disappeared.

1.4. References

(1). Yang, Y.; Liu, J., Flexibly driving micro flow in a Lab-on-Chip system via dry porous structure. *Forschung im Ingenieurwesen* **2009,** *73* (4), 219-229.
(2). Gray, J.; Luan, B., Protective coatings on magnesium and its alloys—a critical review. *Journal of alloys and compounds* **2002,** *336* (1), 88-113.
(3). Il'darkhanova, F.; Mironova, G.; Bogoslovsky, K.; Men'shikov, V.; Bykov, E., Development of paint coatings with superhydrophobic properties. *Protection of Metals and Physical Chemistry of Surfaces* **2012,** *48* (7), 796-802.
(4). Bear, J., *Dynamics of fluids in porous media*. DoverPublications. com: 2013.
(5). Chai, J.; Liu, S.; Yang, X., Molecular dynamics simulation of wetting on modified amorphous silica surface. *Applied surface science* **2009,** *255* (22), 9078-9084.
(6). Miller, J.; Veeramasuneni, S.; Drelich, J.; Yalamanchili, M.; Yamauchi, G., Effect of roughness as determined by atomic force microscopy on the wetting properties of PTFE thin films. *Polymer Engineering & Science* **1996,** *36* (14), 1849-1855.
(7). Yuan, Q.; Zhao, Y.-P., Precursor film in dynamic wetting, electrowetting, and electro-elasto-capillarity. *Physical Review Letters* **2010,** *104* (24), 246101.
(8). Leroy, F.; Müller-Plathe, F., Interfacial Excess Free Energies of Solid-Liquid Interfaces by Molecular Dynamics Simulation and Thermodynamic Integration. *Macromol. Rapid Commun.* **2009,** *30*, 864-870.
(9). Leroy, F.; Müller-Plathe, F., Rationalization of the Behavior of Solid-Liquid Surface Free Energy of Water in Cassie and Wenzel Wetting States on Rugged Solid Surfaces at the Nanometer Scale. *Langmuir* **2011,** *27*, 637-645.
(10). Leroy, F.; Müller-Plathe, F., Solid-Liquid Surface Free Energy of Lennard-Jones Liquid on Smooth and Rough Surfaces computed by Molecular Dynamics using the Phantom-Wall Method. *J. Chem. Phys.* **2010,** *133*, 044101-044111.
(11). Rafiee, J.; Mi, X.; Gullapalli, H.; Thomas, A. V.; Yavari, F.; Shi, Y.; Ajayan, P. M.; Koratkar, N. A., Wetting Transparency of Graphene. *Nature Materials* **2012,** *11*, 217-222.
(12). Israelachvili, J. N., *Intermolecular and surface forces: revised third edition*. Academic press: 2011.
(13). Ren, H.; Xu, S.; Wu, S.-T., Effects of gravity on the shape of liquid droplets. *Optics Communications* **2010,** *283* (17), 3255-3258.
(14). Shaw, D. J.; Costello, B., Introduction to colloid and surface chemistry: Butterworth-Heinemann, Oxford, 1991. Elsevier: 1993.
(15). Wenzel, R. N., Resistance of solid surfaces to wetting by water. *Industrial & Engineering Chemistry* **1936,** *28* (8), 988-994.
(16). Cassie, A. B. D.; Baxter, S., Wettability of porous surfaces. *Transactions of the Faraday Society* **1944,** *40* (0), 546-551.
(17). Delmas, M.; Monthioux, M.; Ondarçuhu, T., Contact angle hysteresis at the nanometer scale. *Physical Review Letters* **2011,** *106* (13), 136102.
(18). De Gennes, P.-G., Wetting: statics and dynamics. *Reviews of modern physics* **1985,** *57* (3), 827.
(19). Sedev, R.; Petrov, J.; Neumann, A., Effect of swelling of a polymer surface on advancing and receding contact angles. *Journal of colloid and interface science* **1996,** *180* (1), 36-42.
(20). Extrand, C.; Kumagai, Y., Contact angles and hysteresis on soft surfaces. *Journal of colloid and interface science* **1996,** *184* (1), 191-200.

(21). Bonn, D.; Eggers, J.; Indekeu, J.; Meunier, J.; Rolley, E., Wetting and spreading. *Reviews of modern physics* **2009,** *81* (2), 739.
(22). Werder, T.; Walther, J. H.; Jaffe, R. L.; Halicioglu, T.; Koumoutsakos, P., On the Water-Carbon Interaction for Use in Molecular Dynamics Simulations of Graphite and Carbon Nanotubes. *J. Phys. Chem. B* **2003,** *107*, 1345-1352.
(23). Sendner, C.; Horinek, D.; Bocquet, L.; Netz, R. R., Interfacial water at hydrophobic and hydrophilic surfaces: Slip, viscosity, and diffusion. *Langmuir* **2009,** *25*, 10768-10781.
(24). Sedlmeier, F.; Janecek, J.; Sendner, C.; Bocquet, L.; Netz, R. R.; Horinek, D., Water at polar and nonpolar solid walls (Review). *Biointerphases* **2008,** *3*, FC23-FC39.
(25). Shih, C. J., Wang, Q. H., Lin, S., Park, K. C., Jin, Z., Strano, M. S., & Blankschtein, D. , Breakdown in the Wetting Transparency of Graphene. *Phys. Rev. Lett.* **2012,** *109*, 176101-176106.
(26). Machlin, E. S., On Interfacial Tension at a Rigid Apolar Wall–Water Interface. *Langmuir* **2012,** *28*, 16729-16732.
(27). Garcia, R.; Osborne, K.; Subashi, E., Validity of the "Sharp-Kink Approximation" for Water and Other Fluids. *J. Phys. Chem. B* **2008,** *112*, 8114.
(28). Dietrich, S., in Phase Transitions and Critical Phenomena. Domb, C. L., J. L., Ed. Academic: London: 1988; Vol. 12, p 1.
(29). Dietrich, S.; Napiorkowski, M., Analytic results for wetting transitions in the presence of van der Waals tails. *Phys. Rev. A* **1991,** *43* (1861).
(30). Dietrich, S.; Schick, M., Order of wetting transitions. *Phys. Rev. B* **1986,** *33*, 4952-4968.
(31). Israelachvili, J. N., *Intermolecular and Surface Forces, 3rd edn.* Academic Press: 2011.
(32). Chandler, D., Insight Review: Interfaces and the Driving Force of Hydrophobic Assembly. *Nature* **2005,** *437*, 640-647.
(33). Huang, H. M.; Geissler, P. L.; Chandler, D., Scaling of Hydrophobic Solvation Free Energies. *J. Phys. Chem. B.* **2001,** *105*, 6704-6709.
(34). Ben-Naim, A., A simple model for demonstrating the relation between solubility, hydrophobic interaction and structural changes in the solvent. *J. Chem. Phys.* **1978,** *82*, 874-885.
(35). Sanchez, I. C.; Truskett, T. M.; In 't Veld, P. J., Configurational Properties and Corresponding States in Simple Fluids and Water. *J. Phys. Chem. B* **1999,** *103*, 5106–5116.
(36). van der Vegt, N. F. A.; Trzesniak, D.; Kasumaj, B.; van Gunsteren, W. F., Energy-Entropy Compensation in the Transfer of Nonpolar Solutes from Water to Co-Solvent/Water Mixtures. *ChemPhysChem* **2004,** *5*, 144-147.
(37). Ben-Amotz, D.; Underwood, R., Unraveling water's entropic mysteries: a unified view of nonpolar, polar, and ionic hydration. *Acc. Chem. Res.* **2008,** *41*, 957-967.
(38). Zwanzig, R. W., High-Temperature Equation of State by a Perturbation Method. I. Nonpolar Gases. **1954,** *22*, 1420-1427.
(39). Schravendijk, P.; Van Der Vegt, N. F., From hydrophobic to hydrophilic solvation: an application to hydration of benzene. *J. Chem. Theory Comput.* **2005,** *1*, 643-652.
(40). Mugele, F., Fundamental challenges in electrowetting: from equilibrium shapes to contact angle saturation and drop dynamics. *Soft Matter* **2009,** *5* (18), 3377-3384.
(41). Mugele, F.; Baret, J.-C., Electrowetting: from basics to applications. *Journal of Physics: Condensed Matter* **2005,** *17* (28), R705.
(42). Berge, B., Electrocapillarity and wetting of insulator films by water. *Comptes Rendus De L Academie Des Sciences Serie II* **1993,** *317* (2), 157-163.
(43). Quilliet, C.; Berge, B., Electrowetting: a recent outbreak. *Current Opinion in Colloid & Interface Science* **2001,** *6* (1), 34-39.

(44). Verheijen, H.; Prins, M., Reversible electrowetting and trapping of charge: model and experiments. *Langmuir* **1999,** *15* (20), 6616-6620.
(45). Kang, K. H., How electrostatic fields change contact angle in electrowetting. *Langmuir* **2002,** *18* (26), 10318-10322.
(46). Drygiannakis, A. I.; Papathanasiou, A. G.; Boudouvis, A. G., On the connection between dielectric breakdown strength, trapping of charge, and contact angle saturation in electrowetting. *Langmuir* **2008,** *25* (1), 147-152.
(47). Zhang, J.; Van Meter, D.; Hou, L.; Smith, N.; Yang, J.; Stalcup, A.; Laughlin, R.; Heikenfeld, J., Preparation and analysis of 1-chloronaphthalene for highly refractive electrowetting optics. *Langmuir* **2009,** *25* (17), 10413-10416.
(48). Vallet, M.; Vallade, M.; Berge, B., Limiting phenomena for the spreading of water on polymer films by electrowetting. *The European Physical Journal B-Condensed Matter and Complex Systems* **1999,** *11* (4), 583-591.
(49). Quinn, A.; Sedev, R.; Ralston, J., Influence of the electrical double layer in electrowetting. *The Journal of Physical Chemistry B* **2003,** *107* (5), 1163-1169.
(50). Chen, L.; Bonaccurso, E., Electrowetting-from Statics to Dynamics. *Advances in Colloid and Interface Science* **2013**.
(51). Hasan, T.; Scardaci, V.; Tan, P. H.; Bonaccorso, F.; Rozhin, A. G.; Sun, Z.; Ferrari, A. C., In *Molecular- and Nano-Tubes*, Hayden, O.; Nielsch, K., Eds. Springer Science and Business Media: New York, 2011; pp 279-354.
(52). Cohen-Tanugi, D.; Grossman, J. C., Water Desalination Across Nanoporous Graphene. *Nano Lett.* **2012,** *12*, 3602-3608.
(53). Kim, H.; Abdala, A. A.; Macosko, C. W., Graphene/polymer nanocomposites. *Macromolecules* **2010,** *43*, 6515-6530.
(54). Berashevich, J.; Chakraborty, T., *Phys. Rev. B.* **2009,** *80*, 033404.
(55). Wehling, T. O.; Lichtenstein, A. I.; Katsnelson, M. I., *Appl. Phys. Lett.* **2008,** *93*, 202110.
(56). Yavari, F.; Kritzinger, C.; Gaire, C.; Song, L.; Gulapalli, H.; Borca-Tasciuc, T.; Ajayan, P. M.; Koratkar, N., *small* **2010,** *6*, 2535.
(57). Gordillo, M.; Marti, J., Structure of water adsorbed on a single graphene sheet. *Physical Review B* **2008,** *78* (7), 075432.
(58). Wang, S. R.; Zhang, Y.; Abidi, N.; Cabrales, L., Wettability and Surface Free Energy of Graphene Films. *Langmuir* **2009,** *25*, 11078-11081.
(59). Shin, Y. J.; Wang, Y.; Huang, H.; Kalon, G.; Wee, A. T. S.; Shen, Z.; Bhatia, C. S.; Yang, H., Surface-energy engineering of graphene. *Langmuir* **2010,** *26* (6), 3798-3802.
(60). Jaffe, R. L.; Gonnet, P.; Werder, T.; Walther, J. H.; Koumoutsakos, P., Water–Carbon Interactions 2: Calibration of Potentials using Contact Angle Data for Different Interaction Models. *Mol. Simul.* **2003,** *30*, 205-216.
(61). Shih, C. J.; Wang, Q. H.; Lin, S.; Park, K. C.; Jin, Z.; Strano, M. S.; Blankschtein, D., Breakdown in the Wetting Transparency of Graphene. *Phys. Rev. Lett.* **2012,** *109*, 176101.
(62). Jamadagni, S. N.; Godawat, R.; Garde, S., Hydrophobicity of Proteins and Interfaces: Insights from Density Fluctuations. *Annu. Rev. Chem. Biomol. Eng.* **2011,** *2*, 147-171.
(63). Godawat, R.; Jamadagni, S. N.; Garde, S., Characterizing hydrophobicity of interfaces by using cavity formation, solute binding, and water correlations. *Proc. Natl. Acad. Sci. USA* **2009,** *106*, 15119–15124.
(64). Patel, A. J.; Varilly, P.; Jamadagni, S. N.; Acharya, H.; Garde, S.; Chandler, D., Extended surfaces modulate hydrophobic interactions of neighboring solutes. *Proc. Natl. Acad. Sci. USA* **2011,** *108*, 17678–17683.

(65). Castner, E. W.; Wishart, J. F., Spotlight on ionic liquids. *Journal of Chemical Physics* **2010,** *132*, 120901.
(66). Zhou, F.; Liang, Y.; Liu, W., Ionic liquid lubricants: designed chemistry for engineering applications. *Chemical Society Reviews* **2009,** *38* (9), 2590-2599.
(67). Ye, C.; Liu, W.; Chen, Y.; Yu, L., Room-temperature ionic liquids: a novel versatile lubricant. *Chemical Communications* **2001,** (21), 2244-2245.
(68). Han, X.; Armstrong, D. W., Ionic liquids in separations. *Accounts of chemical research* **2007,** *40* (11), 1079-1086.
(69). Berthod, A.; Ruiz-Angel, M.; Carda-Broch, S., Ionic liquids in separation techniques. *Journal of Chromatography A* **2008,** *1184* (1), 6-18.
(70). Aslanov, L.; Valetskii, P.; Zakharov, V.; Kabachii, Y. A.; Kochev, S. Y.; Romanovskii, B.; Yatsenko, A., Heterogeneous catalysis in ionic liquids: The heck reaction of bromobenzene with styrene over palladium supported on mesoporous carbon. *Petroleum Chemistry* **2008,** *48* (5), 360-365.
(71). Welton, T., Room-temperature ionic liquids. Solvents for synthesis and catalysis. *Chemical Reviews* **1999,** *99* (8), 2071-2084.
(72). Armand, M.; Endres, F.; MacFarlane, D. R.; Ohno, H.; Scrosati, B., Ionic-liquid materials for the electrochemical challenges of the future. *Nature materials* **2009,** *8* (8), 621-629.
(73). de Souza, R. F.; Padilha, J. C.; Gonçalves, R. S.; Dupont, J., Room temperature dialkylimidazolium ionic liquid-based fuel cells. *Electrochemistry communications* **2003,** *5* (8), 728-731.
(74). Wang, P.; Zakeeruddin, S. M.; Moser, J.-E.; Grätzel, M., A new ionic liquid electrolyte enhances the conversion efficiency of dye-sensitized solar cells. *The Journal of Physical Chemistry B* **2003,** *107* (48), 13280-13285.
(75). Nakamoto, H.; Watanabe, M., Brønsted acid–base ionic liquids for fuel cell electrolytes. *Chemical Communications* **2007,** (24), 2539-2541.
(76). Lee, S.-Y.; Ogawa, A.; Kanno, M.; Nakamoto, H.; Yasuda, T.; Watanabe, M., Nonhumidified intermediate temperature fuel cells using protic ionic liquids. *Journal of the American Chemical Society* **2010,** *132* (28), 9764-9773.
(77). Palacio, M.; Bhushan, B., A review of ionic liquids for green molecular lubrication in nanotechnology. *Tribology Letters* **2010,** *40* (2), 247-268.
(78). Nainaparampil, J.; Phillips, B.; Eapen, K.; Zabinski, J., Micro–nano behavior of DMBI-PF6 ionic liquid nanocrystals: large and small-scale interfaces. *Nanotechnology* **2005,** *16* (11), 2474.
(79). Liu, Y.; Zhang, Y.; Wu, G.; Hu, J., Coexistence of liquid and solid phases of BMIM-PF6 ionic liquid on mica surfaces at room temperature. *Journal of the American Chemical Society* **2006,** *128* (23), 7456-7457.
(80). Sha, M.; Wu, G.; Fang, H.; Zhu, G.; Liu, Y., Liquid-to-solid phase transition of a 1, 3-dimethylimidazolium chloride ionic liquid monolayer confined between graphite walls. *The Journal of Physical Chemistry C* **2008,** *112* (47), 18584-18587.
(81). Sha, M.; Wu, G.; Liu, Y.; Tang, Z.; Fang, H., Drastic phase transition in ionic liquid [Dmim][Cl] confined between graphite walls: new phase formation. *The Journal of Physical Chemistry C* **2009,** *113* (11), 4618-4622.
(82). Rivera-Rubero, S.; Baldelli, S., Influence of water on the surface of hydrophilic and hydrophobic room-temperature ionic liquids. *Journal of the American Chemical Society* **2004,** *126* (38), 11788-11789.
(83). Baldelli, S., Influence of water on the orientation of cations at the surface of a room-temperature ionic liquid: A sum frequency generation vibrational spectroscopic study. *The Journal of Physical Chemistry B* **2003,** *107* (25), 6148-6152.

(84). Neilson, G.; Adya, A. K.; Ansell, S., 8 Neutron and X-ray diffraction studies on complex liquids. *Annual Reports Section" C"(Physical Chemistry)* **2002,** *98*, 273-322.
(85). Oh, S.; Kauffmann, Y.; Scheu, C.; Kaplan, W.; Rühle, M., Ordered liquid aluminum at the interface with sapphire. *Science* **2005,** *310* (5748), 661-663.
(86). Atkin, R.; Abedin, S. Z. E.; Hayes, R.; Gasparotto, L. H.; Borisenko, N.; Endres, F., AFM and STM studies on the surface interaction of [BMP] TFSA and [EMIm] TFSA ionic liquids with Au (111). *The Journal of Physical Chemistry C* **2009,** *113* (30), 13266-13272.
(87). Bowers, J.; Vergara-Gutierrez, M. C.; Webster, J. R., Surface ordering of amphiphilic ionic liquids. *Langmuir* **2004,** *20* (2), 309-312.
(88). Dubois, P.; Marchand, G.; Fouillet, Y.; Berthier, J.; Douki, T.; Hassine, F.; Gmouh, S.; Vaultier, M., Ionic liquid droplet as e-microreactor. *Analytical chemistry* **2006,** *78* (14), 4909-4917.
(89). Galiński, M.; Lewandowski, A.; Stępniak, I., Ionic liquids as electrolytes. *Electrochimica Acta* **2006,** *51* (26), 5567-5580.
(90). Daub, C. D.; Bratko, D.; Leung, K.; Luzar, A., Electrowetting at the nanoscale. *The Journal of Physical Chemistry C* **2007,** *111* (2), 505-509.
(91). Daub, C. D.; Bratko, D.; Luzar, A., Nanoscale wetting under electric field from molecular simulations. In *Multiscale Molecular Methods in Applied Chemistry*, Springer: 2012; pp 155-179.
(92). Song, F. H.; Li, B. Q.; Liu, C., Molecular Dynamics Simulation of Nanosized Water Droplet Spreading in an Electric Field. *Langmuir* **2013,** *29* (13), 4266-4274.
(93). Raj, B.; Dhindsa, M.; Smith, N. R.; Laughlin, R.; Heikenfeld, J., Ion and liquid dependent dielectric failure in electrowetting systems. *Langmuir* **2009,** *25* (20), 12387-12392.
(94). Feng, G.; Qiao, R.; Huang, J.; Dai, S.; Sumpter, B. G.; Meunier, V., The importance of ion size and electrode curvature on electrical double layers in ionic liquids. *Physical Chemistry Chemical Physics* **2011,** *13*, 1152–1161.
(95). Feng, G.; Zhang, J.; Qiao, R., Microstructure and capacitance of the electrical double layers at the interface of ionic liquids and planar electrodes. *The Journal of Physical Chemistry C* **2009,** *113* (11), 4549-4559.
(96). Kislenko, S. A.; Samoylov, I. S.; Amirov, R. H., Molecular dynamics simulation of the electrochemical interface between a graphite surface and the ionic liquid [BMIM][PF6]. *Physical Chemistry Chemical Physics* **2009,** *11* (27), 5584-5590.
(97). Paneru, M.; Priest, C.; Sedev, R.; Ralston, J., Static and dynamic electrowetting of an ionic liquid in a solid/liquid/liquid system. *Journal of the American Chemical Society* **2010,** *132* (24), 8301-8308.

2. Molecular Dynamics Simulation of Wetting: Technical Issues

2.1. Introduction

Before discussing the simulation results for the questions addressed in Chapter 1, we explain here the method to calculate some of the quantities related to the wetting like surface tension and contact angle by molecular dynamics (MD) simulations, and some of the technical issues are also addressed. We start in the following with a short overview on MD simulation.

2.2. Molecular dynamics simulations

In the following, we summarize the main principle of a MD simulation: at the first step, the interaction potentials between the atoms in the system are defined. The total interaction can be divided to bonded and non-bonded interactions. The bonded interactions can be written as sum of the bond, angle and torsion potentials, while the summation of the Lennard-Jones and the Coulomb potentials are used to model the non-bonded interactions. The Lennard-Jones potential can be written as following:

$$u(r) = 4\varepsilon\left(\left(\frac{\sigma}{r}\right)^{12} - \left(\frac{\sigma}{r}\right)^{6}\right) \qquad (2\text{-}1)$$

where ε is the interaction energy at the minimum potential, σ representing the radius of the atoms and r is the separation between the atoms. Using the total interaction potential between the atoms, the total force on each atom can be calculated. By solving the Newton's equation of motion, the position and the velocity of the atoms during time are calculated. To do so, time is discretized to a small value defined as dt. To make the simulation computationally less expensive as possible the larger values of dt are more favorable, while to have a correct dynamics dt should be smaller than 10% of the smallest oscillation time in the system. To solve the equation of the motion different algorithms like Verlet or leap-frog can be used.[1] To remove the effect of the interfaces in MD simulations, periodic boundary conditions are usually used. Since at very large distances, the interaction potential between the atoms is zero, a cutoff value is used for possible interacting atoms in the system. A typical value for the Lennard-Jones potential is 2.5 times the distance where the potential is zero at finite distances. After running the simulation and

collecting the trajectory of the system during the time one could calculate different physical properties of the system by taking average during the time. In this chapter, the technical details of MD simulations for studying the wetting properties are given. There are several open source software available like NAMD[2], AMBER[3], CHARMM[4], LAMMPS[5], GROMACS[6]. In this thesis the molecular dynamics code GROMACS is used.

2.2.1. Force field derivation for MD simulations

Main challenging part of the force field in the wetting simulation is the interaction of the liquid with the surface. The solid-liquid interaction parameters are developed in a way that the droplet simulation reproduces the macroscopic contact angle of the liquid on the surface. Werder et al.[7] parameterized the interactions between the SPC/E (extended simple point charge) water model and the graphite surface. In the following, we explain the procedure to develop the force field as an example for water on graphene.

To develop the interaction parameters, the first step is to place a drop of liquid molecules on the surface and run simulation with different interaction parameters (which lead to contact angle values close to the experimental one) between the surface and the liquid. By using a linear interpolation for the variation of the contact angle ($1+\cos\theta$) versus the interaction parameter ε_{CO} (between the carbon of surface and the oxygen of water) first estimation can be made for the parameter, which reproduce the experimental contact angle (θ). The value of σ_{CO} is equal to 0.392 nm and kept constant.[7] Before proceed further with the development of the solid-liquid interaction, the reason for the linear dependence $1+\cos\theta \propto \varepsilon_{CO}$ for small change of ε_{CO} is given.

As mentioned in Chapter 1, the work of adhesion (W_a) is defined by:

$$W_a = \gamma_{sv} + \gamma_{lv} - \gamma_{sl} = \gamma_{lv}(1+\cos\theta) \qquad (2\text{-}2)$$

Suppose there is no contribution of interfacial entropy to the work of adhesion, W_a will be equal to the interactions of all water molecules with the surface and is given by (assuming homogeneous solid and liquid densities ρ_s and ρ_l)

$$W_a = -\rho_l \int_{z^*}^{r_c} u_{ws}^{(1)}(z)dz \qquad (2\text{-}3)$$

where $u_{ws}^{(1)}(z)$ is the interaction energy of a single liquid molecule with the surface at a distance z from the surface, r_c is the cut-off for the solid-liquid interactions, z^* is defined by $u_{ws}^{(1)}(z^*) = 0$.[8] The eq. (2-3) can be written as a function of the intermolecular liquid-solid interaction potential $u(z)$ as following:

$$W_a = -2\pi\rho_s\rho_l \int_{z^*}^{r_c} dz \int_z^{r_c} dr(r^2 - zr)u(r) \qquad (2\text{-}4)$$

Since the Lennard-Jones potential in eq. (2-1) depends linearly on ε_{CO}, therefore according to eq. (2-4) the work of adhesion will be a linear function of the solid-liquid interaction energy ε_{CO}. Then using eq. (2-2) linear dependence of $1+\cos\theta \propto \varepsilon_{CO}$ follows:

$$1+\cos\theta = \frac{W_a}{\gamma_{lv}} \propto \varepsilon_{CO} \qquad (2\text{-}5)$$

It is worth to mention that, neglecting the interfacial entropy contributions is the main assumption to derive eq. (2-5) and adding this contribution could lead to no-linearity when the range of the change in ε_{CO} is wide. However, as soon as we are changing ε_{CO} around the target value the linearity would be valid. In Chapter 4, a simple theoretical model is proposed for computing the interfacial entropy of water at rigid hydrophobic surfaces. The interfacial entropy, which is not considered in existing mean field models of the work of adhesion, is evaluated from the fluctuations of the water-surface dispersion energy at the single particle level, and represents the configurational bias imposed on the fluid molecules by the attractive external potential of the surface. Figure 2.1 shows the change in the contact angle of water on diamond[8] and graphite[7] as a function of the interaction parameter ε_{CO}. The figure shows a linear dependence of $1+\cos\theta$ to ε_{CO} with some deviations at small values of ε_{CO}. We will discuss this issue in Chapter 4.

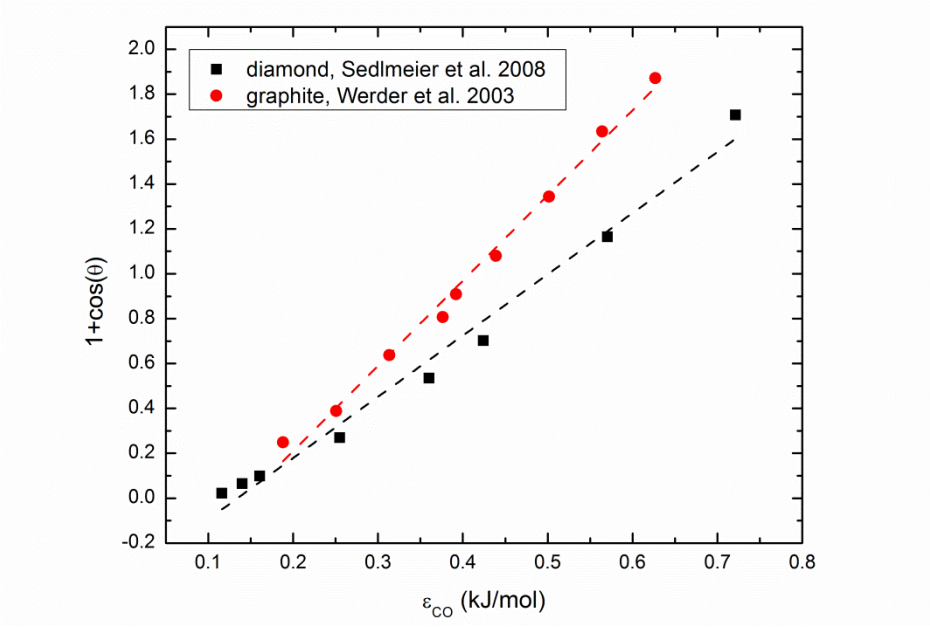

Figure 2.1. Contact angle of water on diamond and graphite as a function of the interaction parameter ε_{CO}.

For small droplet sizes, since the number of atoms at the contact-line is comparable to the total number of atoms in the droplet, line tension may change the value of the contact angle. Line tension is the work done to create a unit length of the contact line. Since the molecules at the contact-line are in contact with the three phases, they will be at different energetic states than those at the interfaces or those in the center of the droplet. Such differences will lead to having the effect of the line tension. By considering the effect of the line tension, the Young equation is modified as following: [9]

$$\cos\theta = \frac{\gamma_{sv} - \gamma_{sl}}{\gamma_{lv}} - \frac{\tau}{\gamma_{lv} r_B} \qquad (2\text{-}6)$$

Therefore, according to equation (2-6) by changing the size of a droplet on a surface its contact angle changes.

In the next step to develop the solid-liquid interaction energy, drops of different sizes are then simulated on the surface using the estimated value of the interaction parameter in the previous step. By using eq. (2-6), the value of the line tension and the contact angle of a macroscopic droplet (θ_∞) can be calculated. The effect of the line tension on the interaction parameter can be taken into account by comparing the value of the contact angle used for the calibration of the first part (experimental value) with θ_∞. This difference shows how the line tension changes the contact angle of small droplets.

The strategy adopted here is much faster than the one used by Werder at al.[7] or recently by Scocchi et al.[10], where first the simulation of different droplet sizes have been run for different interaction parameters between the surface and the liquid, and then by plotting θ_∞ versus the interaction parameter and using a linear fit to the data points, the corresponding value reproducing the experimental contact angle was derived.

The effect of line tension on the contact angle can be excluded by simulation a cylindrical droplet, where the contact-line has infinite length. Periodic boundary conditions are applied such that the droplet is infinite in one direction. The contact angle is calculated by fitting the projection of the droplet on the plain normal to the cylinder axis with a circle.[11]

2.2.2. Cut-off artifact

As it was mentioned above, the non-bonded interactions are truncated at a cut-off radius to reduce the number of computations. Our experience in the simulation of liquid droplets shows that choosing the right value of the cut-off is very critical, and it could lead to strong artifact in the system. In Chapter 6, a droplet of 2000 ion pairs of [BMIM][BF_4] ionic liquid was simulated using the coarse-grained potential developed by Merlet et al.[12] The cut-off was set to 1.6 nm, as the authors suggested. Simulating a spherical droplet (cut out from a bulk simulation) in the vacuum for at least 15 ns, where the non-bonded interactions are simply truncated at the cut-off leads to a pancake shape droplet. The cut-off artifacts can be avoided by shifting the non-bonded potentials to zero at the cut-off. The modification of the non-bonded interactions can be turned on in GROMACS[6] by using the option *shift* for the van der Waals interactions in the *mdp* file.

2.3. Surface tension measurement

The change in the intermolecular forces at the interface will lead the change in the normal and parallel components of the pressure at the interface. Kirkwood and Buff developed a theory where they have expressed the surface tension in terms of the change in the pressure components as following:[13]

$$\gamma_{lv} = \int_{-\infty}^{\infty} \left[P_N - P_T\right] dz \qquad (2\text{-}7)$$

In order to calculate the liquid-vapor surface tension with MD, a simulation of a liquid-vapor interface is carried out. To do so, the box size of an equilibrated system is doubled in the *z*-direction, and a simulation under constant temperature (T), volume (V) and number of atoms (N), NVT, conditions is performed for enough time to equilibrate the system. Using eq. (2-7) surface tension will follow:[14]

$$\gamma_{lv} = \frac{L_z}{4}\left(2P_{zz} - (P_{xx} + P_{yy})\right) \qquad (2\text{-}8)$$

where L_z is the box size perpendicular to the interface. It is important to notice that the thickness of the film should be enough large to prevent the system size effects. For very thin liquid films, the liquid-vapor interfaces may influence on each other and the film becomes unstable which is also dependent on the temperature of the system.[15]

2.3.1. Effect of constraint

Since in principal, the kinetic part of the pressure are the same in the parallel and normal to the liquid-vapor interface, only the virial part of the pressure remains in eq. (2-2). Some authors have already used this approach by subtracting the diagonal components of the virial tensor in parallel and normal to the interface.[8] It is very important to note that if the constraints are used to freeze some degree of freedom of the molecules of liquid, since the constraints remove kinetic energy, and at the surface, water molecules will have an average orientation with respect to the surface, therefore the kinetic energy tensor is non-uniform. Therefore, the kinetic energy in the parallel and normal to the interface will not be the same. In such conditions, both the kinetic and the virial part of the pressure are needed to be considered in eq. (2-8).

2.3.2. Tail correction

As it is mentioned before a cut-off value is used to calculate the non-boned interactions. Introducing the cut-off in the calculations leads to an error in estimating the surface tension. One can calculate the contribution of the long-range interactions as following: first, the density profile of the liquid along the interface ($\rho(z)$) is calculated. Then the profile is fitted to a hyperbolic tangent function:

$$\rho(z) = \frac{1}{2}(\rho_l + \rho_v) - \frac{1}{2}(\rho_l - \rho_v)\tanh[(z - z_0)/d] \qquad (2\text{-}9)$$

where ρ_l, ρ_v, z_0 and d are derived by the fitting. The fitting has been done on both interfaces and the average values are taken. Using the fitting parameters obtained from eq. (2-9) the correction term to the surface tension due to introducing the cutoff in the calculation of the forces can be calculated by[16-17]

$$\gamma_{tail} = \int_0^1 \int_{r_c}^{\infty} 12\pi(\rho_l - \rho_v)^2 \coth\left(\frac{2rs}{d}\right)\left(\frac{3s^2 - s}{r^3}\right) dr ds \qquad (2\text{-}10)$$

MD simulations of Vega et al.[14] for most common water models such as SPC[18], SPC/E[19], TIP3P[20] and TIP4P[20] showed that the correction of the surface tension is in the order of 2-4 mN/m.

2.4. Contact angle measurement

Several ways have been proposed in literature to calculate the contact angle of a droplet on a surface by MD simulations, which lead to similar values for the contact angle. In this thesis, we follow the procedure developed by de Ruijter et al.[21] for the contact angle calculations. In this approach, at the first step, the droplet is divided into layers in *z* direction with a thickness of 0.5 Å. Then each layer is divided into radial bins, where each bin are located at $r_i = \sqrt{i\delta A/\pi}$ for $i = 1 \cdots N_{bin}$ to have same volume for all the elements. The base area for each bin is considered to be $\delta A = 95$ Å^2. In the next step, density profile for each layer is determined and then fitted to a hyperbolic function to find out the radius of each layer. At the end, a circle is fitted to the droplet profile and extrapolated to the surface to calculate the contact angle and the base radius. The points in the droplet profile at the top of the droplet where the corresponding density value measured in the central bin is below the half of the bulk density of the liquid, and also the points below a height of 8 Å from the surface are not taken into account for the circular fit, because the statistics would be too poor.

2.5. References

(1). Frenkel, D.; Smit, B., *Understanding molecular simulation: from algorithms to applications*. Access Online via Elsevier: 2001.

(2). Phillips, J. C.; Braun, R.; Wang, W.; Gumbart, J.; Tajkhorshid, E.; Villa, E.; Chipot, C.; Skeel, R. D.; Kale, L.; Schulten, K., Scalable molecular dynamics with NAMD. *Journal of computational chemistry* **2005,** *26* (16), 1781-1802.

(3). Salomon-Ferrer, R.; Case, D. A.; Walker, R. C., An overview of the Amber biomolecular simulation package. *Wiley Interdisciplinary Reviews: Computational Molecular Science* **2012**.

(4). Brooks, B. R.; Brooks, C. L.; Mackerell, A. D.; Nilsson, L.; Petrella, R. J.; Roux, B.; Won, Y.; Archontis, G.; Bartels, C.; Boresch, S., CHARMM: the biomolecular simulation program. *Journal of computational chemistry* **2009,** *30* (10), 1545-1614.

(5). FrantzDale, B.; Plimpton, S. J.; Shephard, M. S., Software components for parallel multiscale simulation: an example with LAMMPS. *Engineering with Computers* **2010,** *26* (2), 205-211.

(6). Hess, B.; Kutzner, C.; Spoel, D. V. D.; Lindahl, E., GROMACS 4: Algorithms for Highly Efficient, Load-Balanced, and Scalable Molecular Simulation. *J. Chem. Theory Comput.* **2008,** *4*, 435-447.

(7). Werder, T.; Walther, J. H.; Jaffe, R. L.; Halicioglu, T.; Koumoutsakos, P., On the Water-Carbon Interaction for Use in Molecular Dynamics Simulations of Graphite and Carbon Nanotubes. *J. Phys. Chem. B* **2003,** *107*, 1345-1352.

(8). Sedlmeier, F.; Janecek, J.; Sendner, C.; Bocquet, L.; Netz, R. R.; Horinek, D., Water at polar and nonpolar solid walls (Review). *Biointerphases* **2008,** *3*, FC23-FC39.

(9). Gibbs, J. W., On the equilibrium of heterogeneous substances. *Trans Conn.Acad.* **1878,** *3*, 343.

(10). Scocchi, G.; Sergi, D.; D'Angelo, C.; Ortona, A., Wetting and Contact-Line Effects for Spherical and Cylindrical Droplets on Graphene Layers: A Comparative Molecular-Dynamics Investigation. *Phys. Rev. E* **2011,** *84*, 061602-061608.

(11). Rafiee, J.; Mi, X.; Gullapalli, H.; Thomas, A. V.; Yavari, F.; Shi, Y.; Ajayan, P. M.; Koratkar, N. A., Wetting Transparency of Graphene. *Nature Materials* **2012,** *11*, 217-222.

(12). Merlet, C.; Salanne, M.; Rotenberg, B., New coarse-grained models of imidazolium ionic liquids for bulk and interfacial molecular simulations. *J. Phys. Chem. C* **2012,** *116*, 7687-7693

(13). Kirkwood, J. G.; Buff, F. P., The statistical mechanical theory of surface tension. *The Journal of chemical physics* **1949,** *17*, 338.

(14). Vega, C.; Miguel, E. d., Surface Tension of the Most Popular Models of Water by using the Test-Area Simulation Method. *J. Chem. Phys* **2007,** *126*, 154707-154710.

(15). Weng, J.-G.; Park, S.; Lukes, J. R.; Tien, C.-L., Molecular dynamics investigation of thickness effect on liquid films. *The Journal of chemical physics* **2000,** *113*, 5917.

(16). Alejandre, J.; Tildesley, D.; Chapela, G. A., Molecular dynamics simulation of the orthobaric densities and surface tension of water. *J. Chem. Phys.* **1995,** *102*, 4574-4583.

(17). Blokhuis, E.; Bedeaux, D.; Holcomb, C.; Zollweg, J., Tail corrections to the surface tension of a Lennard-Jones liquid-vapor interface. *Molecular Physics* **1995,** *85* (3), 665-669.

(18). Berendsen, H. J. C.; Postma, J. P. M.; Gunsteren, W. F.; Hermans, J., Interaction Models for Water in Relation to Protein Hydration. In *Intermolecular Forces*, Pullman, B., Ed. Springer Netherlands: 1981; Vol. 14, pp 331-342.

(19). Berendsen, H. J. C.; Grigera, J. R.; Straatsma, T. P., The Missing Term in Effective Pair Potentials. *J. Phys. Chem.* **1987,** *91*, 6269-6271.
(20). Jorgensen, W. L.; Chandrasekhar, J.; Madura, J. D.; Impey, R. W.; Klein, M. L., Comparison of simple potential functions for simulating liquid water. *The Journal of chemical physics* **1983,** *79*, 926.
(21). De Ruijter, M. J.; Blake, T.; De Coninck, J., Dynamic wetting studied by molecular modeling simulations of droplet spreading. *Langmuir* **1999,** *15* (22), 7836-7847.

3. What is the Contact Angle of Water on Graphene?

3.1. Introduction

Due to exceptional properties of graphene a lot of researches have been focused on different properties of graphene and there is a high interest to use graphene in different industrial applications. Graphene is expected to find applications in numerous domains of nanotechnology as varied as optoelectronics[1] and water desalination[2] among others. The dispersion of graphene flakes in polymers[3] or the interaction of graphene sheets with aqueous solutions of salts strongly depends on the wetting properties of graphene. Graphene has already been recognized as a hydrophobic material. However, a quantitative knowledge of its wetting properties is still missing. Therefore, the precise characterization of these properties is of crucial importance and became a topic of investigation very recently. We call graphene the two dimensional planar material made up of a monolayer of carbon atoms in contrast to other authors who use the term graphene to describe materials composed of a few carbon layers.

A simple way to address the wetting properties of graphene with respect to water is to measure the contact angle of a water droplet deposited on an isolated graphene surface. Measuring a contact angle in this precise case depends on the possibility to isolate and to suspend monolayers of carbon atoms. Moreover, the dimensions of such samples should be sufficiently extended to support liquid droplets that are large enough so that they do not evaporate too fast. The material should be free of roughness as this factor may significantly influence the results of the measurements. Although obtaining such experimental conditions may be a challenge, several experimental works have addressed the question of the wetting properties of graphene. It was shown that in the case of SiC coated with graphene contact angle measurements on different number of graphene layers showed no thickness dependence on the number of layers.[4] This finding was generalized and it was shown that water had a different contact angle on a single graphene layer depending on the type of supporting substrate.[5-6] In the recent study of Wang *et al*.,[7] graphene monolayers or a stack of a very few graphene layers were produced through chemical exfoliation of natural graphite flakes. The contact angle of water was measured on several such flakes. The influence of the supporting substrate was removed by stacking several

flakes on top of each other. Under these conditions, it was found that water had a contact angle of 98.3º on graphite, while this quantity increased to 127º on graphene. Such a high value would promote graphene to be the most hydrophobic smooth material. Indeed, the most direct competitor would be crystalline *n*-perfluoroeicosane which yields a contact angle of water of 119°.[8] However, the measurements of the contact angle reported above were done on a film composed of several graphene flakes. These experimental conditions may have led to a sample exhibiting significant ruggedness and thus may explain the origin of the high value of the contact angle.[4] Scocchi *et al.*[9] recently formulated the idea that those measurements may be seen as the most reliable characterization of the contact angle of water on graphene in the ideal condition of a flat surface free of defects. These authors developed a new empirical force field for the water-carbon interaction on the basis of the contact angle of 127º. On the basis of the experimental works of Wang *et al.*[7], Shin *et al.*[4] and Rafiee *et al.*[5] performed between 2009 and 2012, we note that a value of approximately 90-95° seems to be an acceptable estimate of the contact angle of water on graphite. The question we address in the present work is whether a value of the contact angle on a monolayer of graphene of the order of 127° is compatible with a value of the contact angle of approximately 90-95° on graphite.–Shih *et al.*[6] have very recently contributed to this issue by developing a theory according to which the contact angle of water on monolayer graphene is 96°.

Besides recent achievements in the experimental approach to the characterization of the wetting properties of graphene, quantum based simulation methods recently made significant progresses. Indeed, recent advances in electronic density functional theory which account for the van der Waals interactions in the interaction energies made it possible to better describe the interactions between single water molecules or small water clusters and solid surfaces such as graphite or graphene (see ref. [10] and references therein). Quantum molecular dynamics (QMD) simulations were recently employed to study a water droplet on graphene. A value of the contact angle of 87° was obtained.[11] It must be noted that the droplet employed in these computations contained only 125 water molecules. This small number suggests that the result may strongly be affected by the line-tension, i.e. an important size effect which has been characterized both in experiments[12] and in molecular simulations.[13-15] Moreover, the stability of such small droplets may be questioned from the standpoint of experiments,[16] although submicrometer-sized droplets have recently been observed at the step-edges of graphene surfaces.[17] Nevertheless, it must be noted that the value obtained in the QMD study mentioned above is close to the range of

values commonly accepted for the contact angle of water on graphite, i.e. around 90°. Despite the uncertainty that characterizes that result, it strongly contrasts with the experimental value of 127° in the experimental work mentioned previously.

In the present article, we show that the value of 127° for the contact angle of water on graphene is an overestimation of the actual value. To that end, we develop a theoretical argumentation based on interfacial thermodynamics. The development of this model is supported by classical molecular dynamics (MD) simulations. We reproduce the result previously obtained both analytically and by molecular simulations which shows that the contact angle of a water droplet on graphite is insensitive to the number of carbon atoms layers as long as this number is larger than or equal to three.[5-6, 18] We show that a value of 127° for the contact angle of water on graphene is obtained by means of an interaction potential between water and graphene that is incompatible with the accepted value of the contact angle of approximately 90° on graphite. Our work delivers important information about the wetting properties of graphene and leads to multiple conclusions. Besides the importance of the information about contact angles on graphene in the context of experimental materials science, the precise knowledge of such a macroscopic property is required to generate reliable interaction potentials that are employed in molecular simulations. Such a topic is illustrated in the reviews by Werder *et al.*[13] and by Alexiadis and Kassinos[19] in the context of the molecular modeling of the interactions between water and carbon based materials. From a more fundamental point of view, the theoretical approach we develop shows that the work of adhesion of water on graphite or graphene is mainly due to the interaction energy between water and these surfaces. On the basis of the theory of solvation, we introduce the idea that the remaining part is entropic in nature and finds its origin in the fluctuations of the water-substrate interaction energy. This contribution is overlooked in the theories based on the approach of Hamaker which is employed in the work of Rafiee *et al.*[5] and Shih *et al.*[6] for example.

To reach our conclusions, we develop a model to connect the variations of the work of adhesion on graphene-based substrates to the change in the interaction potential between water and these substrates. We employ MD simulations to probe the assumptions we formulate. Our argumentation requires that interfacial tensions, contact angles, potential interaction energies and interaction potentials of a single water molecule with the surfaces are computed. In Section 3.2, we describe the systems we studied and provide technical details on how these quantities were obtained. The results of the related calculations and the derivation of the model are

presented and discussed in Section 3.3 before the conclusions of our work are summarized in the last section. The reader mostly interested in the results of this study may read Section 3.2.1 before directly reading Section 3.3.

3.2. Methodology

3.2.1. Free Energy Calculations

We computed the interfacial tension between water and graphite. To that end, we employed the thermodynamic integration-based phantom-wall algorithm implemented in a modified version of the MD package YASP.[20] Although this algorithm has been described in details elsewhere,[20-21] we recall its main features because it is one of the key elements of the derivation of our thermodynamic model. Our computations were carried out using periodic boundary conditions in all directions of space. Therefore, graphite was modeled as a slab and water was present on both sides of it (see ref [20] for details about the implementation). According to the phantom-wall algorithm, graphite was reversibly turned into a flat repulsive surface. This transformation was realized by the action of two walls (the phantom walls) which became the repulsive surfaces mentioned above at the end of the process. The walls were initially present within the graphite slab but were far enough from water not to interact with it. They were progressively symmetrically displaced in the direction perpendicular to the interface. Thus, the interaction with the water molecules was progressively established while graphite was insensitive to them. This interaction yielded water to be lifted off from the graphite substrate. At the end of the process, the walls were displaced far enough from their initial positions so that water only interacted with them and no longer with graphite. The free energy change of the process is the work required to lift off water from graphite by the action of the walls. Note that this process was conducted at constant cross sectional area of the solid substrate, constant pressure, constant temperature and constant number of particles. Consequently, the Gibbs free energy change per unit of cross-sectional area is also the difference in interfacial tension between the initial and final systems. Note that a pressure×volume term has to be taken into account to include the possible volume change of the system in connection with the transformation mentioned above.[20] To describe the interactions between water and the repulsive walls, we employed a planar Weeks-Chandler-Andersen (WCA) potential[22] which is dependent on the water-wall distance. In this case, it was shown by Chandler and coworkers[23-24] that the related interfacial tension is the

surface tension of water γ_{lv}. Indeed, water tends to avoid the repulsive surface by forming a thin liquid-vapor interface in its vicinity. Therefore, the interfacial tension that describes such an interface is γ_{lv}. In summary, we computed the difference in interfacial tension $\Delta\gamma$ between a water-repulsive surface interface characterized by the interfacial tension γ_{lv} and the water-graphite interface characterized by the interfacial tension γ_{sl}. We also independently determined γ_{lv} by means of the so-called mechanical route.[25] Thus, γ_{sl} was finally obtained through $\gamma_{sl}= \gamma_{lv}-\Delta\gamma$. Such computations have already been carried out by one of the present authors in the context of carbon-based materials with the exception that poorly attractive phantom walls were employed.[26]

The SPC/E model of water was used[27] in combination with the interaction potential of Werder *et al.* between water and graphite.[13] According to this model, the water-carbon interaction is modeled by means of a 12-6 Lennard-Jones potential between the carbon and the oxygen atoms. The distance and energy parameters are σ=0.319 nm and ε=0.392 kJ/mol, respectively. These values warrant that the contact angle of droplets free of the effect of the line tension reproduces the macroscopic experimental value of 86° against which the intermolecular interactions was optimized.[13] No electrostatic interaction is taken into account between water and graphite. The internal dynamics of graphite was modeled through the potential of Bedrov and Smith.[28] The cross-sectional area of the system was 4.26×3.69 nm^2. The graphite slab contained seven stacked graphene sheets although water only interacted with the first two top such layers on each side of the slab due to the value of the interaction cut-off. The system contained 4158 molecules of water. The electrostatic interactions were treated by means of the reaction field method with an infinite reaction field dielectric constant. The cut-off distance for the water-water interactions was 1.5 nm, while it was 1.0 nm for the carbon-water interactions and carbon-carbon interactions. The thermostat and barostat of Berendsen *et al.*[27] were used to maintain temperature and pressure at 298 K (with a coupling constant of 0.2 ps) and 101.3 kPa (with a coupling constant of 2.0 ps), respectively. The computations consisted of equilibration runs of 250 ps followed by production runs of 500 ps. Data was extracted every 1 ps for further statistical analysis.

3.2.2. Contact Angle Calculations

The study of the contact angles of water droplets containing 4000 molecules were carried out with GROMACS.[29] We performed simulations with graphene-based systems in which the number of graphene monolayers *n* in the sample was varied between *n*=1-6. In these simulations, the carbon atoms were fixed at the crystallographic positions of the graphite lattice with a carbon-carbon distance of 0.142 nm and an interlayer distance of 0.34 nm. The SPC/E model of water was employed to describe water-water interactions. The electrostatic interactions were computed by means of the particle mesh Ewald (PME) technique.[30] The model of Jaffe *et al.*[18] was employed for the water-carbon interactions. In this model, the interactions are described identically to the model of Werder *et al.*[13] mentioned in the free energy calculations with the exception that a cut-off distance of 2.0 nm is employed. Consequently, the Lennard-Jones distance and energy parameters are σ_{CO}=0.319 nm and ε_{CO}=0.357 kJ/mol so as to reproduce the value of the macroscopic contact angle of water on graphite, too. Note that the models of Werder *et al.*[13] and the model of Jaffe *et al.*[18] yield identical results as far as the structure of water in the vicinity of graphite is concerned. In order to model the graphene system with a macroscopic contact angle of 127° (noted *n*=1* in what follows), we used a procedure similar to the one recently developed by Scocchi *et al.*[9] to obtain the values of the Lennard-Jones parameters between the oxygen and carbon atoms. In accord with this study, we found values of σ_{CO}=0.319 nm and ε_{CO}=0.205 kJ/mol. This force-field was used in combination with a cut-off of 2.0 nm. The computations were performed in the canonical ensemble by means of the Nosé-Hoover thermostat with a coupling constant of 0.2 ps.

It must be noted that we performed simulations with droplets of which the size yields a deviation from the macroscopic contact angle. Due to the effect of line-tension, the contact angle of the droplets that include 4000 water molecules on graphite has a value of 90.2±0.3° in our computations whereas the value of 86° is obtained for larger droplets free of line-tension. The values of the surface tension of water in the reaction field and the PME simulations agree within the uncertainty. At 298K, the reaction-field treatment yields a value of 59.1±1.3 mJ/m^2 whereas the PME computations lead to a value of 60.3±1.8 mJ/m^2.

3.2.3. Interaction Energies and Potentials Calculations

Films having a thickness of approximately 6 nm and containing 8000 water molecules were employed to compute the time averaged total potential interaction energy $u_{ws,n}$ of water with the systems n=1-6 and n=1* previously defined. The cross-sectional area of the systems was 6.396×6.389 nm^2. $u_{ws,n}$ was obtained following:

$$u_{ws,.n} = \frac{1}{N_t}\sum_{i=1}^{N_t}\left(\sum_{j=1}^{N_{C,n}}\sum_{k=1}^{N_O} v_{jk}(r)\right) \qquad (3\text{-}1)$$

In eq. (3-1) N_t refers to the number of independent configurations used to calculate the average, $N_{C,n}$ is the number of carbon atoms in the system with n carbon layers and N_O is the number of oxygen atoms (i.e. water molecules) in the films. v_{jk} is the inter-atomic interaction potential between the carbon and oxygen atoms at a distance r apart. The configurations of the system employed to compute $u_{ws,n}$ were obtained by means of MD simulations with GROMACS in the canonical ensemble similarly to the contact angle calculations. To that end, simulations of 10 ns were used and 5000 configurations separated by 2 ps were extracted.

We also computed the average interaction potentials V between single water molecules and the surfaces n=1-6 and n=1* by means of

$$V_n(z) = \frac{1}{D}\iint_D \sum_{j=1}^{N_{C,n}} v_j(x,y,z)dxdy \qquad (3\text{-}2)$$

Note that V only depends on the height z of the water molecules above the planar surfaces n=1-6 and n=1*. In practice, the continuous summation in eq. (3-2) is performed by discretizing the xy plane parallel to the carbon surfaces into surface elements having an area of 0.05×0.05 nm^2. A single water molecule is placed on a lattice point at a given z distance above the surface. The total interaction energy between the water molecule and graphite is computed over the domain of integration D. D is determined by the interaction cut-off used in the contact angle calculations. This operation is repeated until water has been placed on each lattice point of the unit cell of graphite. The average value of the interaction potential energies in eq. (3-2) leads to V at the given height z.

3.3. Results and Discussion

3.3.1 Enthalpy and Entropy of the Work of Adhesion

In order to show that a value of 127° of the contact angle θ of water on a graphene monolayer is inconsistent with a value of 90° on graphite, we derive a relationship between the work of adhesion W_a of water on the surfaces n=1-6 and n=1* and the interaction potential V between water and these surfaces. We start with Young's equation according to which the equilibrium contact angle θ of a macroscopic droplet placed on a flat solid substrate can be described by:[31]

$$\gamma_{lv}\cos\theta = \gamma_{sv} - \gamma_{sl} \qquad (3\text{-}3)$$

where γ_{lv}, γ_{sv} and γ_{sl} are the liquid-vapor, solid-vapor and the solid-liquid interfacial tensions, respectively. Although θ and γ_{lv} can be obtained by independent measurements, this is not the case for γ_{sv} and γ_{sl}.[32] Therefore, only the difference γ_{sv}-γ_{sl} is directly accessible from experiments. In the case of low vapor density fluids like water and poorly wettable substrates like graphene and graphite, we assume that the contribution of γ_{sv} to the contact angle is much lower than γ_{sl}. In fact, this assumption has already been quantitatively verified by molecular simulations in the case of water on graphite.[26, 33] It can also be noted that Werder *et al.*[13] showed by means of MD simulations that both flexible and rigid models of graphite yield the same contact angle of water in addition to the fact that γ_{sv} exactly cancels out in the limit of rigid substrates.[34] Under that condition, eq. (3-3) yields:

$$\Delta\gamma = \gamma_{lv} - \gamma_{sl} = \gamma_{lv}(1+\cos\theta) \qquad (3\text{-}4)$$

Eq. (3-4) can be interpreted as the result of a phantom-wall calculation as mentioned in Section 3.2.1. Indeed, Δγ is the difference in interfacial tension between a system characterized by γ_{lv} where water interacts with a purely repulsive substrate and a system with the interfacial tension γ_{sl} where water interacts with a carbon-based solid surface. The fact that the interfacial tension of the repulsive interface is γ_{lv} and that γ_{sv} is a negligible quantity yields $\Delta\gamma$ to be the work of adhesion W_a=γ_{lv}(1+cosθ) of water on the graphene-based substrates. Furthermore, the quantity $A\Delta\gamma$=A(γ_{lv} -γ_{sl}) is the difference in the excess interfacial Gibbs free energy when a surface like graphite or graphene is turned into a repulsive surface. It is equal to the Gibbs free energy change of the transformation provided that the number of water molecules and the number of particles in the substrate remain constant, and that the transformation is performed at constant temperature, constant cross-sectional area and constant pressure normal to the interfaces. The Gibbs free energy change $A\Delta\gamma$ can be written as the sum of an enthalpy contribution and an

entropy contribution: $A\Delta\gamma = \Delta H - T\Delta S$. According to eq. (3-4), there is a relationship between $\Delta\gamma$ and $\cos\theta$. Consequently, the computation of ΔH and ΔS and the study of the temperature dependence of $\Delta\gamma$ may be compared to possible experimental determinations of $\cos\theta$ at different temperatures. This is particularly important to address the reliability of the computations of $\Delta\gamma$. The temperature dependence of $A\Delta\gamma$ was obtained by means of MD through phantom-wall computations in the case of water on graphite in the temperature range 283-328K. It is shown in Figure 3.1 that there is a linear relationship between $\Delta\gamma$ and temperature in the range that was sampled. We fitted a linear equation to the simulation data and found $\Delta S/A$=0.140±0.017 mJ/m^{2}K and $\Delta H/A$=103.7±5.1 mJ/m^2. The value of $\Delta\gamma$ at each temperature has been reported in Table 3.1.

Table 3.1. Interfacial tensions and contact angles values of water on graphite depending on temperature.

Temperature	Δγ / mJ/m²	γ_{lv}	γ_{sl}	θ
283K	64.1±0.5	61.3±1.3	2.8±1.8	87.4±0.1
298K	62.0±0.5	59.1±1.3	2.9±1.8	87.2±0.1
313K	60.0±0.6	56.4±1.3	3.6±1.9	86.4±0.1
328K	57.8±0.6	53.2±1.3	4.6±1.9	85.0±0.2

ΔS is the change in entropy between the repulsive surface system and the graphite system. It is interesting to note that ΔS has a positive value. In order to understand the physical meaning of this result, we reported in Figure 3.2 the mass-density distribution of water in the direction perpendicular to the surface of graphite (black curve). This plot was obtained from the analysis of our MD simulations. Two relatively intense maxima can be observed on the plot. This is interpreted as water forming two layers on graphite, as was already obtained in previous studies.[13, 26] In contrast, the interface with the purely repulsive substrate features no layering of water (see the dashed line in Figure 3.2). This is actually a consequence of water preserving its hydrogen-bonding network by forming a thin liquid-vapor interface in the vicinity of the repulsive hydrophobic surface as was mentioned in Section 3.2.1. We can conclude that the configurations of water close to graphite are more constrained than close to the repulsive surface. This result explains why entropy is gained (ΔS>0) when water is moved from the

structured interface on graphite to the virtually unconstrained interface on the repulsive substrate. We will comment in details the origin of the positive sign of ΔH later in the text.

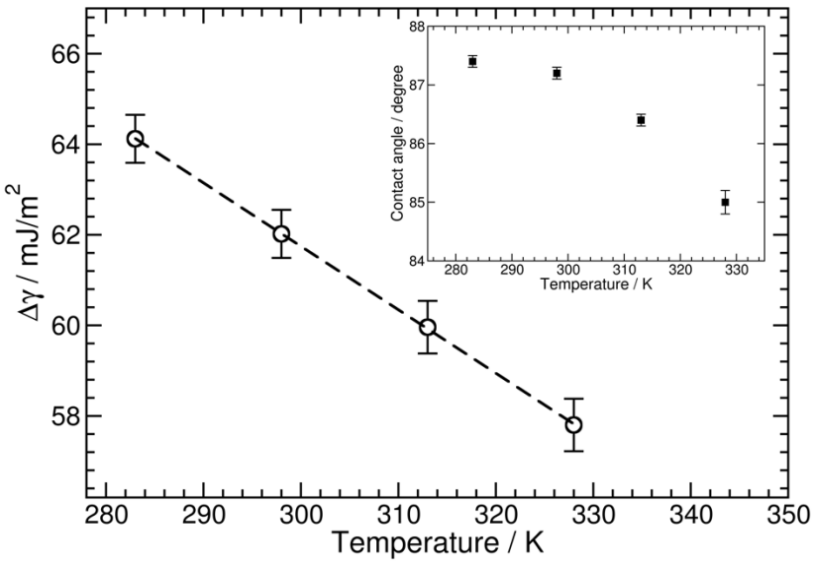

Figure 3.1. Temperature variations of Δγ. The white circles are the simulation results. The dashed line represents a linear regression to the simulations. Inset: Temperature variation of water contact angle on graphite as predicted by the MD simulations.

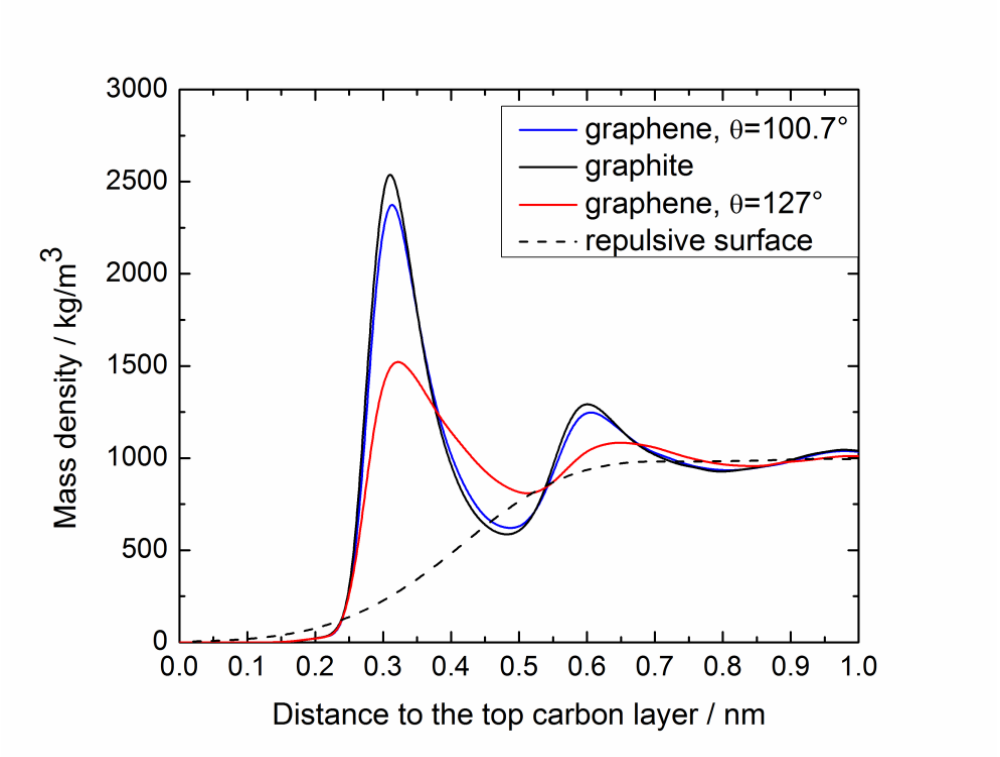

Figure 3.2. Water mass-density distribution as a function of the distance to the top layer of carbon atoms of graphite and graphene. Black curve: water-graphite. Blue curve: water-graphene with θ=100.7°. Red curve: water-graphene with θ=127°. Dashed curve: water in contact with the repulsive surface

One may wonder whether the values of ΔS and ΔH obtained in the simulations are in any manner comparable to experiments. This raises the question as to whether the model employed in the computations is able to capture the temperature dependence of the contact angle of water on graphite. Despite the apparent simplicity of the system at hand, no conclusive experiments have been reported yet. Osborne recently discussed the difficulties encountered in such an experimental study.[35] In fact, the measurements are very sensitive to the experimental conditions and it is even difficult to discriminate between both the situations where θ may increase or decrease with temperature. In this context, the test of the validity of the values of ΔS and ΔH relies on theoretical and simulation works that aim to make up for the momentary lack of experimental results. Garcia *et al.*[36] recently predicted by means of a theoretical analytical approach based on the sharp-kink approximation that the contact angle of water on graphite should decrease with temperature.[36] This trend is in line with the work carried out by Choong[33] by means of the Monte Carlo simulations scheme developed by Errington and successive coworkers[37] and the work of Dutta *et al.*[38] performed by means of MD simulations. However, these studies show that the temperature dependence of the contact angle is relatively weak below the boiling point of water. We employed our results for γ_{lv} and γ_{sl} in Table 3.1 to compute the temperature dependence of θ in the range 283-328K by means of eq. (3-1) in which we neglected γ_{sv} as stated above. The result is shown in the inset of Figure 3.1. The trend we obtained is consistent with the studies of Garcia *et al.*[36], Dutta *et al.*[38] and Choong.[33] In order to be more quantitative, we extracted the value of ΔS and ΔH per unit area from the interfacial tensions in the work of Choong at 300K and 350K and assumed linear dependence of $\Delta\gamma$ on temperature. The values we obtained are in agreement with our own result for $\Delta S/A$ (0.137 mJ/m^{2}K and 0.140±0.017 mJ/m^{2}K, respectively) and $\Delta H/A$ (99.2 mJ/m^2 and 103.7±5.1, respectively). Based on those comparisons, we are confident that our study follows the trends outlined in the earlier theoretical and simulation studies that predict that the contact angle of water on graphite is a decreasing function of temperature.

3.3.2 Work of Adhesion and Interaction Potentials

Before we proceed further with our argumentation, we should mention that the MD simulations to which we will refer in what follows deal with water droplets on graphite and different models of graphene systems as detailed in Section 3.2.2. We performed simulations of water droplets on the surfaces n=1 to n=6 and calculated the respective contact angles. The results are reported in Table 3.2 and plotted in Figure 3.3. It can be seen that the contact angle on graphite converges at n=3. A comparable behavior was recently reported both experimentally and in MD simulations.[5] It can also be observed that a value of the contact angle of 100.7° is observed on the n=1 surface (i.e. graphene) without modification of the intermolecular interaction between water and the carbon atoms. This observation contrasts with the value of 127° and is in line with the idea that the contact angle on graphite and graphene may only differ by a few degrees as was also noted by Shih *et al.*[6]

Table 3.2. Thermodynamic data for the water graphite and water graphene systems. The uncertainty on $\Delta H_{ws}/A$ is of the order of 0.1% and was omitted.

	θ	$\gamma_{lv}(1+\cos\theta)$ **(mJ/m²)**	$\frac{\Delta H_{ws}}{A}$ **(mJ/m²)**	$\frac{T\Delta S_{ws}}{\Delta H_{ws}}$	$\frac{W_{a,n}}{W_{a,n=6}}$	$\frac{\Delta H_{ws,n}}{\Delta H_{ws,n=6}}$	E_b **kJ/mol**
***n*=1**	100.7±0.4	49.1±2.2	76.9	0.36±0.02	0.82±0.01	0.85	-5.22
***n*=2**	91.3±0.3	58.9±1.9	87.9	0.33±0.01	0.98±0.01	0.97	-5.70
n=3	89.7±0.3	60.6±1.8	90.1	0.33±0.01	1.01±0.01	0.99	-5.78
***n*=4**	89.6±0.2	60.7±1.7	90.7	0.33±0.01	1.01±0.01	1.00	-5.80
***n*=5**	90.4±0.3	59.9±1.8	90.8	0.34±0.01	1.00±0.01	1.00	-5.81
***n*=6**	90.2±0.3	60.1±1.8	90.7	0.34±0.01	1	1	-5.81
n*=1	127.0±0.3	24.0±2.7	35.8	0.33±0.03	0.40±0.01	0.39	-3.00

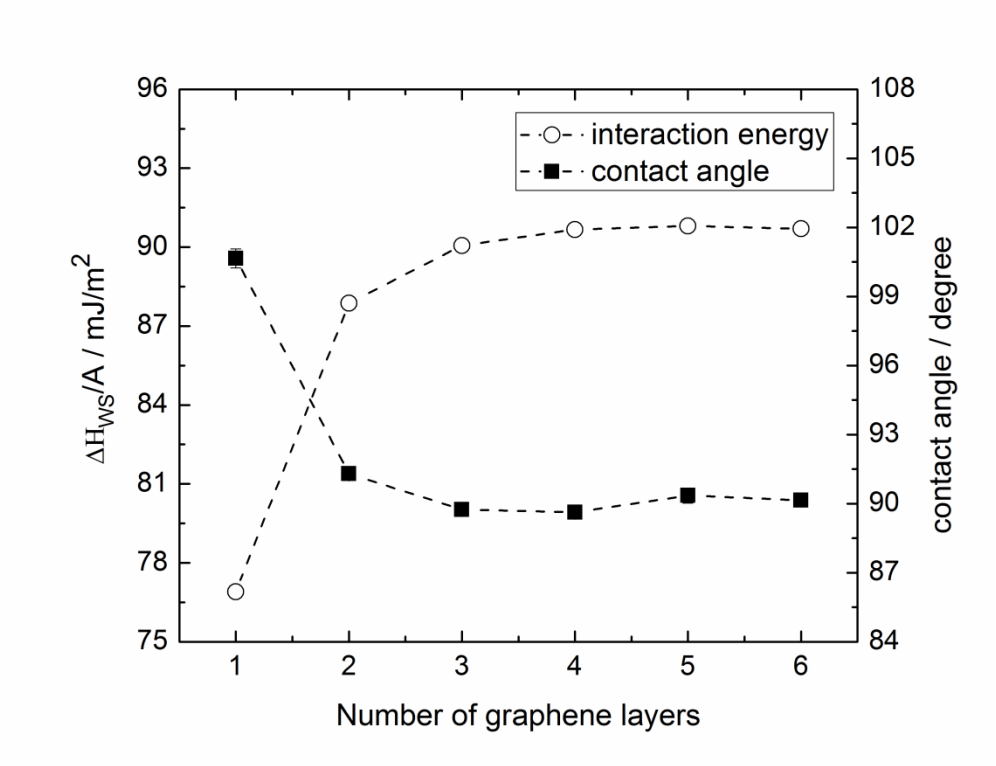

Figure 3.3. Water-substrate potential interaction energy with respect to the number of carbon layers in the substrate (black circles). Contact angle variation with respect to the number of carbon layers in the substrate (black squares). The dashed line is guide to the eye. The error bars are smaller than the symbols.

We note that the change in enthalpy ΔH defined above arises from two contributions. On the one hand, when graphite or graphene are turned into the purely repulsive surface, there is a change in the interactions between water and the actual substrate. We call ΔH_{ws} this contribution to ΔH. On the other hand, the change in the water structure in the vicinity of graphite or graphene (as is illustrated in Figure 3.2) and the repulsive substrate yields a change in the water-water interactions. Indeed, it can be observed in Figure 3.2 that graphite (n=6) and both models of graphene (n=1 and n=1*) yield water to form layers (black, blue and red curves, respectively), although the intensity of the first maximum in water mass density is lower in the case of n=1* (θ=127°) than in the case of n=1 (θ=100.7°). The effect of the change in the water structure between the carbon surfaces and the repulsive interface on the change in enthalpy is quantified by a contribution ΔH_{ww}. The enthalpy change ΔH is the sum of two contributions, $\Delta H=\Delta H_{ws}+\Delta H_{ww}$. Note that there is no change in ΔH arising from the interactions within the solid because these interactions remain unchanged in the phantom-wall calculations (see Section

3.2.1). In order to compute the enthalpy changes, we use the relationship $\Delta H=\Delta U+P\Delta V$, where U is the internal energy, P the pressure and V the volume. The water layering in the vicinity of the surfaces yields the change in PV per unit area to be of the order of 0.1 mJ/m^2 at 100 kPa, which is negligible when compared with the energies featured previously. Therefore, the change in enthalpy was obtained assuming that $\Delta H\approx\Delta U$. Moreover, since the systems have the same number of particles there is no change in the total kinetic energy and $\Delta U=\Delta u$, where u is the total interaction potential energy. In our computations, the interatomic interaction potentials are based on Lennard-Jones and Coulomb pair interactions. Therefore, u can be written as a sum of three contributions $u=u_{ww}+u_{ws}+u_{ss}$. u_{ws} is the total interaction potential energy arising from the water-substrate interactions, whereas u_{ww} is the total interaction potential energy arising from the water-water interactions and u_{ss} is the total potential interaction energy within the solid. Thus, we obtain the relationships $\Delta H_{ws}=\Delta u_{ws}$ and $\Delta H_{ww}=\Delta u_{ww}$ which show that the enthalpy changes can be directly obtained from the changes in the interaction potential energies. Note that $\Delta u_{ss}=0$ for the reason that there is no change of interactions within the substrate. Combining $\Delta H=\Delta H_{ws}+\Delta H_{ww}$ and $A\Delta\gamma=\Delta H-T\Delta S$ with eq. (3-2) yields:

$$W_a=\gamma_{lv}(1+\cos\theta)=\frac{1}{A}(\Delta H_{ws}+\Delta H_{ww}-T\Delta S) \qquad (3\text{-}5)$$

Note that eq. (3-5) arises from the equality between the work of adhesion and the free energy change $\Delta\gamma$ of turning a carbon-based surface into a repulsive wall. $\Delta\gamma$ can be interpreted as the difference in solvation free energy per unit area between two such surfaces. It was shown in the framework of the theory of solvation that the contribution of the solvent-solvent interaction to the free energy of solvation is strictly enthalpy-entropy compensating.[39,40] In other words, there is no contribution of these interactions to the solvation free energy. This result yields the enthalpy term ΔH_{ww} in eq. (3-5) to be exactly compensated by an entropy term in $-T\Delta S$. Thus, ΔH_{ww}-$T\Delta S$ simplifies to -$T\Delta S_{ws}$, where ΔS_{ws} is the entropy change in connection with the interaction between water and both the carbon-based substrates and the repulsive surface. Eq. (3-5) takes the following form:

$$W_a=\frac{1}{A}(\Delta H_{ws}-T\Delta S_{ws}) \qquad (3\text{-}6)$$

Another result of the solvation theory is that the entropy contribution to the free energy of solvation arises from the fluctuations in the solute-solvent interactions.[41,42] Therefore, the work of adhesion can be understood as arising from the water-substrate interaction strength ($\Delta H_{ws}/A$) and the fluctuations of these interactions (-$T\Delta S_{ws}/A$). This interpretation is inline with the work

of Garde and coworkers[43] who showed that the fluctuations in water density in the vicinity of solid-substrates play a key role in determining the hydrophilic/hydrophobic nature of substrates. We computed the value of ΔH_{ws} in eq. (3-6) as the total water-substrate interaction potential energy $-u_{ws}$ by means of MD simulations for all the values of n (see Section 3.2.3). It must be recalled that water tends to minimize the interaction with the repulsive surface. Consequently, we observed that the potential interaction energy between water and the repulsive substrates is several orders of magnitude smaller than in the case of the carbon-based surfaces and could be neglected. We plotted in Figure 3.3 the variations of $\Delta H_{ws}/A$ (i.e. $-u_{ws,n}/A$) as a function of the number of carbon layers. It can be observed that this quantity is independent of the number of layers if n>2. Such a behavior was also observed for the contact angle (Figure 3.3). We assumed that the relationship in eq. (3-5) holds true for all the systems studied here. The values of γ_{lv}, θ and $\Delta H_{ws}/A$ were employed to obtain $-T\Delta S_{ws}$. It can be seen in Table 3.2 that the quantity $T\Delta S_{ws}$ represents approximately 33% of ΔH_{ws} in all cases. Note that this result was obtained using the value of γ_{lv} of the model employed in our computations (60.3 mJ/m^2). Values of approximately 17% are obtained if the experimental value of γ_{lv} (72 mJ/m^2) is considered. This observation suggests that $\Delta H_{ws}/A$ is the main contribution to the work of adhesion W_a. However, the entropy contribution must be taken into account to obtain a quantitative description, as mentioned above. The roughly constant ratio between $T\Delta S_{ws}$ and ΔH_{ws} leads to the following relationship:

$$\frac{W_{a,n}}{W_{a,n=6}} \approx \frac{\Delta H_{ws,n}}{\Delta H_{ws,n=6}} \qquad (3\text{-}6)$$

It can be observed in Table 3.2 that very good agreement exists between both the independent determinations of the ratio between the works of adhesion and the right-hand side of eq. (3-6). Eq. (3-6) shows that there is a direct relationship between the change in the work of adhesion and the change in the water substrate interaction potential energy. $\Delta H_{ws}/A$ can also be defined following:

$$\frac{\Delta H_{ws}}{A} = \int_0^\infty V(z)\rho(z)dz \qquad (3\text{-}7)$$

where $V(z)$ is the total interaction potential between a given surface and a water molecule located at a distance z from this surface (see Section 3.2.3) and $\rho(z)$ is the water number-density distribution perpendicular to the surface. We have reported in Figure 3.4 the computed variations of V(z) for water interacting with graphite and graphene (both for θ=100.7° and

127°). We quantitatively verified that these variations could be described by the following analytical form $V(z)=4\pi\varepsilon d(\sigma^{12}/5z^{10}-\sigma^{6}/2z^{4})$,[44] where σ and ε are the Lennard-Jones distance and energy parameters of the non-bonded interactions between the carbon atoms and the water molecules, while d is the surface density of carbon atoms in a graphene sheet (d=38.1 nm^{-2}). It can be noted that analytical form is short-ranged when compared to the form derived from the approach of Hamaker for other materials such as metals where the dispersion part of the potential is proportional to $1/z^3$.[45] In the case of graphite (n=6), the variations of V can be fitted to $V(z)=A/z^{10}-B/z^{4}-C/z^{3}$ where the $1/z^3$ term takes into account the carbon layers that are added to the top layer in agreement with the Steele potential.[46]

Recent quantum calculations reported results for the equilibrium distance and binding or adsorption energy of water molecules on graphene and graphite.[10, 47] These computations were performed with a single water molecule and therefore do not include the collective effects that arise from a computation including several molecules. In single molecule calculations, the most stable configuration for water is obtained when the two bonds are oriented towards the carbon surfaces.[10] Such a configuration may not be realistic in a system including several water molecules as it would imply that two hydrogen bonds per water molecule are sacrificed. Instead, it was shown that water tends to minimize the number of such sacrificed hydrogen bonds in the vicinity of graphite[26] and other substrate that do not form hydrogen bonds with water. The empirical force-fields used in our classical MD simulations implicitly include such many-particles effects because the water–carbon Lennard-Jones interaction parameters were optimized to reproduce the contact angles of water, i.e. a collective property. Nevertheless, the single molecule quantum computations yield a good indication of how equilibrium distances and binding/adsorption energies of water vary between graphite and graphene. The interaction potential V related to the intermolecular interactions in our MD simulations have an equilibrium distance of 0.319 nm for graphene (both for θ=100.7° and 127°) and 0.3175 nm for graphite (see Figure 3.4). These values compare well with recent single molecule quantum calculations (0.32-0.34 nm).[10, 47] The minimum of the interaction potential V is the binding energy E_b of water on the related surface. We reported in Table 3.2 this energy for the systems n=1-6 and n=1*. In the case of graphite, quantum calculations studies led to average values of the binding energy of -13.1 kJ/mol[10] and -15 kJ/mol,[47] while average values of -10.4 kJ/mol[10] and -13.3 kJ/mol[47] were obtained for graphene. These values are overestimates of the results obtained by means of empirical force-fields. This observation may be explained by the fact that these results were

obtained by means of computations carried out on a single water molecule, as noted above. Here again, precise experimental data is lacking to perform a complete comparison.

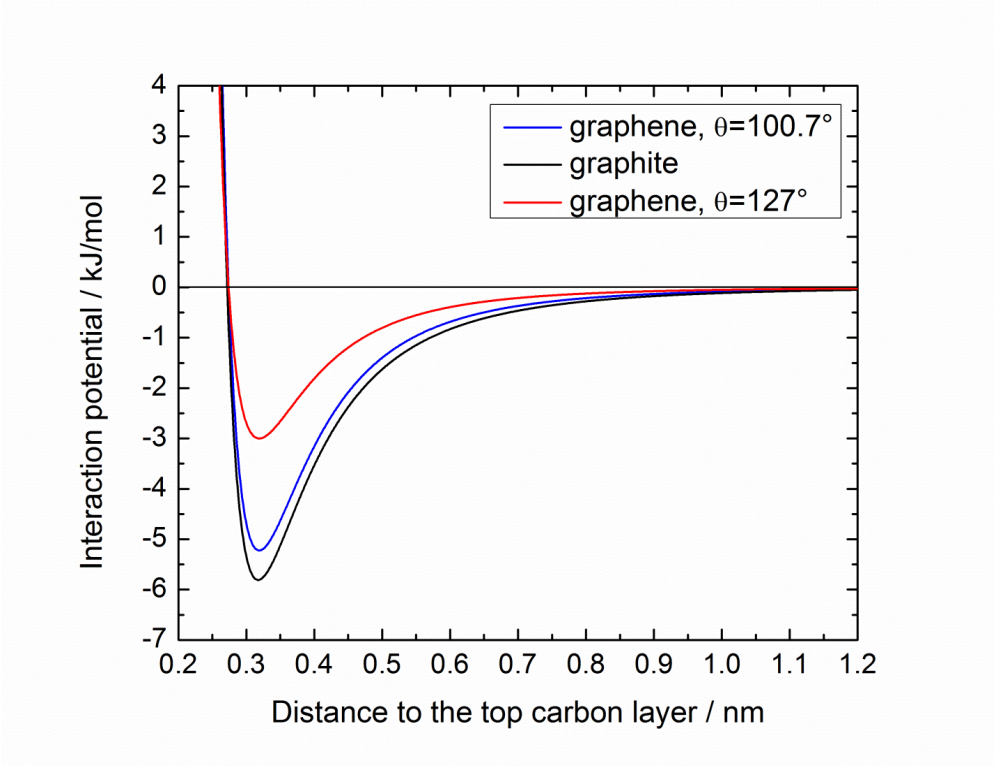

Figure 3.4. Potential interaction energy for a single water molecule in interaction with graphite and graphene as a function of the distance to the surface. Black curve: Graphene (θ=100.7°), Red curve: Graphite, Blue curve (θ=127°).

It can be noted that the ratio $E_{b,n=1}/E_{b,n=6}$=0.90, while $E_{b,n=1^*}/E_{b,n=6}$=0.52. Interestingly the corresponding ratios between the binding energy on graphene and on graphite obtained in the quantum computations mentioned above are in the range 0.8-0.9, which is consistent with the results obtained by means of the force-field of Jaffe *et al.* that yields θ=100.7° on graphene (n=1) and θ≈90.2° on graphite (n>2). Furthermore, it has been suggested in experiments that only a very few layers of carbon atoms are necessary to obtain the contact angle of water on graphite.[4-5] Our study shows that the main part of the interaction between water and graphite is achieved with two layers of carbon atoms. This is in clear contrast with $E_{b,n=1^*}/E_{b,n=6}$≈0.52. Indeed, this value suggests that if graphite were built by stacking layers of carbon atoms that lead to θ=127°, the first such layer would contribute to only approximately half of the interaction between a water molecule and graphite. In other words, both the first and second layer of carbon atoms

would approximately have the same contribution to the interaction potential between water and graphite. This is in contradiction with the short range nature of the interaction energy between a water molecule and graphene as is illustrated in Figure 3.4. Indeed, it can be seen that V vanishes at a distance shorter than 1 nm from the surfaces. An interpretation in terms of the work of adhesion of water can also be given. If we assume that two to three graphene layers are sufficient to establish a value of approximately 90° on graphite, a value of 127° on a graphene monolayer implies that the work of adhesion of water on this monolayer represents only 40% of the work of adhesion of water on graphite (see Table 3.2). This is again in contradiction with the fact that the interaction between water and graphite is mainly established through the first two carbon layers. Indeed, the fact that two layers are sufficient to establish the graphite-water interaction yields the conclusion that the work of adhesion of water on a graphene monolayer should be significantly larger than 50% of the work of adhesion of water on graphite. We conclude that the value of the contact angle for $n=1^*$, i.e. $\theta=127°$ is an overestimate of the actual value. In contrast, the smooth transition in contact angle from graphite to graphene generated by the model yielding $\theta=100.7°$ and the agreement on the ratio between binding energies obtained in quantum calculations suggest that this value of the contact angle should be considered as a more realistic experimental expectation. Assuming that the ratio between the work of adhesion on graphene and graphite is of the order of 0.82-0.85 (see Table 3.2), we anticipate that the contact angle of water on a graphene monolayer is of the order of 95-100°.

3.4. Conclusion

We have developed a thermodynamic model supported by MD simulations to address the unresolved question of the contact angle of water on a graphene monolayer. In particular, we have addressed the question of whether the value of 127° recently suggested in the literature is compatible with the accepted value of approximately 90-95° on graphite. We have established a connection between the change in the work of adhesion of water on both these materials and the change in the water-surface interaction potential. We have shown that a change in θ from 90° on graphite to 127° on graphene yields a change in the work of adhesion which is incompatible with the short-range nature of the interaction potentials between water and these carbon materials. We also have shown that the water-substrate interaction energy is the main contribution to the work of adhesion of water. However, the entropy contribution cannot be neglected to obtain a

quantitative description of the work of adhesion. We interpret the work of adhesion as arising from the strength of the water-substrate interaction and from the fluctuations of this interaction. Further work is required to assess whether this interpretation is general or if it is restricted to the present systems. Finally, we anticipate that the contact angle of water on a monolayer of graphene is of the order of 95-100°. The same conclusion was very recently reached by Shih *et al*.[6] by means of a theory and simulations supported by experimental evidence.

3.5. References

1. Hasan, T.; Scardaci, V.; Tan, P. H.; Bonaccorso, F.; Rozhin, A. G.; Sun, Z.; Ferrari, A. C., In *Molecular- and Nano-Tubes*, Hayden, O.; Nielsch, K., Eds. Springer Science and Business Media: New York, 2011; pp 279-354.
2. Cohen-Tanugi, D.; Grossman, J. C., Water Desalination Across Nanoporous Graphene. *Nano Lett.* **2012,** *12*, 3602-3608.
3. Kim, H.; Abdala, A. A.; Macosko, C. W., Graphene/polymer nanocomposites. *Macromolecules* **2010,** *43*, 6515-6530.
4. Shin, Y. J.; Wang, Y. Y.; Huang, H.; Kalon, G.; Wee, A. T. S.; Shen, Z. X.; Bhatia, C. S.; Yang, H., Surface-Energy Engineering of Graphene. *Langmuir* **2010,** *26*, 3798-3802.
5. Rafiee, J.; Mi, X.; Gullapalli, H.; Thomas, A. V.; Yavari, F.; Shi, Y.; Ajayan, P. M.; Koratkar, N. A., Wetting Transparency of Graphene. *Nature Materials* **2012,** *11*, 217-222.
6. Shih, C. J.; Wang, Q. H.; Lin, S.; Park, K. C.; Jin, Z.; Strano, M. S.; Blankschtein, D., Breakdown in the Wetting Transparency of Graphene. *Phys. Rev. Lett.* **2012,** *109*, 176101.
7. Wang, S. R.; Zhang, Y.; Abidi, N.; Cabrales, L., Wettability and Surface Free Energy of Graphene Films. *Langmuir* **2009,** *25*, 11078-11081.
8. Nishino, T.; Meguro, M.; Nakamae, K.; Matsushita, M.; Ueda, Y., The Lowest Surface Free Energy Based on -CF3 Alignment. *Langmuir* **1999,** *15*, 4321-4323.
9. Scocchi, G.; Sergi, D.; D'Angelo, C.; Ortona, A., Wetting and Contact-Line Effects for Spherical and Cylindrical Droplets on Graphene Layers: A Comparative Molecular-Dynamics Investigation. *Phys. Rev. E* **2011,** *84*, 061602-8.
10. Ambrosetti, A.; Silvestrelli, P. L., Adsorption of Rare-Gas Atoms and Water on Graphite and Graphene by van der Waals-Corrected Density Functional Theory. *J. Phys. Chem. C* **2011,** *115*, 3695-3702.
11. Li, H.; Zeng, X. C., Wetting and Interfacial Properties of Water Nanodroplets in Contact with Graphene and Monolayer Boron-Nitride Sheets. *ACS Nano* **2012,** *6*, 2401-2409.
12. Amirfazli, A.; Neumann, A. W., Status of the Three-Phase Line Tension: a Review. *Adv. Colloid Interface Sci.* **2004,** *110*, 121-41.
13. Werder, T.; Walther, J. H.; Jaffe, R. L.; Halicioglu, T.; Koumoutsakos, P., On the Water-Carbon Interaction for Use in Molecular Dynamics Simulations of Graphite and Carbon Nanotubes. *J. Phys. Chem. B* **2003,** *107*, 1345-1352.
14. Weijs, J. H.; Marchand, A.; Andreotti, B.; Lohse, D.; Snoeijer, J. H., Origin of Line Tension for a Lennard-Jones Nanodroplet. *Phys. Fluids* **2011,** *23*, 022001-11.
15. Binder, K.; Block, B.; Das, S. K.; Virnau, P.; Winter, D., Monte Carlo Methods for Estimating Interfacial Free Energies and Line Tensions. *J. Stat. Phys.* **2011,** *144*, 690.
16. Ritchie, J. A.; Yazdi, J. S.; Bratko, D.; Luzar, A., Metastable Sessile Nanodroplets on Nanopatterned Surfaces. *J. Phys. Chem. C* **2012,** *116*, 8634–8641.
17. Cao, P. X., K.; Varghese, J.O.;Heath, J.R., The Microscopic Structure of Adsorbed Water on Hydrophobic Surfaces under Ambient Conditions5586. *Nano Lett.* **2011,** *11*, 5581-5586.
18. Jaffe, R. L.; Gonnet, P.; Werder, T.; Walther, J. H.; Koumoutsakos, P., Water–Carbon Interactions 2: Calibration of Potentials using Contact Angle Data for Different Interaction Models. *Mol. Simul.* **2003,** *30*, 205-216.
19. Alexiadis, A.; Kassinos, S., Molecular Simulation of Water in Carbon Nanotubes. *Chem. Rev.* **2008,** *108*, 5014-5034.

20. Leroy, F.; Müller-Plathe, F., Interfacial Excess Free Energies of Solid-Liquid Interfaces by Molecular Dynamics Simulation and Thermodynamic Integration. *Macromol. Rapid Commun.* **2009,** *30*, 864-70.
21. Leroy, F.; Müller-Plathe, F., Solid-Liquid Surface Free Energy of Lennard-Jones Liquid on Smooth and Rough Surfaces computed by Molecular Dynamics using the Phantom-Wall Method. *J. Chem. Phys.* **2010,** *133*, 044101-11.
22. Weeks, J. D.; Chandler, D.; Andersen, H. C., Role of repulsive forces in forming the equilibrium structure of simple liquids. *J. Chem. Phys.* **1971,** *54*, 5237-5247.
23. Huang, H. M.; Geissler, P. L.; Chandler, D., Scaling of Hydrophobic Solvation Free Energies. *J. Phys. Chem. B.* **2001,** *105*, 6704-6709.
24. Chandler, D., Insight Review: Interfaces and the Driving Force of Hydrophobic Assembly. *Nature* **2005,** *437*, 640-647.
25. Vega, C.; Miguel, E. d., Surface Tension of the Most Popular Models of Water by using the Test-Area Simulation Method. *J. Chem. Phys* **2007,** *126*, 154707-10.
26. Leroy, F.; Müller-Plathe, F., Rationalization of the Behavior of Solid-Liquid Surface Free Energy of Water in Cassie and Wenzel Wetting States on Rugged Solid Surfaces at the Nanometer Scale. *Langmuir* **2011,** *27*, 637-645.
27. Berendsen, H. J. C.; Grigera, J. R.; Straatsma, T. P., The Missing Term in Effective Pair Potentials. *J. Phys. Chem.* **1987,** *91*, 6269-6271.
28. Bedrov, D.; Smith, G. D., Molecular Dynamics Simulation Study of the Structure of Poly(ethylene oxide) Brushes on Nonpolar Surfaces in Aqueous Solution. *Langmuir* **2006,** *22*, 6189-6194.
29. Hess, B.; Kutzner, C.; Spoel, D. V. D.; Lindahl, E., GROMACS 4: Algorithms for Highly Efficient, Load-Balanced, and Scalable Molecular Simulation. *J. Chem. Theory Comput.* **2008,** *4*, 435-447.
30. Essmann, U.; Perera, L.; Berkowitz, M. L.; Darden, T.; Lee, H.; Pedersen, L. G., A Smooth Particle Mesh Ewald Method. *J. Chem. Phys.* **1995,** *103*, 8577-8593.
31. Young, T., An Essay on the Cohesion of Fluids. *Phil. Trans. R. Soc. Lond.* **1805,** *95*, 65-87.
32. Marmur, A., Soft contact: measurement and interpretation of contact angles. *Soft Matter* **2006,** *2*, 12-17.
33. Choong, W. K. The Determination of Contact Angle of Water on Graphite Surface: Using Grand-Canonical Transition Matrix Monte Carlo. The State University of New York at Buffalo, September 2007.
34. Machlin, E. S., On Interfacial Tension at a Rigid Apolar Wall-Water Interface. *Langmuir* **2012,** *28*, 16729.
35. Osborne, K. L. Temperature-Dependence of the Contact Angle of Water on Graphite, Silicon, and Gold. Worcester Polytechnic Institute, April 2009.
36. Garcia, R.; Osborne, K.; Subashi, E., Validity of the "Sharp-Kink Approximation" for Water and Other Fluids. *J. Phys. Chem. B* **2008,** *112*, 8114-8119.
37. Grzelak, E. M.; Errington, J. R., Computation of Interfacial Properties via Grand Canonical Transition Matrix Monte Carlo Simulation. *J. Chem. Phys.* **2008,** *128*, 014710-10.
38. Dutta, R. C.; Khan, S.; Singh, J. K., Wetting transition of Water on Graphite and Boron-Nitride Surfaces: A Molecular Dynamics Study. *Fluid Phase Equilibria* **2011,** *302*, 310-315.
39. Ben-Naim, A., A simple model for demonstrating the relation between solubility, hydrophobic interaction, and structural changes in the solvent. *J. Phys. Chem.* **1978,** *82*, 874–885.
40. Yu, H. A.; Karplus, M., A thermodynamic analysis of solvation. *J. Chem. Phys.* **1988,** *89*, 2366.

41. Schravendijk, P.;van der Vegt, N. F. A., From hydrophobic to hydrophilic solvation: an application to hydration of benzene. *J. Chem. Theory Comput.* **2005,** *1*, 643-652.
42. van der Vegt, N. F. A.; Lee, M.E.; Trzesniak, D.; Gunsteren, W. F. V., Enthalpy–Entropy Compensation in the Effects of Urea on Hydrophobic Interactions. *J. Phys. Chem. B* **2006,** *110*, 12852-12855.
43. Godawat, R.; Jamadagni, S. N.; Garde, S., Characterizing hydrophobicity of interfaces using cavity formation, solute binding, and water correlations. *Proc. Natl. Acad. Sci.* **2009,** *106*, 15119 - 15124.
44. Daoulas, K. C.; Harmandaris, V. A.; Mavrantzas, V. G., Detailed Atomistic Simulation of a Polymer Melt/Solid Interface: Structure, Density, and Conformation of a Thin Film of Polyethylene Melt Adsorbed on Graphite. *Macromolecules* **2008,** *38*, 5780-5795.
45. Butt, H.-J.; Kappl, M., *Surface and Interfacial Forces*. John Wiley and Sons: 2010.
46. Gatica, S. M.; Johnson, J. K.; Zhao, X. C.; Cole, M. W., Wetting transition of water on graphite and other surfaces. *J. Chem. Phys. B* **2004,** *108*, 11704.
47. Rubes, M. N., P.; Vondrasek, J.; Bludsky, O. , Structure and Stability of the Water–Graphite Complexes. *J. Phys. Chem. C* **2009,** *113*, 8412–8419.

4. Interfacial entropy of water on rigid hydrophobic surfaces

4.1. Introduction

When a water droplet is put in contact with a rigid surface, one key contribution to the system's interfacial thermodynamics is the loss of entropy of the interfacial water molecules. While the molecules gain energy due to the attractive interactions with the surface, they lose entropy because the same attractions tend to reduce their configuration degrees of freedom. We have recently shown in the case of graphene and graphite that this entropy contribution is not negligible.[1] Mean-field descriptions of the work of adhesion, i.e. the work required to transform a solid-liquid interface into a solid-vapor interface and a liquid-vapor interface, only consider the contribution of the solid-liquid interaction energy and neglect the contribution of the interfacial entropy.[2-5] In these approaches, the so-called sharp-kink approximation (SKA) is employed. The SKA assumes that the thickness of the solid-liquid interface is zero and density of the liquid changes from zero to its bulk value at a specific distance from the surface.[6-9] Alternatively to the SKA, the liquid particles may be assumed to be spatially distributed following a Boltzmann distribution to account for the water layer-structure in the vicinity of hydrophilic to moderately hydrophobic surfaces.[4] However, such an approach does not explicitly take entropy into account either. In the present work, we show that the interfacial entropy can be estimated from the knowledge of the interaction potential between water and hydrophobic surfaces. To that end, a simple theoretical model is developed to calculate the entropy change of water on a rigid hydrophobic solid surface, relative to water at the liquid-vapor interface. It has been recognized that the interface hydrophobicity has a weak correlation with water density next to the interface while the water density fluctuations provide a clear picture of hydrophobicity.[10-12] Simulation results show that at the hydrophobic interfaces where there is a week solid-liquid interactions the density fluctuation is high and gradually decreases with making the solid-liquid interaction stronger and making the surface more hydrophilic.[10-12] Weak water-substrate interactions hence promote enhanced molecular scale flexibility or “softness” of interfacial water with correspondingly larger entropy, while strong water-substrate interactions promote larger rigidity of interfacial water and reduced entropy. Water’s interfacial entropy contribution to macroscopic wettability can in principle be obtained from computer simulations by considering the energy fluctuations of an ensemble of fluid molecules in the external attractive tail of the

liquid-solid dispersion potential, but is treated in this work at single particle level in order to arrive at an analytically simple model. The resulting single particle model is solved analytically and assumes that fluctuations of interaction energies of individual water molecules with the surface are uncorrelated. This assumption reduces the many-body problem to a simple calculation of the excess entropy of a single water molecule in a box with a linear dimension determined by the range of the external potential. It will be shown that the corresponding estimates of the interfacial entropy of water on graphene, graphite and diamond are in a good agreement with the exact values calculated by molecular dynamics (MD) simulation. Our results further show that the SKA induces an error in estimating the interaction energy that is compensated by the error introduced by not considering the entropy.

4.2. Methodology

4.2.1. Models and Simulation Details

The SPC/E water model[13] is used, where the O-H bond length and H-H distance are constrained to 0.1 and 0.1633 nm, respectively, using the SETTLE[14] algorithm within GROMACS.[15] The partial charges on the oxygen and the hydrogen atoms of water are −0.8476e and +0.4238e, respectively, and the oxygen-oxygen Lennard-Jones interaction has the following parameters: ε_{OO}=0.6502 kJ/mol and σ_{OO}=0.3166 nm. The electrostatic interactions are computed by means of the particle mesh Ewald (PME) technique.[16] Two graphene models with the macroscopic contact angles of 96° (model GM1) and 127° (model GM2) and the corresponding Lennard-Jones parameters of ε_{CO}=0.357 kJ/mol (GM1) and 0.205 kJ/mol (GM2) are used. The value of σ_{CO}=0.319 nm is the same for both cases. In the case of graphite, the model of Werder et al.[17] is used where graphite consists of two graphene layers. The carbon atoms are fixed at the crystallographic positions of the graphite lattice with a carbon-carbon distance of 0.142 nm and an interlayer distance of 0.34 nm. For the graphene models, the cutoff distance for the interactions is set to 2 nm.

A slab of water having a thickness of approximately 6 nm and containing 8000 water molecules has been simulated in order to compute the time averaged total solid-liquid interaction energy U_{ws} for graphene and graphite. The dimensions of the simulation box are 6.396 nm × 6.39 nm × 24.0 nm. The interaction energies are obtained by means of MD simulations in the canonical ensemble (T=300 K) by means of the Nosé-Hoover thermostat[18-19] with a coupling constant of

0.2 ps. Simulations of 10 ns are used and 5000 configurations separated by 2 ps are extracted. The cutoff for the water-graphite model is 1.0 nm.

The range of interaction parameter ε_{CO} investigated in the case of graphite is the same as Werder's work,[17] where ε_{CO} changes between 0.0940 and 0.6270 kJ/mol with a rise of 0.0627 kJ/mol. The value of σ_{CO}=0.319 nm is fixed for all the cases. To measure the macroscopic contact angle of water at different values of ε_{CO} a cylindrical droplet consist of 4000 water molecules is placed on the surface. By applying the periodic boundary condition in y-direction the droplet will have a infinite length in this direction. The dimensions of the simulation box are 39.35 nm × 2.13 nm × 20.0 nm. The simulation of the droplet is run in the NVT ensemble at 300 K for 3 ns to obtain a relaxed water droplet on the substrate, and then the sample evolves for 2 ns for data collection. The droplet profile is then calculate in the x-z plane and by fitting a circle to the profile, the contact angle is calculated.[20] It has been shown recently that the contact angle of a drop of 4000 water molecules in the described conformation is not system-size dependent.[20]

4.2.2. Water-Surface Interaction Potential

The single-particle entropy, discussed later on in Section 3.3.3, requires the knowledge of the z-dependent external potential describing the single molecule (water) – surface interaction. The external potential in case of a graphene layer ($V_g(z)$) is calculated as following:

$$V_g(z) = d\iint_D u_{water-carbon}(r)dxdy = 4\pi\varepsilon_{CO}d\left(\frac{\sigma_{CO}^{12}}{5z^{10}} - \frac{\sigma_{CO}^{6}}{2z^{4}}\right) - 4\pi\varepsilon_{CO}d\left(\frac{\sigma_{CO}^{12}}{5r_C^{10}} - \frac{\sigma_{CO}^{6}}{2r_C^{4}}\right) \qquad (4\text{-}1)$$

where d is the number density of carbon atoms in graphene (38.1 nm^{-2}), $u_{water\text{-}carbon}(r)$ is the Lennard-Jones interaction between an oxygen of water and a carbon atom, D is the part of the graphene surface within the range of the interaction cutoff (r_c). It should be mentioned that we are using here the SPC/E water model in which there is no interaction between the hydrogens of water and the carbons of the surface.

For graphite with N graphene layers the interaction potential of a water molecule with the surface ($V_G(z)$) can be derived from the interaction energy for a single graphene layer (eq. (4-1)):

$$V_G(z) = \sum_i V_g(z_i) = 4\pi\varepsilon_{CO}d\sum_{i=0}^{N-1}\left(\frac{\sigma_{CO}^{12}}{5(z+i\cdot h_0)^{10}} - \frac{\sigma_{CO}^{6}}{2(z+i\cdot h_0)^{4}}\right) - 4N\pi\varepsilon_{CO}d\left(\frac{\sigma_{CO}^{12}}{5r_C^{10}} - \frac{\sigma_{CO}^{6}}{2r_C^{4}}\right) \qquad (4\text{-}2)$$

where h_0 is the interlayer distance of graphite (0.34 nm). For our calculations, we used two graphene layers as graphite.[17] The same approach as eq. (4-1) is used to calculate the interaction potential of a single water molecule with diamond.[1] The simulation details and the structure of

diamond was taken from Ref. 3, where the oxygen-carbon interaction parameters are chosen to be ε_{CO}=0.337 kJ/mol and σ_{CO}=0.42 nm.

4.3. Theory and Results

4.3.1. Interfacial Thermodynamics

We start with Young's equation for the equilibrium contact angle θ of a macroscopic droplet placed on a flat solid substrate:

$$\gamma_{lv}\cos\theta = \gamma_{sv} - \gamma_{sl} \qquad (4\text{-}3)$$

In eq. (4-3) γ_{lv}, γ_{sv} and γ_{sl} are the liquid-vapor, solid-vapor and the solid-liquid interfacial tensions, respectively. The work of adhesion (W_a) for low vapor density fluids like water and poorly wettable substrates like graphene and graphite is equal to the difference in the liquid-vapor and the solid-liquid interfacial tensions due to the negligible contribution of γ_{sv}. Using eq. (4-3) we obtain

$$W_a = \Delta\gamma = \gamma_{lv} - \gamma_{sl} = \gamma_{lv}(1+\cos\theta) \qquad (4\text{-}4)$$

We now consider a thermodynamic process where an attractive surface like graphite is turned into a purely repulsive surface (being modelled with a WCA potential[21-22]), provided that the number of water molecules, the number of particles in the substrate, the temperature T, the cross-sectional area A and the pressure normal to the interfaces are maintained constant. This thermodynamic process has extensively been discussed in our previous contribution.[1] It is important to note that the repulsive nature of the final surface plays a key role. Indeed, it was shown that the interfacial tension of the corresponding water-substrate interface is the liquid-vapor interfacial tension, owing to the fact that water tends to form a liquid-vapor like interface in the vicinity of such a surface.[23-24] Therefore, the free energy change of the thermodynamic process of turning an attractive surface in a repulsive wall is $A\Delta\gamma$. This quantity can be written as the sum of an enthalpy contribution (ΔH) and an entropy contribution ($-T\Delta S$), i.e. $A\Delta\gamma=\Delta H-T\Delta S$.[1] The entropy contribution is ignored in mean-field models, which furthermore consider only the water-substrate potential energy contribution to ΔH which we shall refer to as ΔU_{WS} in the text below.[25] An additional contribution arising from the difference between the internal energies of water at the solid and vapor interfaces appears in ΔH but is exactly enthalpy-entropy compensating in the work of adhesion as will be discussed below. This additional contribution results from differences in water structure at the two interfaces and the corresponding

differences in water-water interactions. Note that there is no contribution in ΔH and ΔS arising from the atoms within the solid because the structure and internal interatomic interactions of the solid remain unchanged upon the transformation from the rigid attractive to the rigid repulsive wall.[1]

4.3.2. Thermodynamic Perturbation Theory

The quantity $A\Delta\gamma$ can thus be understood as the change in Gibbs energy of transforming an attractive surface like graphite into a purely repulsive surface. In other words, $A\Delta\gamma$ (which is proportional to the work of adhesion) represents the Gibbs energy of *desolvating* the attractive tail of the liquid-solid dispersion potential. Such potentials for two models of graphene and diamond are shown in Figure 4.1.

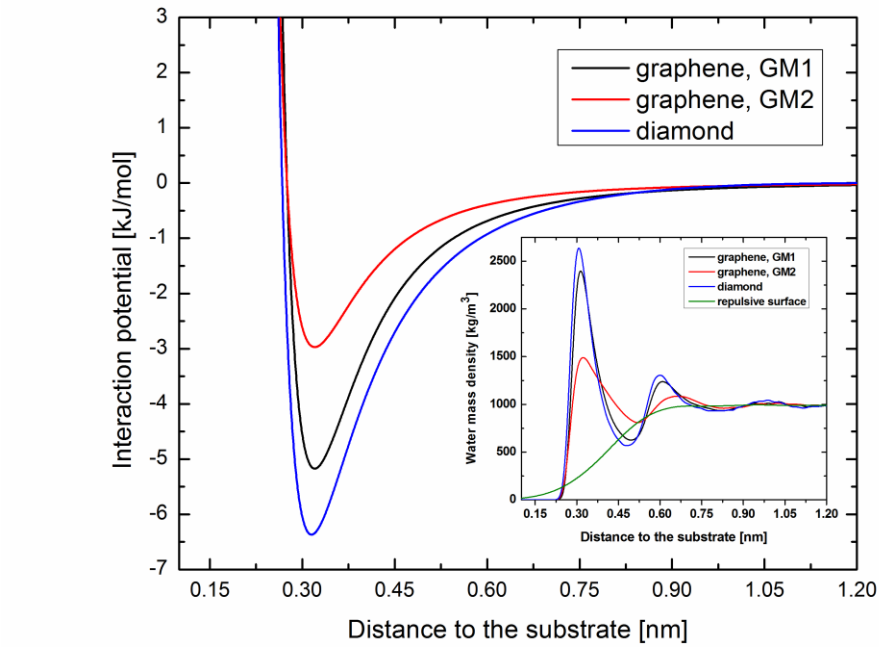

Figure 4.1. Potential energy of interaction for a single water molecule on graphene (described with models GM1 and GM2) and diamond as a function of the distance to the surface, where the macroscopic contact angle of water are 96° (GM1), 127° (GM2) and 100.7° respectively. The inset shows the corresponding water mass density distribution (300 K).

In that desolvation process, the internal energy of the liquid phase changes due to notable differences in water structures at the attractive and repulsive surfaces (see inset in Figure 4.1) and corresponding changes in water-water interactions. However, these changes are exactly

enthalpy-entropy compensating and do not feature in the work of adhesion as can be seen from a statistical mechanics analysis (see Ref. 1 and references therein). This point will be discussed later in the text. Free energy perturbation (FEP) theory[26] provides an expression for the Gibbs energy of desolvating the attractive tail

$$W_a = -\frac{\beta^{-1}}{A}\ln\left\langle \exp\left[-\beta(V_R - V_A)\right]\right\rangle_A \tag{4-5}$$

where $\beta^{-1} = k_B T$ with k_B the Boltzmann constant and T the absolute temperature, V_R denotes the potential energy of interaction of the liquid with the repulsive (WCA) surface, V_A denotes the potential energy of interaction of the liquid with the attractive surface and $\langle\cdots\rangle_A$ denotes an average over the configurational distribution of the liquid molecules in contact with the attractive surface at temperature T. Since $V_A - V_R$ represents the attractive dispersion interaction for liquid configurations in contact with the attractive surface we can write

$$\begin{aligned} W_a &= -\frac{\beta^{-1}}{A}\ln\left\langle \exp\left[\beta V_{disp}\right]\right\rangle_A \\ &= \frac{1}{A}\left[-\left\langle V_{disp}\right\rangle_A - \beta^{-1}\ln\left\langle \exp\left[\beta\delta V_{disp}\right]\right\rangle_A\right] \equiv \frac{1}{A}(\Delta H_{WS} - T\Delta S_{WS}) \end{aligned} \tag{4-6}$$

where $V_{disp} = V_A - V_R$ is the total solid-liquid dispersion energy and $\delta V_{disp} = V_{disp} - \left\langle V_{disp}\right\rangle_A$ denotes the fluctuation of this quantity. $\Delta U_{WS} \equiv -\left\langle V_{disp}\right\rangle_A$ represents the energy contribution to the work of adhesion while $\Delta S_{WS} \equiv k_B \ln\left\langle \exp[\beta\delta V_{disp}]\right\rangle_A \geq 0$ represents the entropy contribution, which, due to its positive sign, disfavors wetting of the attractive surface.[27] The terms ΔU_{WS} and ΔS_{WS} have a simple physical significance. $-\Delta U_{WS}/A$ represents the solid-liquid dispersion energy per unit area, $-\Delta S_{WS}$ represents the entropy loss of the interfacial fluid due the configurational bias imposed on the fluid molecules by the attractive external potential of a solid wall.[28-30] Note that ΔS_{WS} does not represent the thermodynamic entropy ΔS, which features another contribution ΔS_{WW} arising from changes in water-water interactions (ΔU_{WW}) and the corresponding changes in the configurational degrees of freedom of the fluid molecules, i.e. $\Delta S = \Delta S_{WS} + \Delta S_{WW}$.[31-34] The water-water contribution equals $\Delta S_{WW} = \frac{\Delta U_{WW}}{T}$, and exactly cancels in the work of adhesion, as was originally shown by Ben-Naim in his studies of hydrophobic hydration and association.[31] The quantity of interest here, ΔS_{WS}, has in earlier solvation studies been referred to as the

interaction entropy,[28] solute-solvent entropy[29] or fluctuation entropy.[34] We further note that in mean field models, $W_a = \frac{\Delta U_{WS}}{A}$ because fluctuations are ignored which yields $\Delta S_{WS} = 0$.

4.3.3. Single-Particle Model

Molecular simulations may be used to evaluate the averages in eqs. 5 and 6. Since in this work we are interested in deriving a simple analytical model, we conjecture that correlated contributions of different water molecules to δV_{disp} (eq. (4-6)) can be ignored. With this conjecture, $\left\langle \exp[\beta \delta V_{disp}] \right\rangle_A$ factorizes into a product of N_W identical terms, i.e. ΔS_{WS} reduces to a sum of N_W identical single-molecule entropy contributions, with N_W the number of water molecules affected by the attractive tail of the liquid-solid dispersion potential. We thus reduce the problem of evaluating ΔS_{WS} to the calculation of the excess entropy, ΔS_1, of a single particle in a box with a linear dimension determined by the range of the attractive dispersion potential $V(z)$ acting between the wall and the particle:

$$\begin{aligned} \Delta S_{WS} &= N_W \Delta S_1 \\ &= N_W k_B \ln \left\langle \exp[\beta \delta V(z)] \right\rangle_A \\ &= N_W k_B \ln \left[\int_z^{z_{\max}} P_A(z) \exp[\beta \delta V(z)] dz \right] \end{aligned} \tag{4-7}$$

where $\delta V(z) = V(z) - \left\langle V(z) \right\rangle_A$ is the energy fluctuation of a water molecule located at a distance z from the surface and the probability density $P_A(z)$ reads

$$P_A(z)dz = \frac{\exp[-\beta V(z)]dz}{\int_{z_{\min}}^{z_{\max}} \exp[-\beta V(z)]dz} \tag{4-8}$$

The average $\langle \cdots \rangle_A$ is obtained assuming the particle to be Boltzmann distributed (with probability density $P_A(z)$) in the potential $V(z)$ bounded by z_{min} and z_{max}, which are the minimum distance from the surface where the density of water is non-zero and the maximum distance from the surface where the water molecule is affected by $V(z)$, respectively. It can be seen in Figure 4.1 that the water-surface interaction potential both in the case of graphene and diamond becomes negligible at a distance of the order of 1 nm. Moreover, no layer structure of water is observed in the mass distribution beyond this distance (inset of Figure 4.1). Thus, it seems clear that z_{max} should be chosen to be of the order of 1 nm. The dependence of the

interfacial entropy on the choice of z_{max} will be discussed later in the text. We however emphasize that z_{max} is not a freely adjustable parameter. ΔS_1 (eq. (4-7)) is a function of z_{min} and z_{max} which vanishes in the limit $z_{max} \to \infty$, i.e. the entropy of a particle in a box with an attractive wall is identical to the entropy of a particle in a box with a repulsive wall if the box is large in comparison with the range of the potential. The answer to the question how to meaningfully chose z_{max} is provided by Eq. (4-6), which shows that fluctuations δV_{disp} of the attractive solid-liquid interaction energy determine the entropy ΔS_{WS}. Only those water molecules located within the range of the attractive external potential contribute to the energy fluctuation, while water molecules located outside this range do not contribute. z_{max} must therefore be chosen according to the range of the external potential.

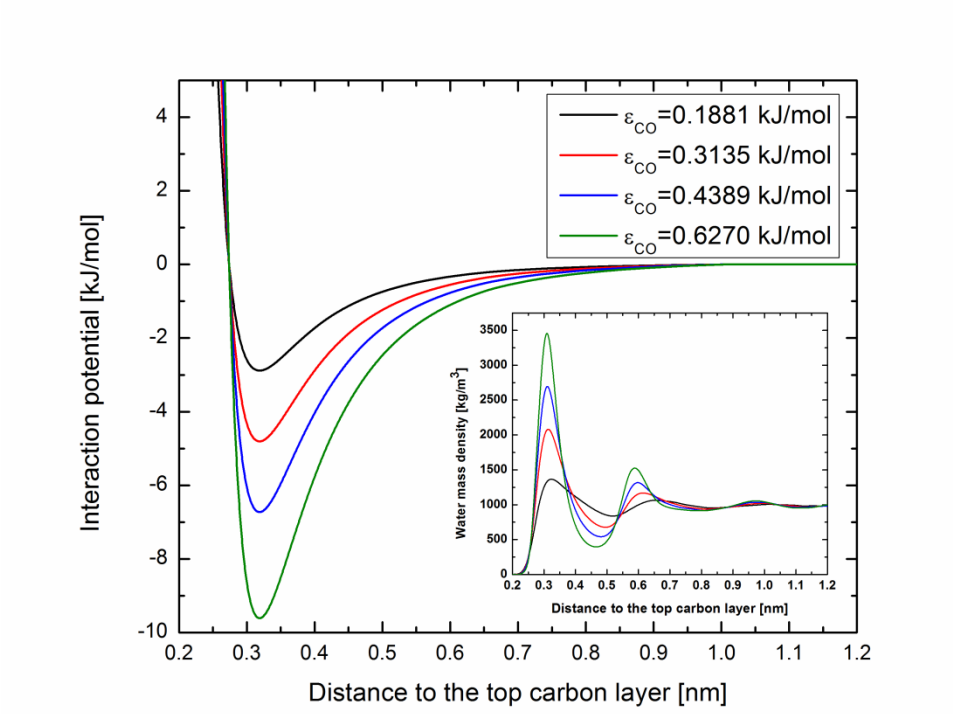

Figure 4.2. Potential energy of interaction for a single water molecule on graphite as a function of the distance to the surface for different Lennard-Jones interaction strengths ε_{CO}. The inset shows the corresponding water mass density distribution (300 K).

Since we assumed a Boltzmann distribution of the molecules in the water-surface interaction potential, computing N_W in eq. (4-7) following this assumption seems to be the most direct choice. However, this choice neglects the possible packing of molecules which occurs close to the surface. We have performed MD simulations of water on graphite using the model of Werder et

al.[17] to determine the actual value of N_W. In this model, SPC/E water interacts with the graphite surface through Lennard-Jones interactions between the carbon and oxygen atoms. We present in the inset of Figure 4.2 the water mass-density distribution on graphite obtained from simulations where the strength of the interaction between water and graphite (i.e. the energy parameter ε_{CO} of the Lennard-Jones potential) was tuned to yield values of the contact angle in the range 30-150°. It can be seen that even at low values of ε_{CO}, density oscillations are present, illustrating the packing of water molecules mentioned above. We compare in Table 4.1 the actual surface number density of water molecules in the surface region between z_{min} and z_{max}, obtained from the simulation of a slab of water on the surface, i.e. $N_W / A = \int_{z_{\min}}^{z_{\max}} \rho_l(z)dz$, where $\rho_l(z)$ is the water number density distribution and N_W^B/A obtained from the same formula where $r_l(z)$ is replaced with $\rho_0 \exp(-\beta V(z))$ (Boltzmann distribution). It can be observed that the calculations carried out following the Boltzmann distribution overestimate the actual surface number density. Only in the limit of weak dispersive interactions (hydrophobic substrates), the values are comparable. We also report in Table 4.1 the quantity N_W^{SKA} obtained following the SKA between z_{min} and z_{max}. It can be seen that the assumption of uniform bulk water density leads to estimates of N_W in very good agreement with the simulations in the full range of the interaction strengths. This result may be explained by the relatively low compressibility of water and by the fact that water has to maintain its hydrogen bonding network also close to the surfaces. Although we adopt a single molecule formalism to derive the interfacial entropy from the fluctuations in the water-surface interaction energy, the correlation between water molecules cannot be completely ignored when counting the number of molecules affected by these fluctuations. We thus assume that an effective number of water molecules have to be taken into account and this number can be reliably estimated from the SKA. We have used the values of N_W from the last column of Table 4.1 (SKA values) in performing the calculations of the interfacial entropy with the theoretical model (eq. (4-7)).

Table. 4.1. Number of water molecules between z_{min} (the minimum distance from the surface where the water density is non-zero: 0.22-0.25 nm) and z_{max} (0.88 nm) on graphite for different values of ε_{CO} obtained following the distribution of Boltzmann (N_W^B) for T=300 K, by integrating

the water mass density distribution (N_W) and by assuming that the density is equal to the bulk water value (N_W^{SKA}) at 300 K.

ε_{CO} (kJ/mol)	N_W^B/A (nm^{-2})	N_W/A (nm^{-2})	N_W^{SKA}/A (nm^{-2})
0.0940	24.9	18.6	22.4
0.1254	26.6	19.5	22.0
0.1567	28.5	20.3	22.0
0.1881	30.8	20.8	22.0
0.2508	36.4	21.6	21.6
0.3135	43.9	22.2	21.6
0.3762	54.2	22.7	21.6
0.4389	68.3	23.0	21.6
0.5016	87.6	23.3	21.2
0.5643	114.5	23.6	21.2
0.6270	151.9	23.8	21.2

4.3.4. Comparison of Theoretical Predictions with Computer Simulations

It is interesting to see how the interfacial entropies estimated by our theoretical model compare with the exact results obtained from the MD simulations. The MD simulations are used to evaluate (i) ΔU_{WS} for a slab of water on the surface and (ii) the contact angle of a cylindrical droplet on the surface. The exact value of the interfacial entropy $T\Delta S_{WS}$ is next obtained by subtracting W_a (obtained using eq. (4-4)) from ΔU_{WS} Since water tends to minimize the interaction with the repulsive surface by forming a thin liquid-vapor interface (see inset of Figure 4.1), the potential interaction energy between water and the repulsive substrates is several orders of magnitude smaller than in the case of the carbon-based surfaces like graphite and could be neglected in ΔU_{WS}, as was shown in our previous work.[1] In the following, we compare the interfacial entropies estimated by our theoretical model for water on graphene, graphite and diamond with the corresponding values from MD simulation.

4.3.4.1 Interfacial Entropy for Graphene

In our recent study, we considered two graphene models which lead to the macroscopic contact angle of 96° (GM1) and 127° (GM2) for water.[1] The interaction potentials of a single water molecule ($V(z)$) with the GM1 and GM2 substrates are shown in Figure 4.1.[35] The interfacial entropies $T\Delta S_{WS}/A = (\Delta U_{WS} - W_a)/A$ for GM1 and GM2 are 27.8±2.2 mJ/m^2 and 11.8±2.7 mJ/m^2, respectively (for comparison, the entropy for vapor-liquid surface creation amounts to

42 mJ/m^2 at 300 K for the SPC/E water model.[1]) We present in Table 4.2 the value for the interfacial entropies for GM1 and GM2 using different values of z_{max} estimated by means of eq. (4-7). It can be observed that quantitative agreement is found in both cases for the values of z_{max} lower than 1 nm. The discrepancy between the exact and predicted values increases with z_{max}, a value of around 0.85 nm yields the best agreement. A value of 0.88 nm is approximately obtained when summing up the values of two water molecular diameters and the atomic radius of a carbon atom. Moreover, it can be seen both in Figure 4.1 and Figure 4.2, that no influence of the external field generated by the carbon surface can be observed beyond that distance. We also report in Table 4.2 the value of the interaction potential at the distance z_{max}. In all cases, $V(z_{max})$ is negligible in comparison with the depth of the potential.

Table 4.2. Interfacial entropy $T\Delta S_{WS}$ (T=300 K) for the two models of graphene GM1 and GM2 depending on the interaction potential boundary parameter z_{max}.

	GM1		GM2	
z_{max} (nm)	$T\Delta S_{WS}$ (mJ/m^2)	$V(z_{max})$ (kJ/mol)	$T\Delta S_{WS}$ (mJ/m^2)	$V(z_{max})$ (kJ/mol)
0.8	25.8	−0.23	11.2	−0.14
0.88	29.6	−0.15	12.2	−0.09
1.0	35.0	−0.08	13.5	−0.05
1.1	38.9	−0.05	14.4	−0.03
1.2	42.9	−0.03	15.2	−0.02

4.3.4.2. Interfacial Entropy for Graphite

Using the proposed theoretical model we now investigate the variation of the solid-liquid interfacial entropy for graphite with respect to the change in the nature of the external potential by varying the carbon-water Lennard-Jones parameter ε_{CO}. The interaction potentials of a single water molecule with graphite for four values of ε_{CO} are shown in Figure 4.2 Figure 4.3 shows the interfacial entropies obtained from the simulations and the theoretical single particle model. In the corresponding calculations, the value of z_{max} is set to 0.88 nm to obtain a lower bound estimate of the interfacial entropy and set to 1.1 nm to obtain an upper bound. The contribution of the interfacial entropy to the work of adhesion increases with increasing the strength of the solid-liquid interaction, as it is expected, since when the water molecules are bound strongly to the surface the fluctuations in solid-water interactions are usually large. Removing these

attractions leads to an increase of the interfacial entropy. The results in Figure 4.3 further show that the single particle theoretical model provides good predictions for water on hydrophobic surfaces (θ>90°). On hydrophilic interfaces (θ<90°) the model fails to describe the interfacial entropy correctly and predicts too high values of $T\Delta S_{WS}$. The main contribution to the interfacial entropy results from water molecules exploring the region around the minimum of the solid-liquid interaction potential. On hydrophilic surfaces, strong surface-water interactions introduce enhanced water-water correlations as evidenced by the increased density oscillation observed in the inset of Figure 4.2. This means that fluid molecules located in the second layer explore a region of the potential where the entropy cost is smaller, leading to a smaller overall entropy $T\Delta S_{WS}$ in comparison with the prediction of the theoretical model.

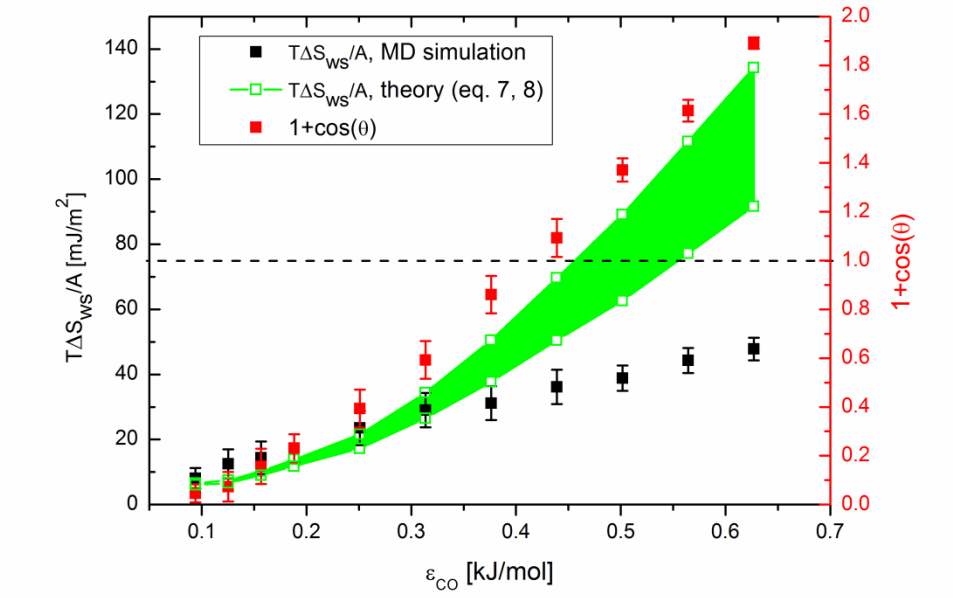

Figure 4.3. Interfacial entropy of water (300 K) on graphite versus the Lennard-Jones parameter ε_{CO} obtained from MD simulations (black symbols) and the theoretical model, eqs. 7 and 8 (green symbols). The theoretical model has been applied using z_{max}=1.1 nm (upper symbols) and z_{max}=0.88 nm (lower symbols) in order to provide upper and lower bound theoretical estimates of the interfacial entropy. The values of 1+cos(θ) obtained from the simulations for different ε_{CO} are also included (red symbols; right vertical axis). The horizontal dashed line delimits contact angles higher and lower than 90°.

4.3.4.3. Interfacial Entropy for Diamond

A similar calculation as for graphene and graphite was performed for diamond, where the macroscopic contact angle of water is 100.7°. The interaction potential of a single water molecule and the number density of water on the diamond substrate are shown in Figure 4.1. The interfacial entropy of water obtained from the simulations is equal to 53.8 (±5.4) mJ/m^2, which is in reasonable agreement with the value estimated by the theoretical model which yields 44.4 mJ/m^2 using z_{max}=0.88 nm and 61.4 mJ/m^2 using z_{max}=1.1 nm.

4.3.5. The sharp-kink Approximation

The solid-liquid interaction energy ΔU_{WS} in eq. (4-6) for a slab of water on graphite can be calculated numerically as following:

$$\Delta U_{WS} / A = -\langle V(z) \rangle_A / A = -\int_{z_{\min}}^{z_{\max}} \rho_l(z) V(z) dz \qquad (4\text{-}9)$$

In the SKA, the liquid density is assumed to go abruptly from its bulk value (ρ_0) to zero at a certain distance z_{min} above the substrate. Thus, the solid-liquid interaction energy (eq. (4-9)) in this approximation can be obtained as:

$$\Delta U_{WS} / A = -\rho_0 \int_{z_{\min}}^{z_{\max}} V(z) dz \qquad (4\text{-}10)$$

Different values have been used in the literature for z_{min}. Sendner et al.[2] used a distance from the surface where $V(z)$ turns from repulsive to attractive, while in the work of Garcia et al.[6] z_{min} coincides with the minimum of the potential. A further possibility is to choose the value of z_{min} where the potential is equal to k_BT. Here, we calculate ΔU_{WS} with these three different values for z_{min} and compare the results with exact values obtained by eq. (4-9). The comparison of the results is shown in Figure 4.4. As it is shown, the SKA underestimates the solid-liquid interaction energy especially for large values of ε_{CO}. The closest value of ΔU_{WS} to the exact ones can be obtained when z_{min} equals the distance where the $V(z)$ is zero. Taking a smaller or bigger value for z_{min} decreases the slope of ΔU_{WS} versus ε_{CO}. The inset of Figure 4.4 shows the difference between the predicted values of ΔU_{WS} by the SKA (z_{min} equals to the distance where the $V(z)$ is zero) and the exact values along with the solid-liquid interfacial entropy calculated in the previous section. It is interesting to note that at the intermediate values of ε_{CO}, where ε_{CO} is close to the actual value for the water-graphite interaction (ε_{CO} = 0.392 kJ/mol), the error introduced by the SKA in estimating the solid-liquid interaction energy by coincidence cancels the error of ignoring the interfacial entropy in this approximation. In other words, what the SKA is doing

wrong in estimating the interaction energy is compensated by the fact that it is not considering the interfacial entropy.

We finally point out that by assuming linear response of the fluid, an analysis based on free energy perturbation theory yields $W_a \cdot A = -\frac{1}{2}\langle V_{disp} \rangle_A = \Delta U_{WS}/2$. This result is exact provided that the distribution of V_{disp} is Gaussian and the fluctuations $\langle \delta V_{disp}^2 \rangle$ are equal on the attractive (water on graphite) and repulsive (water on a repulsive wall) energy surfaces.[36] Our analysis shows that the energy fluctuations are indeed Gaussian on all surfaces considered in this work (data not shown), however, $T\Delta S_{WS} < \Delta U_{WS}/2$ when $\varepsilon_{CO} > 0.25$ kJ/mol. The linear response assumption therefore neither holds on hydrophobic surfaces (graphene, graphite) nor on hydrophilic ones.

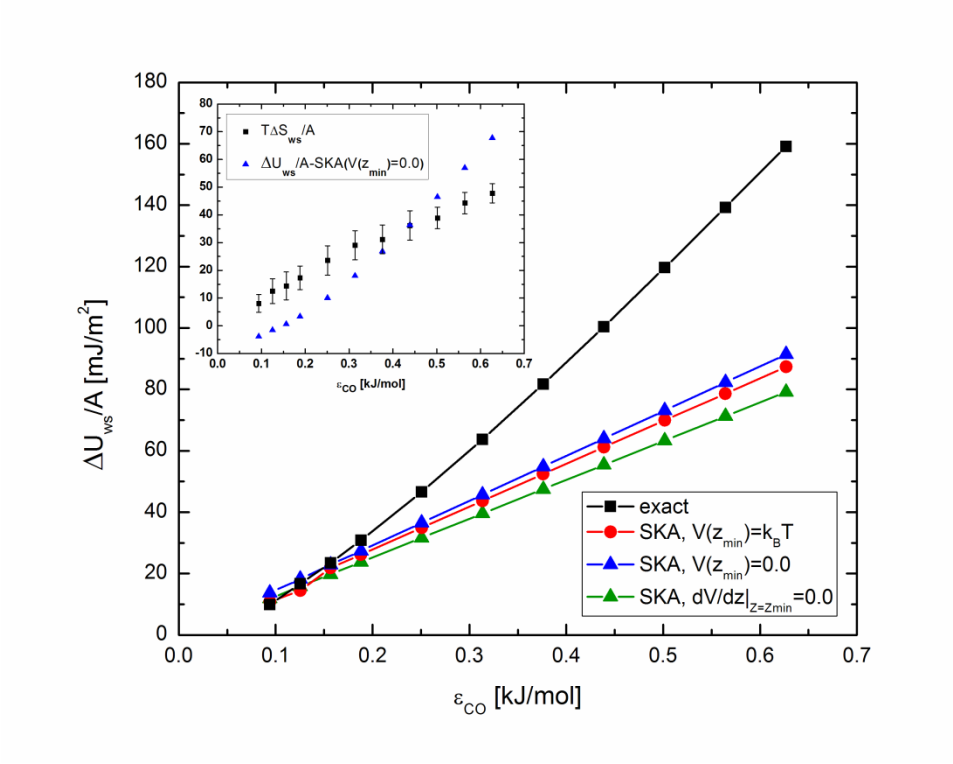

Figure 4.4. The solid-liquid interaction energy (300 K) versus the Lennard-Jones parameter ε_{CO} calculated by using eq. (4-9) and using the sharp-kink approximation with different values of z_{min} (eq. (4-10)). The lines are guide to the eye. Inset shows the difference between the predicted values of ΔU_{WS} by the SKA (z_{min} equals the distance where the $V_G(z)$ is zero) and the exact values along with the solid-liquid interfacial entropy shown in Figure 4.3.

4.4. Conclusions

In summary, we have shown that the interfacial entropy of fluids in contact with rigid planar surfaces disfavors wetting, contributing as much as ~30% to the work of adhesion of water on hydrophobic surfaces such as graphite, graphene and diamond. While significant water structuring occurs on these weakly attractive surfaces with corresponding changes in water entropy, these changes in "water structure" are always perfectly enthalpy-entropy compensating and are therefore not affecting the equilibrium contact angle. Prompted by the analogy between wetting and solvation processes a model has been proposed which describes the contribution of the interfacial entropy of the fluid to the work of liquid-solid adhesion in terms of fluctuations of the attractive fluid-substrate interaction energy. Assuming independent energy fluctuations of the individual fluid molecules in the near-surface region, the interfacial entropy reduces to a sum of single-molecule entropies, which can be computed analytically and represent the biasing of the fluid molecules' configuration space by the external (molecule-substrate) interaction potential. Based on a comparison with data from molecular simulations we have shown that this simple model provides qualitatively accurate predictions of water's entropy contribution to the work of adhesion for rigid hydrophobic walls including graphene, graphite and diamond. The emerging picture is that fluid molecules win some liquid-solid interaction energy and lose some entropy upon wetting the substrate. A greater energy gain is generally accompanied with a greater entropy loss, which can be estimated at single-particle level provided that the molecule-surface interaction potential is known. Our work further demonstrates that the sharp-kink approximation, commonly used to estimate the liquid-solid adhesion energy, underestimates the real value of the energy on hydrophobic surfaces. In mean field models of water on graphite, this error is exactly compensated by not considering the interfacial entropy.

4.5. References

(1). Taherian, F.; Marcon, V.; van der Vegt, N. F. A.; Leroy, F., What is the Contact Angle of Water on Graphene? *Langmuir* **2013,** *29*, 1457-1465.
(2). Sendner, C.; Horinek, D.; Bocquet, L.; Netz, R. R., Interfacial water at hydrophobic and hydrophilic surfaces: Slip, viscosity, and diffusion. *Langmuir* **2009,** *25*, 10768-10781.
(3). Sedlmeier, F.; Janecek, J.; Sendner, C. B., L.; Netz, R. R.; Horinek, D., Water at polar and nonpolar solid walls (Review). *Biointerphases* **2008,** *3*, FC23-FC39.
(4). Shih, C. J., Wang, Q. H., Lin, S., Park, K. C., Jin, Z., Strano, M. S., & Blankschtein, D. , Breakdown in the Wetting Transparency of Graphene. *Phys. Rev. Lett.* **2012,** *109*, 176101-176106.
(5). Machlin, E. S., On Interfacial Tension at a Rigid Apolar Wall–Water Interface. *Langmuir* **2012,** *28*, 16729-16732.
(6). Garcia, R.; Osborne, K.; Subashi, E., Validity of the "Sharp-Kink Approximation" for Water and Other Fluids. *J. Phys. Chem. B* **2008,** *112*, 8114-8119.
(7). Dietrich, S., in Phase Transitions and Critical Phenomena. Domb, C. L., J. L., Ed. Academic: London: 1988; Vol. 12, p 1.
(8). Dietrich, S.; Napiórkowski, M., Analytic results for wetting transitions in the presence of van der Waals tails. *Phys. Rev. A* **1991,** *43*, 1861-1885.
(9). Dietrich, S.; Schick, M., Order of wetting transitions. *Phys. Rev. B* **1986,** *33*, 4952-4968.
(10). Jamadagni, S. N.; Godawat, R.; Garde, S., Hydrophobicity of Proteins and Interfaces: Insights from Density Fluctuations. *Annu. Rev. Chem. Biomol. Eng.* **2011,** *2*, 147-171.
(11). Godawat, R.; Jamadagni, S. N.; Garde, S., Characterizing hydrophobicity of interfaces by using cavity formation, solute binding, and water correlations. *Proc. Natl. Acad. Sci. USA* **2009,** *106*, 15119–15124.
(12). Patel, A. J.; Varilly, P.; Jamadagni, S. N.; Acharya, H.; Garde, S.; Chandler, D., Extended surfaces modulate hydrophobic interactions of neighboring solutes. *Proc. Natl. Acad. Sci. USA* **2011,** *108*, 17678–17683.
(13). Berendsen, H. J. C.; Grigera, J. R.; Straatsma, T. P., The Missing Term in Effective Pair Potentials. *J. Phys. Chem.* **1987,** *91*, 6269-6271.
(14). Miyamoto, S.; Kollman, P. A., SETTLE: An analytical version of the SHAKE and RATTLE algorithms for rigid water models. *J. Comput. Chem.* **1992,** *13*, 952-962.
(15). Hess, B.; Kutzner, C.; Spoel, D. V. D.; Lindahl, E., GROMACS 4: Algorithms for Highly Efficient, Load-Balanced, and Scalable Molecular Simulation. *J. Chem. Theory Comput.* **2008,** *4*, 435-447.
(16). Essmann, U.; Perera, L.; Berkowitz, M. L.; Darden, T.; Lee, H.; Pedersen, L. G., A Smooth Particle Mesh Ewald Method. *J. Chem. Phys.* **1995,** *103*, 8577-8593.
(17). Werder, T.; Walther, J. H.; Jaffe, R. L.; Halicioglu, T.; Koumoutsakos, P., On the Water-Carbon Interaction for Use in Molecular Dynamics Simulations of Graphite and Carbon Nanotubes. *J. Phys. Chem. B* **2003,** *107*, 1345-1352.
(18). Nose, S., A molecular dynamics method for simulations in the canonical ensemble. *Mol. Phys.* **1984,** *52*, 255-268.
(19). Hoover, W. G., Canonical dynamics: equilibrium phase-space distributions. *Phys. Rev. A* **1985,** *31*, 1695-1697.
(20). Rafiee, J.; Mi, X.; Gullapalli, H.; Thomas, A. V.; Yavari, F.; Shi, Y.; Ajayan, P. M.; Koratkar, N. A., Wetting Transparency of Graphene. *Nature Materials* **2012,** *11*, 217-222.

(21). Chandler, D.; Weeks, J. D.; Andersen, H. C., Van der Waals Picture of Liquids, Solids, and Phase Transformations. *Science* **1983,** *220*, 787-794.
(22). Weeks, J. D.; Chandler, D.; Andersen, H. C., Role of Repulsive Forces in Determining the Equilibrium Structure of Simple Liquids. *J. Chem. Phys.* **1971,** *54*, 5237-5248.
(23). Leroy, F.; Müller-Plathe, F., Rationalization of the Behavior of Solid-Liquid Surface Free Energy of Water in Cassie and Wenzel Wetting States on Rugged Solid Surfaces at the Nanometer Scale. *Langmuir* **2011,** *27*, 637-645.
(24). Huang, D. M.; Geissler, P. L.; Chandler., D., Scaling of hydrophobic solvation free energies. *J. Phys. Chem. B* **2001,** *105*, 6704–6709.
(25). *The pressure-volume contribution PΔV to the enthalpy change is of order 0.1 mJ/m2 at 101.3 kPa and can be ignored. It may thus be assumed that ΔH≈ ΔU.*
(26). Zwanzig, R. W., High-Temperature Equation of State by a Perturbation Method. I. Nonpolar Gases. **1954,** *22*, 1420-1427.
(27). *follows from the Gibbs inequality (also known as Bogoliubov or Feynman inequality):* .
(28). Sanchez, I. C.; Truskett, T. M.; In 't Veld, P. J., Configurational Properties and Corresponding States in Simple Fluids and Water. *J. Phys. Chem. B* **1999,** *103*, 5106–5116.
(29). van der Vegt, N. F. A.; Trzesniak, D.; Kasumaj, B.; van Gunsteren, W. F., Energy-Entropy Compensation in the Transfer of Nonpolar Solutes from Water to Co-Solvent/Water Mixtures. *ChemPhysChem* **2004,** *5*, 144-147.
(30). Schravendijk, P.; Van Der Vegt, N. F., From hydrophobic to hydrophilic solvation: an application to hydration of benzene. *J. Chem. Theory Comput.* **2005,** *1*, 643-652.
(31). Ben-Naim, A., A simple model for demonstrating the relation between solubility, hydrophobic interaction and structural changes in the solvent. *J. Chem. Phys.* **1978,** *82*, 874-885.
(32). Yu, H. A.; Karplus, M., A thermodynamic analysis of solvation. *J. Chem. Phys.* **1988,** *89*, 2366-2379.
(33). Peter, C.; van der Vegt, N. F. A., Solvent Reorganization Contributions in Solute Transfer Thermodynamics: Inferences from the Solvent Equation of State. *J. Phys. Chem. B* **2007,** *111*, 7836-7842.
(34). Ben-Amotz, D.; Underwood, R., Unraveling water's entropic mysteries: a unified view of nonpolar, polar, and ionic hydration. *Acc. Chem. Res.* **2008,** *41*, 957-967.
(35). *The approach to calculate the interaction potential of single water molecule with graphene, graphite and diamond is explained in the supporting information.*
(36). Åqvist, J.; Hansson, T., On the Validity of Electrostatic Linear Response in Polar Solvents. *J. Phys. Chem.* **1996,** *100*, 9512-9521.

5. Molecular Simulation of Ionic Liquids at Solid-Liquid Interfaces and Aspects of Electrowetting: a Review

5.1. Introduction

Room temperature ionic liquids (ILs) made of cations and anions have been studied extensively during the last years, and they are used in different industrial applications because of their unique properties. One could prepare new ionic liquids by choosing a suitable combination of cation and anion, varying the symmetry of the cations , relative size of cations and anions or changing the distribution of the charges on the ions.[1]

Ionic liquids has been found in different applications like lubricants,[2-3] batteries,[4-5] heterogeneous catalysis,[6-7] electrochemistry,[8] fuel cells,[9-11] and nanotechnology[12-13]. In all these applications the structure of ILs with a solid surface plays an important role. Several theoretical and experimental works have been performed to study the interfacial properties of ILs. Since ILs are composed of molecules with net charges and the cations and anions could make hydrogen bonds, interaction between a solid surface and ILs can be completely different than the typical liquids. Since ions have a strong interaction with the surface, the mobility of the ions at the interface is reduced and the liquid may changed to the solid phase.[14-17]

Different experimental methods have been used to investigate the structural properties of ILs at the solid surface like neutron scattering,[23] X-ray,[20-21] sum-frequency spectroscopy[18-19] or atomic force microscopy[22]. Several different ILs deposited on silica, mica, graphene and graphite surfaces, or on more reactive surfaces such as metals, and TiO_2 have been studied experimentally or by using molecular dynamics (MD) simulations. All the investigations of the ILs at the solid interfaces have shown strong layering of the liquid. The orientation of the imidazolium ring of the cations at the interface was shown experimentally to be dependent on the length of the alkyl tail of the cations, type of the anions and on the chemistry of the surface.[24-26] Due to limitation of the experimental methods to investigate the interfacial properties of ILs, MD simulations have been used extensively during last years to study different structure and dynamic properties of ILs at the solid surfaces. In the following, we are reviewing the recent simulation results, where the different factors influencing the interfacial properties of ILs were investigated. Readers

interested specially on the computer simulations of ILs at electrochemical interfaces are referred to recent review of Merlet et al.[27]

5.2. Ionic Liquids at Solid-Liquid Interface

It has been shown by the experimental studies and the MD simulations that properties of the solid–IL interface depend on (i) characteristic of the surface (ii) type of IL and (iii) on the thermodynamic conditions of the interface. Different characteristics of the surface that have been already investigated by MD simulations are the chemical nature of the solid surface (graphene, graphite, SiO_2, TiO_2 rutile, mica and iron surface), surface curvature (flat surfaces and carbon nanotubes), charge on the surface (positively and negatively charged surfaces), confinement of the ILs in the slit like and cylindrical pores, the effect of the size of the confinement and the number of the ion pairs inside the pores. Concerning the properties of the liquid, effect of the size of the cations and the anions and the width of the ionic liquid layer on the solid-liquid and the liquid-vapor interfaces have been studied. The way that also temperature influences the interfacial properties of ILs has been studied. In the following, we review the main results obtained by the MD simulations.

5.2.1. Surface

5.2.1.1. Chemical Nature

MD simulations have been already used to investigated the structure and the dynamic properties of ILs on graphene,[28-31] graphite,[16-17, 32-41] silica,[36, 42-46] TiO_2 rutile,[47] mica[48-49], gold[50] and iron[51] surfaces. Sha et al.[32] reported for the first time the interfacial properties of [BMIM][PF_6] on graphite by using MD simulation. A well defined structure has been shown at the IL-solid interface. Simulation results showed that the IL has the mass density and the electron density of around 90 and 80%, respectively, higher than the bulk values at the solid-liquid interface. Since there is a strong van der Waals interaction between the $[BMIM]^+$ cations and the surface, more cations come close to the surface than anions. Analyzing the orientation of the cations at the interface by MD simulations and by the scanning tunneling microscopy experiment showed that the imidazolium ring of the cations lie parallel to the surface.[52-53]

Similar to the IL graphite interface, higher density of the liquid (approximately 15%) compared to the bulk was also observed at the IL-vacuum interface, however the structuring of the liquid at

the IL-vacuum interface was less than the one at the solid surface.[34] By using MD simulations[16, 54] and also by X-ray reflectivity experiments[55] it was shown that adsorption of $[PF_6]^-$ ions at the IL-vacuum interface leads to the enhancement of the charge density of the liquid at the interface. The structure of [BMIM][NO_3] on rutile [110] was investigated by Liu et al.[47] using MD simulations. Analyzing the orientation of the anions and the cations at the interface showed that anions and the imidazolium rings of the cations are standing almost perpendicular to the surface, the alkyl tails are oriented toward the bulk, while the methyl groups connected to the imidazolium rings are oriented to the surface. As it was observed for graphite surface, in the case of the rutile surface also the cations provide the main contribution to the density profile at the interfacial region. Li et al.[36] compared the interfacial properties of confined [C_4mim][Tf_2N] IL between two solid walls with different surface chemistries. They have simulated the carbon and silica solid walls. Their results showed that presence of hydroxyl groups on the surface of the silica generates roughness on the surface, which decreases the mobility of the ILs at the interface compared to graphene sheets or carbon nanotubes. Simulation results showed that the lateral diffusion of the ions at the solid surface correlates with the density. The ions (cations and anions) diffuse faster at the regions where their corresponding density is lower. High density of the ions corresponds to the low diffusion in the plane.

The diffusion coefficients of $[C_4mim]^+$ in the silica and carbon pores as function of the distance from the solid surface and temperature are reported in Figure 5.1. Results show an increase of the diffusion coefficient versus the distance from the wall and temperature for both silica and carbon pores. It is also shown that in the case of silica pores change in the diffusion coefficient by changing temperature depends on the distance of the ions from the surface; the dynamics of the ions become less sensitive to temperature by getting closer to the silica wall. (layer-1 in Figure 5.1a). However, in the case of carbon pores at different regions analogous temperature dependence of the diffusion was observed. It has been found that the averaged interaction potential per ion versus the distance from the solid wall surface has an oscillatory behavior, while such a behavior was not found in the case of graphene (Figure 5 in ref [36]). Different behavior of the IL in the silica and carbon pores was attributed to different surface structure and different type of interaction between the solid and the liquid.

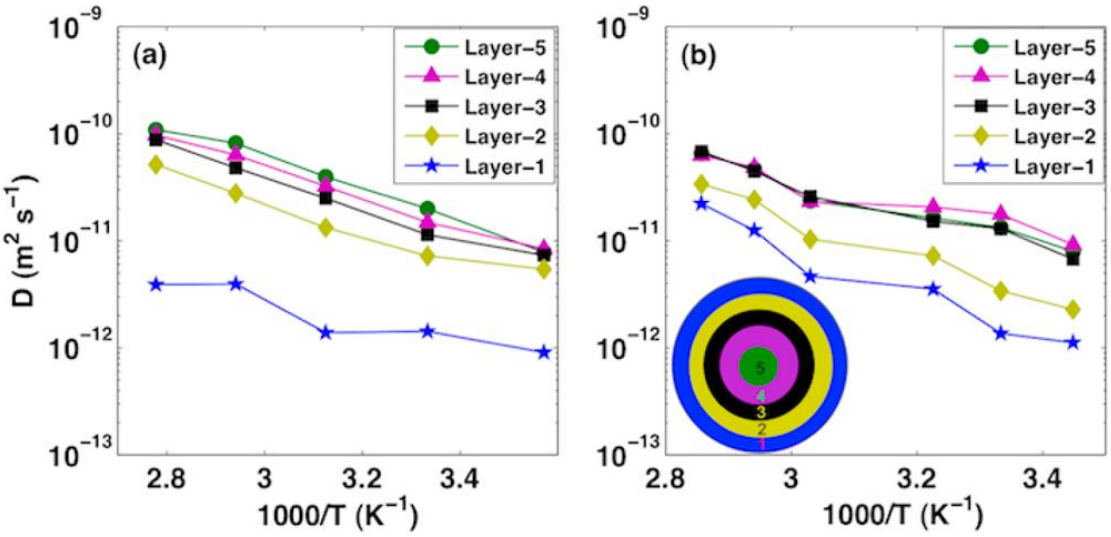

Figure 5.1. The diffusion coefficients of $[C_4mim]^+$ in the silica (a) and carbon pores (b) as function of the distance from the solid surface and temperature. Reproduced with permission from reference 36.

Layering of $[C_nmim][Tf_2N]$ with different lengths of the alkyl tail of the cations (n=2, 4, 6 or 8) on mica surface was studied by Singh Payal et al.[48]. Simulation results showed that the orientation of alkyl tail of cations on mica surface depends on the length of the chain; cations with shorter chains (n=2 or 4) are lie on the surface, while for longer alkyl chains (n=6 or 8) the tails are standing perpendicular to the surface. The same behavior was also observed in the surface force measurements.[56]

Dragoni et al.[49] also studied the interfacial properties of $[BMIM][Tf_2N]$ IL on mica with different surface charge densities. Simulation results showed an oscillatory behavior of the charge and number density profiles of the ions up to 1 nm from the surface. It was observed that at the high surface charge densities, the change in the number of the counter-ions at the interface becomes less pronounced. Investigating the mass density and the electron charge density profiles of the IL at the interface at different temperatures (between 300 and 350 K) showed very low sensitivity of these quantities to the temperature. Simulation results showed that such behavior is independent of the type of the surface, since a similar behavior was also observed in the case of silica surfaces in Ref. 44. Very low sensitivity of the structure of IL at the interface to temperature (glass-like behavior) is due to the strong interaction between the solid and the liquid. The presence of hydrogen bonds between the ions and the surface may push the ions toward the surface. For example in the case of $[BMIM][Tf_2N]$ on silica, the anions are the closest ions to the surface, since they are making hydrogen bonds with surface, but replacing the surface

with mica prevent any hydrogen bonding between the liquid and the surface. Therefore, the cations in this case, due to their higher van der Waals interaction with the surface, will stand closer to the surface.

Mendonça et al.[51] developed the force field parameters for the interaction between several ILs and a metal surface by using the quantum calculations. They studied the structural properties of $[N_{1114}][C_1SO_3]$, $[N_{1114}][C_4SO_3]$, and $[N_{1124}][C_4SO_3]$ ILs at an iron surface. Simulation results showed that the interfacial thickness changes between 0.5 and 1.0 nm depending on the alkyl side chains of the cations and the anions (shorter is the alkyl chains thicker is the interfacial layer). The orientation of the alkyl side chains of the cations and the anions were found to be different: the tails of the cations are mainly flattened on the surface while the anions are mostly standing in the perpendicular direction to the surface. The different in the orientation of the alkyl side chains of the anions and the cations is due to the different chemistry of the ions and the way how they interacting with the surface.

5.2.1.2. Surface Curvature

Studying the different interfacial properties of ILs around and inside carbon nanotubes (CNTs), due to the particular electro- and biochemical properties of ILs and CNTs, became very interesting recently. [57-61] One important factor to be considered in such systems is the effect of the surface curvature on the interfacial properties.[62-63]

Frolov et al.[28] studied the structure of $[C_n\text{mim}][\text{TFSI}]$ with n=2,4 and 8 at the IL-CNT interface with positively and negatively charged surfaces. Simulation results at the zero surface charge density showed a layering of the liquid at the interface, where by making the tail of the cations longer they oriented more parallel to the tube surface. Analyzing the orientation of the ions at the positively and the negatively charged CNTs showed that the anions are always oriented parallel the tube surface independent of the charge of the surface, while the ordering of the actions depends on the charge of the CNT and the length of the alky tail. On the positively charged CNTs, cations are always oriented parallel the surface independent of the length the alkyl chain, while on the negatively charged CNTs with increasing the length of the alkyl tails of the cations the ordering of the cations changes from the perpendicular orientation to the surface to more parallel direction.

Influence of the confinement of $[\text{BMIM}][PF_6]$ IL inside slit like graphitic pores and also inside the CNTs with different diameters on the interfacial properties of the liquid was investigated by

Singh et al.[35, 64] Comparison of the results for the slit like and the cylindrical pores showed that, for both geometries the IL displays a significant layering at the interface, and a low mobility of the ions was observed close the pore wall. In the case of CNTs the ions displayed similar mobility at the interface, while faster diffusion of the cations was observed for slit pores. Additionally, the results showed that the dynamic of the anions in the slit like pores is less sensitive to the distance to the surface.

A cylindrical layering of ILs was also found in the simulation of single and double-layer CNTs dissolved in [EMIM][BF_4].[65-66] Results have shown that depending on the size and the shape of the ions, they may diffuse into the tubes, and have different structures. MD simulation of the filling process of the CNTs by the cations and the anions of [BMIM][PF_6] IL showed that even the number of the cations and the anions in the tube at the end of the process are the same, the cations, due to higher diffusion and stronger van der Waals interaction with the CNT, move prior into the tube.[67] A crystalline structure with high melting point was observed after filling the tube depending on the diameter of the tube, which is in agreement with the experimental studies by Chen et al.[68] The stable crystal structure was observed for temperatures below 500 K, where the number of hydrogen bonds between the ions remains constant. At temperatures higher than 500K and by decreasing the the number of the hydrogen bonds per ions, the crystal structure starts to melt.[69]

5.2.1.3. Charge on the Surface

Depending on the charge of the surface, cations or anions are attracted or pushed away from the surface. The charged surface together with the adsorbed counter-ions forms an electrical double layer (EDL). Several theoretical models have been proposed in the literature to describe the behavior of ions near charged surfaces.[73-74] In the case of ILs, a model that can fit the best with the experimental data is still under discussion.[57-58, 75-76] Since understanding the molecular-level behavior of ILs at the interface with a charged surface is essential for further development, MD simulations have been used extensively to investigate the different interfacial properties.

The effect of surface charges on the ordering of the cations and anions of [BMIM][PF_6] near to a solid surface was investigated by Sha et al.[77]. Simulation results showed that, at very low surface charge densities the strong Columbic interaction between the ions is the dominant interaction at the interface, and the density layers of the ions are overlaps. But by increasing the surface charge density more partitioning of the ionic layers was observed. The formed ELD at high surface

densities (-0.31 e/nm^2) has a thickness of around 1.7 nm, and it was found to be sensitive to the structure and the size of the ions.[77-78] At the charged surfaces, ILs showed more aggregation of the tails, which will suppress more the diffusion of the ions at the interface compared to the uncharged surface.

Feng et al.[42] studied the structural change of [BMIM][NO_3] IL confined between two positively and negatively walls of α-quartz. Results showed that at very low positive charge densities the [BMIM]$^+$ ions will still be present next to the surface due to their stronger van der Waals interaction with the surface. The presence of the cations next to the positively charged surfaces has been also observed in the case of [DMIM][Cl][81] IL on the charged surfaces, and has also been confirmed experimentally.[79,80] The adsorption of the cations at the zero surface charge density will lead to a positive value for the electrical potential drop of the EDL, which can affect the EDL capacitance. The density profiles of cations at the negatively charged surface showed more structuring of the ions at the interface than the anions next to the positively charged surfaces.

Kislenko and coworkers[29] investigated the effect of the charge on the surface (for two surface charge densities: σ=+8.2 μc/cm^2 and σ=-8.2 μc/cm^2) on different structural properties of [BMIM][PF_6] IL near graphene by using MD simulation. It was shown that on the negatively charged surface the anions are pushed away from the surface toward the bulk, and first layer of the ions is made mainly by the cations, while in the case of the positively charged surface cations, due to their strong van der Waals interaction with the surface, can be found even within the first layer of the adsorbed ions. By making the surface charge density more positive, the angular distribution of the imidazolium ring of the cations with respect to the normal to the surface become wider, and it also shifts to higher values, while in the case of negatively charged surfaces the imidazolium rings arrange more parallel to the surface (shifting the distribution to smaller tilt angles). Due to the high packing density of the ions in the first layer and at high negatively charged surfaces some cations can be found with an orientation perpendicular to the surface.[30] The change in the imidazolium ring orientation with the surface charge density has been observed experimentally.[82-83]

The different orientations of the cations and anions next to the positively and negatively charged surfaces will affect the volume charge density at the EDL and consequently the electrical potential drop and the capacitance of the EDL. Such asymmetry in the electrical potential and the volume charge density were also reported for [BMIM][CL] by Lynden-Bell and coworkers.[30] They have shown that the change in the structure of the liquid at the interface upon charging the surface is mainly coming from the change in the structure of the anions at the interface. On the

positively charged surfaces, the anions are absorbed on the surface and replacing the cations that are leaving the interface, while in the case of the negatively charged surfaces, the anions are pushed away from the surface and form a new layer next to the cations. Simulation results showed that on the positively charged surfaces, adsorption of the counter-ions is higher than the co-ions desorption, while on the negatively charged surface the co-ions that are leaving the surface are more than the counter-ions that are adsorbed on the surface. The main changes in the structure and the orientation of the ions upon charging the surface can be seen in Figure 5. 2.

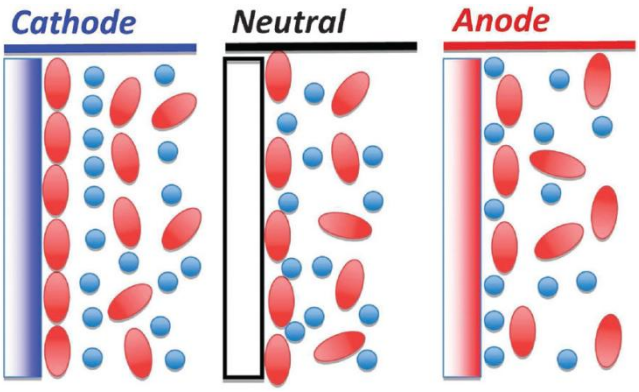

Figure 5.2. The cartoon shows how the density of the ions and the orientation of the cations change upon charging the surface. The red ellipsoids representing the cations and the blue spheres are the anions. Reproduced with permission from reference 30.

5.2.1.4. Confinement and Effect of Pore Size and Pore Loading

Understanding how confining ILs between the surfaces affect their interfacial properties is getting higher attention because of increasing in the use of the ILs in some applications like lubricates, fabrications of the solar cells or IL/CNT composites. Several studies have been focused during the last years on different structural and dynamic properties of ILs inside the slit like and cylindrical pores.[84]

The effect of confinement between two graphite walls on the dynamic properties of [BMIM][PF_6] at the different temperatures (between 300 and 400 K) was studied by Singh et al.[35] Depending on the distance of the ions to the surface the interaction between the ions and the surface and consequently the packing of the ions at the interface change. Therefore the dynamic properties of the ions in the confinement depend strongly on their respective distance to the surface. Simulation results showed that the diffusion of the ions in the lateral direction is almost similar to the diffusion of the ions in the bulk, while their diffusion in the perpendicular direction to the

surface is reduced near to the surface. Such heterogeneity in the dynamic of the ions is mainly related to the packing of the ions next to the surface. The effect of the temperature on the dynamic properties has been shown to be similar to the bulk, where the diffusion of the ions increases with increasing temperature. Simulation results of [BMIM][PF_6] in the confinement with different pore sizes and pore loadings shown no effect on the structure of the ions. However, in the case of [EMIM][TFMSI][37] analyzing the radial distribution function of the ions at different regions inside the slit pores showed that changing the distance between the walls and the number of ions in the confinement introduce small changes in the structure of the ions, while the influence on the dynamic properties was found to be more pronounced. Results showed that the ions will move faster at the interfacial regions with increasing the pore size and decreasing the pore loading. However, the confinement effects on the interfacial properties depend strongly on the chemistry of the ions.

Simulation of [C_4mim][Tf_2N] IL in cylindrical silica and carbon pores showed that the change in the local dynamic also depends on the type of the wall.[36] In the case of confinement in the silica pores, results showed a strong decrease of the mobility of the ions by decreasing the pore loading fraction. Similar trend but with a lower rate was also found in the case of carbon confinement.

Figure 5.3 compares the diffusion coefficients of the cations in the silica and the carbon pores at different temperatures and the number of the ions in the confinement. Results show that independent of the type of the wall the diffusion of the cations is reduced in the confinement compared to the bulk value. With increasing the loading fraction at different temperatures the diffusion of the ions increases. Such dependence is stronger in the case of silica pores. As it is shown in the figure, the diffusion coefficient of the cations close to the silica surface is more or less independent of the temperature at the low loading fraction, while a stronger dependent was found in the case of carbon pores.

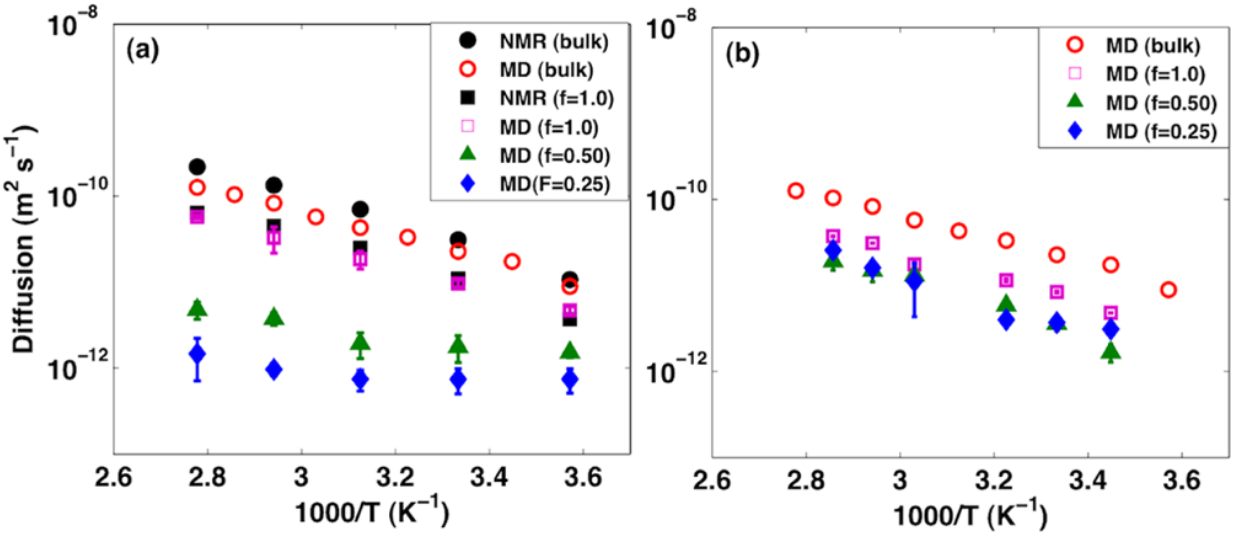

Figure 5.3. The change in the dynamic of the cations inside the cylindrical silica (a) and carbon pores (b) with temperature and the filling fraction of the ions. Reproduced with permission from reference 36.

Simulation results of Sha et al.[16], where they have simulated [DMIM][Cl] IL inside the graphitic slit like pores, have shown that by changing the pore size a transition from liquid to solid phase can be observed. The simulations results reported in Figure 5.4a for different distances between the walls show that the ions display liquid behavior with very high diffusion coefficient for pore sizes between 0.8 and 0.95 nm. For wall distances below 0.8 nm, slowing down the ions by the strong interaction with the walls leads to a transition from liquid to solid phase. Counting the number of nearest-neighbor counter-ions in the solid phase for the monolayer at the wall distances less than 0.8 nm (Figure 5.4a), and for bilayer at wall distances less than 1.15 nm (Figure 5.4b)[17] showed that in the case of monolayer the corresponding number of nearest-neighbor counter-ions is four, while in the case of bilayer it decreases to three. These results showed that number of nearest-neighbor counter-ions in the solid phase formed in the confinement is higher than the corresponding value at the bulk crystalline phase (which was found to be two counter-ions). The higher number of the nearest neighbor counter-ions in the confinement makes the melting point of the IL at the interface twice the corresponding value for bulk.

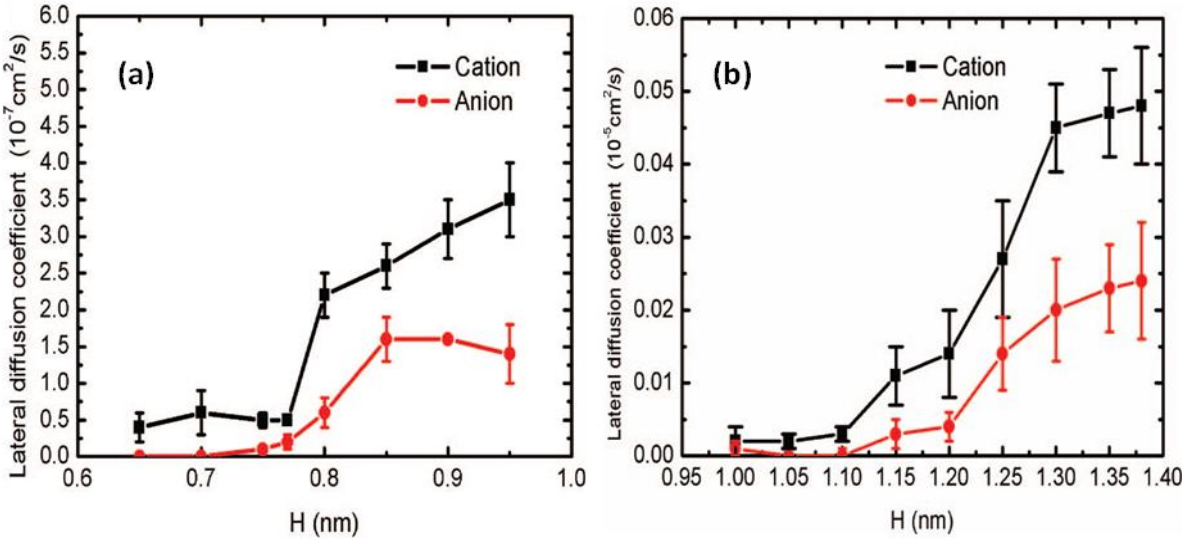

Figure 5.4. In the plane diffusion of $[DMIM]^+$ cations and $[Cl]^-$ anions in the confined (a) monolayer (Reproduced with permission from reference 16) and (b) bilayer (Reproduced with permission from reference 17) states between two graphite walls versus the distance between the walls.

5.2.2. Type of Ionic Liquid

5.2.2.1. Effects of Alkyl Chain Length of Cations

The effect of the length of the alkyl tail of cations on different interfacial properties of the ILs was investigated by MD simulation of [BMIM][PF_6] and [OMIM][PF_6] on a graphite surface.[33] Simulation results showed that for both ILs different parts of the cations are oriented parallel to the surface. However, with increasing the alkyl side chain length aggregation of the polar (the imidazolium ring of the cations and the anions) and non-polar groups (alkyl chain of the cations) can be observed at the interfacial regions.

Dou et al.[41] studied the effect of the alkyl chain length of the cations on the interfacial properties of [$C_n$mim][PF_6] ILs (n = 1, 4, 8, 12) at a graphite surface. Simulation results showed that in the case of [C_1mim][PF_6] since the cations have a symmetric shape, and due to their small sizes, they could pack very easily at the interface, and therefore the number density of the IL shows the highest peak next to the surface compared to the other ILs. By increasing the size of the cations the number density of the ions at the interface decreases. Investigating the change in the structure of the ILs with changing the temperature showed that higher diffusion of the ions in the case of [C_1mim][PF_6] leads to more sensitivity of the density of ions at the interface to the

change in temperature.[85] $[C_1mim][PF_6]$ IL showed a decrease of 17% in the mass density at the first layer by increasing the temperature from 400 to 800 K, while the decrease in the mass density for $[C_4mim][PF_6]$, $[C_8mim][PF_6]$ and $[C_{12}mim][PF_6]$ ILs were found to be 8%, 11% and 10%, respectively. Simulation results showed that the width of the interfacial region, where the density of the IL is affected by the solid surface, depends on the length of the alkyl side chain of the cations. The interfacial thickness of the ILs with shorter alkyl chain of the cations like $[C_1mim][PF_6]$ and $[C_4mim][PF_6]$ was estimated to be around 2 nm, while for the ones with longer chains ($[C_8mim][PF_6]$ and $[C_{12}mim][PF_6]$) high oscillation of the mass density was observed even at higher distances.

5.2.2.2. Size of Anions

Several ILs with anions of different sizes were simulated by Dou et al.[40], where [BMIM][Y] ILs ($[Y]^-$ = $[Cl]^-$, $[PF_6]^-$, and $[Tf_2N]^-$) on graphite at different temperatures (300-800 K). Simulation results showed that ions at the interface mainly diffuse in the parallel direction to the surface, and depending on the size of the anions and their surface electron charge density the lateral diffusion coefficients of the ions changes. Investigating the effect of size of the anions on the change in the structure of the ILs with temperature showed that at low temperatures the structure of ILs with the smaller anions ([BMIM][Cl]) is less sensitive to the change in temperature, because of high surface charge density of anions, while at higher temperatures the change in the structure of the ILs with the smaller anions become more pronounced, since anions with the smaller sizes are moving faster.

5.2.2.3. Influence of Ionic Liquid Film Thickness

Recently, Wang et al.[34] studied the effect of the thickness of $[BMIM][BF_6]$ IL film on the interfacial properties of the liquid at the solid-liquid and the liquid-vacuum interfaces.

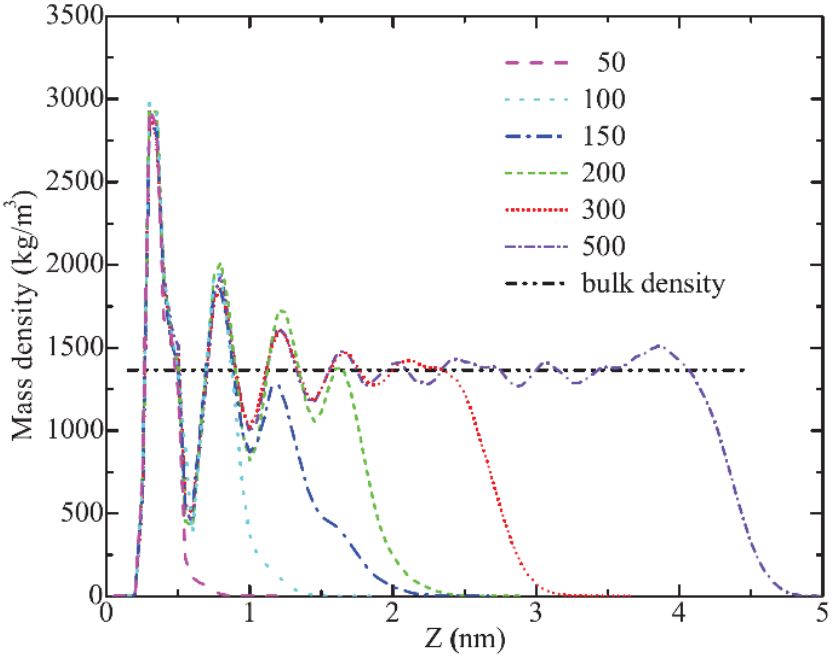

Figure 5.5. The effect of the IL film thickness on the solid-liquid and the liquid-vacuum interfaces for [BMIM][PF_6] on graphene. Reproduced with permission from reference 34.

Simulation results indicated that the different interfacial properties of the ILs at the solid surface like the number and the electron density distribution of the ions (Figure 5.5) and the orientation of cations are independent of the thickness of the IL film. This is due to the fact that the structure of the ions at the solid surface is mainly determined by the strong solid-liquid interaction. Therefore, the liquid-vacuum interface is not able to introduce any considerable changes on the structure of the liquid at the interface with the solid. However, a stronger dependency of the structure of the IL on the film thickness was observed at the vacuum interface. At the thicker IL films, where the effect of the solid-liquid interface on the orientation of the cations at the liquid-vapor interface can be ignored, the orientation distributions of the cations shows several peaks, where some of cations are oriented parallel and some perpendicular to the interface. At very thin liquid films, the orientation of the cations at the vacuum interface is disturbed by the solid surface, and they are mainly oriented parallel to the interface.

5.2.3. Thermodynamics Conditions

Regarding the effect of thermodynamic conditions on the interfacial properties of ILs at the solid-liquid interface, several authors have investigated the influence of temperature, which will be reviewed in the following section.

5.2.3.1. Temperature

Having in mind applications like lubricants where ILs are used at different temperatures, understanding the effect of the temperature on different interfacial properties become very important. Since different interfacial properties at the molecular level are determined by the liquid-liquid and the solid-liquid electrostatic and the van der Waals interactions, the change in the structure of ions at interface with temperature depends on how the solid-liquid and the liquid-liquid interactions response to the change in temperature.

Kislenko et al.[31] reported the first use of MD simulation to investigate the effect of temperature on the interfacial properties of [BMIM][PF_6] IL on graphite. Running the simulations at different temperatures (300, 350, and 400 K) has shown that at higher temperatures the anions show less layering at the interface. In the case of the cations, while the number density of the ions in the first layer decreases with increasing temperature, the intensity of the second layer increases at the higher temperatures.

The strong interaction of the ions in the case of [BMIM][Tf_2N] film on mica[49] and silica[44-45] surfaces lead to only slight change of the structure of the liquid with increasing the temperature from 300 to 350 K. As it was discussed in Section 2.1.1 (and shown in Figure 5.1) the change in the diffusion coefficient of ions at the interface depends on the distance of the ions from the surface, the type of the IL and the type of the surface. It was shown that in the case of silica pores the distance between the ions and the wall has a strong influence on how the diffusion of the ions affected by temperature; for the ions in the vicinity of the silica surface the dynamic is independent of temperature, while for the ions far from the surface the ions moving faster at higher temperatures. Simulation results in the case of pores made of carbon showed that the diffusion increasing with increasing temperature independent of the distance between the ions and the wall. It has been also shown that the number of the ions in the pore affecting the response of the liquid to the temperature dependent on the type of the wall. In the case of silica pores the diffusion of the ions is more sensitive to the change in temperature where the number

of the ions in the confinement is very high, while in the case of carbon pores the amount of the liquid in the confinement is not affecting its response to temperature.

As it was discussed in Section 2, depending on the size of the cations[31, 41] and the anions[40] the interfacial properties of the IL change. It has been shown that the response of the liquid to the temperature at the interface also depends on the size of the ions. As the size of the anions and length of the alkyl side chain of the cations get smaller the change in the number density of the ions at the interface with changing temperature become more pronounced.

5.3. Wetting and Electrowetting

Experimental results of Batchelor et al.[94] showed that the wetting behavior of ILs is quite similar to those liquids which are mostly used as probe fluids (like water, ethylene glycol and etc.) to investigate the wetting properties of a surface: the dependence of the contact angle of both sets of the liquids on the liquid-vapor surface tension followed the same behavior, and both liquids led to the same Zisman critical surface tension (γ_C) of the surface. Several investigations have been also done in the past to use ILs as electrolyte in electrowetting experiments.[88-93] Since ILs are made of cations and anions with controllable molecular structure, they became very good candidates to study the different molecular aspects of wetting and electrowetting. Due to the limitation in experimental methods to characterize the wetting at the molecular level, MD simulations can be used for further analysis at these scales.

Although, a lot of research has been done on the interfacial properties of ILs, as it is reviewed in Section 5.2, understanding the relation between different interfacial properties and the wetting parameters like the contact angle is missing. Cione et al.[95] reported so far the only MD simulation to study the wetting of ILs, where they looked at the equilibrium contact angle of [BMIM][triflate] droplet consisting of 100 ion pairs on a CH_3- and OH-terminated silica. Simulation results showed that the stronger solid-liquid interaction in the case of the OH-terminated silica leads to more spreading of the droplet compared to the CH_3- terminated surface.

Several aspects of electrowetting of ILs were studied experimentally during the last years, [88-93] however no MD simulation has been reported on this topic so far. In Chapter 6, we present first MD simulation on the electrowetting of [BMIM][BF_4]. In Chapter 7, several open questions regarding the solid-liquid interfacial properties of ILs, wetting and also electrowetting of ILs, where MD simulations can be used, are discussed.

5.5. References

(1). Castner, E. W.; Wishart, J. F., Spotlight on ionic liquids. *Journal of Chemical Physics* **2010,** *132*, 120901.

(2). Zhou, F.; Liang, Y.; Liu, W., Ionic liquid lubricants: designed chemistry for engineering applications. *Chemical Society Reviews* **2009,** *38* (9), 2590-2599.

(3). Ye, C.; Liu, W.; Chen, Y.; Yu, L., Room-temperature ionic liquids: a novel versatile lubricant. *Chemical Communications* **2001,** (21), 2244-2245.

(4). Han, X.; Armstrong, D. W., Ionic liquids in separations. *Accounts of chemical research* **2007,** *40* (11), 1079-1086.

(5). Berthod, A.; Ruiz-Angel, M.; Carda-Broch, S., Ionic liquids in separation techniques. *Journal of Chromatography A* **2008,** *1184* (1), 6-18.

(6). Aslanov, L.; Valetskii, P.; Zakharov, V.; Kabachii, Y. A.; Kochev, S. Y.; Romanovskii, B.; Yatsenko, A., Heterogeneous catalysis in ionic liquids: The heck reaction of bromobenzene with styrene over palladium supported on mesoporous carbon. *Petroleum Chemistry* **2008,** *48* (5), 360-365.

(7). Welton, T., Room-temperature ionic liquids. Solvents for synthesis and catalysis. *Chemical Reviews* **1999,** *99* (8), 2071-2084.

(8). Armand, M.; Endres, F.; MacFarlane, D. R.; Ohno, H.; Scrosati, B., Ionic-liquid materials for the electrochemical challenges of the future. *Nature materials* **2009,** *8* (8), 621-629.

(9). de Souza, R. F.; Padilha, J. C.; Gonçalves, R. S.; Dupont, J., Room temperature dialkylimidazolium ionic liquid-based fuel cells. *Electrochemistry communications* **2003,** *5* (8), 728-731.

(10). Wang, P.; Zakeeruddin, S. M.; Moser, J.-E.; Grätzel, M., A new ionic liquid electrolyte enhances the conversion efficiency of dye-sensitized solar cells. *The Journal of Physical Chemistry B* **2003,** *107* (48), 13280-13285.

(11). Nakamoto, H.; Watanabe, M., Brønsted acid–base ionic liquids for fuel cell electrolytes. *Chemical Communications* **2007,** (24), 2539-2541.

(12). Lee, S.-Y.; Ogawa, A.; Kanno, M.; Nakamoto, H.; Yasuda, T.; Watanabe, M., Nonhumidified intermediate temperature fuel cells using protic ionic liquids. *Journal of the American Chemical Society* **2010,** *132* (28), 9764-9773.

(13). Palacio, M.; Bhushan, B., A review of ionic liquids for green molecular lubrication in nanotechnology. *Tribology Letters* **2010,** *40* (2), 247-268.

(14). Nainaparampil, J.; Phillips, B.; Eapen, K.; Zabinski, J., Micro–nano behavior of DMBI-PF6 ionic liquid nanocrystals: large and small-scale interfaces. *Nanotechnology* **2005,** *16* (11), 2474.

(15). Liu, Y.; Zhang, Y.; Wu, G.; Hu, J., Coexistence of liquid and solid phases of BMIM-PF6 ionic liquid on mica surfaces at room temperature. *Journal of the American Chemical Society* **2006,** *128* (23), 7456-7457.

(16). Sha, M.; Wu, G.; Fang, H.; Zhu, G.; Liu, Y., Liquid-to-solid phase transition of a 1, 3-dimethylimidazolium chloride ionic liquid monolayer confined between graphite walls. *The Journal of Physical Chemistry C* **2008,** *112* (47), 18584-18587.

(17). Sha, M.; Wu, G.; Liu, Y.; Tang, Z.; Fang, H., Drastic phase transition in ionic liquid [Dmim][Cl] confined between graphite walls: new phase formation. *The Journal of Physical Chemistry C* **2009,** *113* (11), 4618-4622.

(18). Rivera-Rubero, S.; Baldelli, S., Influence of water on the surface of hydrophilic and hydrophobic room-temperature ionic liquids. *Journal of the American Chemical Society* **2004,** *126* (38), 11788-11789.

(19). Baldelli, S., Influence of water on the orientation of cations at the surface of a room-temperature ionic liquid: A sum frequency generation vibrational spectroscopic study. *The Journal of Physical Chemistry B* **2003,** *107* (25), 6148-6152.
(20). Neilson, G.; Adya, A. K.; Ansell, S., 8 Neutron and X-ray diffraction studies on complex liquids. *Annual Reports Section" C"(Physical Chemistry)* **2002,** *98*, 273-322.
(21). Oh, S.; Kauffmann, Y.; Scheu, C.; Kaplan, W.; Rühle, M., Ordered liquid aluminum at the interface with sapphire. *Science* **2005,** *310* (5748), 661-663.
(22). Atkin, R.; Abedin, S. Z. E.; Hayes, R.; Gasparotto, L. H.; Borisenko, N.; Endres, F., AFM and STM studies on the surface interaction of [BMP] TFSA and [EMIm] TFSA ionic liquids with Au (111). *The Journal of Physical Chemistry C* **2009,** *113* (30), 13266-13272.
(23). Bowers, J.; Vergara-Gutierrez, M. C.; Webster, J. R., Surface ordering of amphiphilic ionic liquids. *Langmuir* **2004,** *20* (2), 309-312.
(24). Fitchett, B. D.; Conboy, J. C., Structure of the room-temperature ionic liquid/SiO2 interface studied by sum-frequency vibrational spectroscopy. *The Journal of Physical Chemistry B* **2004,** *108* (52), 20255-20262.
(25). Romero, C.; Baldelli, S., Sum frequency generation study of the room-temperature ionic liquids/quartz interface. *The Journal of Physical Chemistry B* **2006,** *110* (12), 6213-6223.
(26). Rivera-Rubero, S.; Baldelli, S., Surface characterization of 1-butyl-3-methylimidazolium Br-, I-, PF6-, BF4-,(CF3SO2) 2N-, SCN-, CH3SO3-, CH3SO4-, and (CN) 2N-ionic liquids by sum frequency generation. *The Journal of Physical Chemistry B* **2006,** *110* (10), 4756-4765.
(27). Merlet, C.; Rotenberg, B.; Madden, P. A.; Salanne, M., Computer simulations of ionic liquids at electrochemical interfaces. *Physical Chemistry Chemical Physics* **2013,** *15*, 15781-15792.
(28). Frolov, A. I.; Kirchner, K.; Kirchner, T.; Fedorov, M. V., Molecular-scale insights into the mechanisms of ionic liquids interactions with carbon nanotubes. *Faraday Discussions* **2012,** *154*, 235-247.
(29). Kislenko, S. A.; Samoylov, I. S.; Amirov, R. H., Molecular dynamics simulation of the electrochemical interface between a graphite surface and the ionic liquid [BMIM][PF6]. *Physical Chemistry Chemical Physics* **2009,** *11* (27), 5584-5590.
(30). Lynden-Bell, R. M.; Frolov, A.; Fedorov, M. V., Electrode screening by ionic liquids. *Physical Chemistry Chemical Physics* **2012,** *14* (8), 2693-2701.
(31). Kislenko, S. A.; Amirov, R. H.; Samoylov, I. S., Influence of temperature on the structure and dynamics of the [BMIM][PF6] ionic liquid/graphite interface. *Physical Chemistry Chemical Physics* **2010,** *12* (37), 11245-11250.
(32). Sha, M.; Fuchun, Z.; Guozhong, W.; Haiping, F.; Chunlei, W.; Shimou, C.; Yi, Z.; Jun, H., Ordering layers of [BMIM][PF] ionic liquid on graphite surfaces: Molecular dynamics simulation. *The Journal of chemical physics* **2008,** *128*, 134504.
(33). Wang, S.; Li, S.; Cao, Z.; Yan, T., Molecular dynamic simulations of ionic liquids at graphite surface. *The Journal of Physical Chemistry C* **2010,** *114* (2), 990-995.
(34). Wang, Y.-L.; Laaksonen, A.; Lu, Z.-Y., Influence of ionic liquid film thickness on ion pair distributions and orientations at graphene and vacuum interfaces. *Physical Chemistry Chemical Physics* **2013,** *15* (32), 13559-13569.
(35). Singh, R.; Monk, J.; Hung, F. R., Heterogeneity in the Dynamics of the Ionic Liquid [BMIM+][PF6–] Confined in a Slit Nanopore. *The Journal of Physical Chemistry C* **2011,** *115* (33), 16544-16554.
(36). Li, S.; Han, K. S.; Feng, G.; Hagaman, E. W.; Vlcek, L.; Cummings, P. T., Dynamic and Structural Properties of Room-Temperature Ionic Liquids near Silica and Carbon Surfaces. *Langmuir* **2013,** *29* (31), 9744-9749.

(37). Rajput, N. N.; Monk, J.; Singh, R.; Hung, F. R., On the influence of pore size and pore loading on structural and dynamical heterogeneities of an ionic liquid confined in a slit nanopore. *The Journal of Physical Chemistry C* **2012,** *116* (8), 5169-5181.
(38). Merlet, C.; Salanne, M.; Rotenberg, B., New coarse-grained models of imidazolium ionic liquids for bulk and interfacial molecular simulations. *J. Phys. Chem. C* **2012,** *116*, 7687-7693
(39). Merlet, C.; Salanne, M.; Rotenberg, B.; A. Madden, P., Imidazolium Ionic Liquid Interfaces with Vapor and Graphite: Interfacial Tension and Capacitance from Coarse-Grained Molecular Simulations. *The Journal of Physical Chemistry C* **2011,** *115*, 16613–16618.
(40). Dou , Q.; Sha, M.; Fu, H.; Wu, G., Mass Distribution and Diffusion of [1-Butyl-3-methylimidazolium][Y] Ionic Liquids Adsorbed on the Graphite Surface at 300–800 K. *ChemPhysChem* **2010,** *11* (11), 2438-2443.
(41). Dou, Q.; Sha, M.; Fu, H.; Wu, G., Molecular dynamics simulation of the interfacial structure of [Cnmim][PF6] adsorbed on a graphite surface: effects of temperature and alkyl chain length. *Journal of Physics: Condensed Matter* **2011,** *23* (17), 175001.
(42). Feng, G.; Zhang, J.; Qiao, R., Microstructure and capacitance of the electrical double layers at the interface of ionic liquids and planar electrodes. *The Journal of Physical Chemistry C* **2009,** *113* (11), 4549-4559.
(43). Sieffert, N.; Wipff, G., Ordering of Imidazolium-Based Ionic Liquids at the alpha-Quartz(001) Surface: A Molecular Dynamics Study. *The Journal of Physical Chemistry C* **2008,** *112*, 19590–19603.
(44). Bovio, S.; Podesta, A.; Milani, P.; Ballone, P.; Del Pópolo, M., Nanometric ionic-liquid films on silica: a joint experimental and computational study. *Journal of Physics: Condensed Matter* **2009,** *21* (42), 424118.
(45). Ballone, P.; Del Pópolo, M.; Bovio, S.; Podestà, A.; Milani, P.; Manini, N., Nano-indentation of a room-temperature ionic liquid film on silica: a computational experiment. *Physical Chemistry Chemical Physics* **2012,** *14* (7), 2475-2482.
(46). Coasne, B.; Viau, L.; Vioux, A., Loading-Controlled Stiffening in Nanoconfined Ionic Liquids. *The Journal of Physical Chemistry Letters* **2011,** *2*, 1150–1154.
(47). Liu, L.; Li, S.; Cao, Z.; Peng, Y.; Li, G.; Yan, T.; Gao, X.-P., Well-ordered structure at ionic liquid/rutile (110) interface. *The Journal of Physical Chemistry C* **2007,** *111* (33), 12161-12164.
(48). Singh Payal, R.; Balasubramanian, S., Orientational Ordering of Ionic Liquids near a Charged Mica Surface. *ChemPhysChem* **2012,** *13* (7), 1764-1771.
(49). Dragoni, D.; Manini, N.; Ballone, P., Interfacial Layering of a Room-Temperature Ionic Liquid Thin Film on Mica: A Computational Investigation. *ChemPhysChem* **2012,** *13* (7), 1772-1780.
(50). Hu, Z.; Vatamanu, J.; Borodin, O.; Bedrov, D., A molecular dynamics simulation study of the electric double layer and capacitance of [BMIM][PF6] and [BMIM][BF4] room temperature ionic liquids nearcharged surfaces. *Physical Chemistry Chemical Physics* **2013,** *15*, 14234--14247.
(51). Mendonça, A. C.; Malfreyt, P.; Pádua, A. A., Interactions and Ordering of Ionic Liquids at a Metal Surface. *Journal of Chemical Theory and Computation* **2012,** *8* (9), 3348-3355.
(52). Cyr, D. M.; Venkataraman, B.; Flynn, G. W.; Black, A.; Whitesides, G. M., Functional group identification in scanning tunneling microscopy of molecular adsorbates. *The Journal of Physical Chemistry* **1996,** *100* (32), 13747-13759.
(53). Tao, F.; Bernasek, S. L., Two-dimensional self-assembly of a two-component molecular system: formation of an ordered and homogeneous molecular mesh. *Journal of the American Chemical Society* **2005,** *127* (37), 12750-12751.
(54). Bhargava, B.; Balasubramanian, S., Layering at an ionic liquid-vapor interface: A molecular dynamics simulation study of [BMIM][PF6]. *Journal of the American Chemical Society* **2006,** *128* (31), 10073-10078.

(55). Sloutskin, E.; Ocko, B. M.; Tamam, L.; Kuzmenko, I.; Gog, T.; Deutsch, M., Surface layering in ionic liquids: An X-ray reflectivity study. *Journal of the American Chemical Society* **2005,** *127* (21), 7796-7804.
(56). Perkin, S.; Crowhurst, L.; Niedermeyer, H.; Welton, T.; Smith, A. M.; Gosvami, N. N., Self-assembly in the electrical double layer of ionic liquids. *Chemical Communications* **2011,** *47* (23), 6572-6574.
(57). Kornyshev, A. A., Double-layer in ionic liquids: paradigm change? *The Journal of Physical Chemistry B* **2007,** *111* (20), 5545-5557.
(58). Lockett, V.; Sedev, R.; Ralston, J.; Horne, M.; Rodopoulos, T., Differential capacitance of the electrical double layer in imidazolium-based ionic liquids: Influence of potential, cation size, and temperature. *The Journal of Physical Chemistry C* **2008,** *112* (19), 7486-7495.
(59). El Abedin, S. Z.; Pölleth, M.; Meiss, S.; Janek, J.; Endres, F., Ionic liquids as green electrolytes for the electrodeposition of nanomaterials. *Green Chemistry* **2007,** *9* (6), 549-553.
(60). Izadi-Najafabadi, A.; Yasuda, S.; Kobashi, K.; Yamada, T.; Futaba, D. N.; Hatori, H.; Yumura, M.; Iijima, S.; Hata, K., Extracting the Full Potential of Single-Walled Carbon Nanotubes as Durable Supercapacitor Electrodes Operable at 4 V with High Power and Energy Density. *Advanced Materials* **2010,** *22* (35), E235-E241.
(61). Simon, P.; Gogotsi, Y., Materials for electrochemical capacitors. *Nature materials* **2008,** *7* (11), 845-854.
(62). Feng, G.; Qiao, R.; Huang, J.; Dai, S.; Sumpter, B. G.; Meunier, V., The importance of ion size and electrode curvature on electrical double layers in ionic liquids. *Physical Chemistry Chemical Physics* **2011,** *13*, 1152–1161.
(63). Vatamanu, J.; Hu, Z.; Bedrov, D., Increasing Energy Storage in Electrochemical Capacitors with Ionic Liquid Electrolytes and Nanostructured Carbon Electrodes. *The Journal of Physical Chemistry Letters* **2013,** *4*, 2829−2837.
(64). Singh, R.; Monk, J.; Hung, F. R., A computational study of the behavior of the ionic liquid [BMIM+][PF6−] confined inside multiwalled carbon nanotubes. *The Journal of Physical Chemistry C* **2010,** *114* (36), 15478-15485.
(65). Shim, Y.; Kim, H. J., Solvation of carbon nanotubes in a room-temperature ionic liquid. *ACS Nano* **2009,** *3* (7), 1693-1702.
(66). Shim, Y.; Kim, H. J., Nanoporous carbon supercapacitors in an ionic liquid: a computer simulation study. *ACS Nano* **2010,** *4* (4), 2345-2355.
(67). Dong, K.; Zhou, G.; Liu, X.; Yao, X.; Zhang, S.; Lyubartsev, A., Structural evidence for the ordered crystallites of ionic liquid in confined carbon nanotubes. *The Journal of Physical Chemistry C* **2009,** *113* (23), 10013-10020.
(68). Chen, S.; Wu, G.; Sha, M.; Huang, S., Transition of ionic liquid [BMIM][PF6] from liquid to high-melting-point crystal when confined in multiwalled carbon nanotubes. *Journal of the American Chemical Society* **2007,** *129* (9), 2416-2417.
(69). Dou, Q.; Sha, M.; Fu, H.; Wu, G., Melting Transition of Ionic Liquid [BMIM][PF6] Crystal Confined in Nanopores: A Molecular Dynamics Simulation. *The Journal of Physical Chemistry C* **2011,** *115* (39), 18946-18951.
(70). Abraham, M. H.; Zissimos, A. M.; Huddleston, J. G.; Willauer, H. D.; Rogers, R. D.; Acree, W. E., Some novel liquid partitioning systems: Water-ionic liquids and aqueous biphasic systems. *Industrial & engineering chemistry research* **2003,** *42* (3), 413-418.
(71). Sheldon, R., Catalytic reactions in ionic liquids. *Chemical Communications* **2001,** (23), 2399-2407.
(72). Dupont, J.; de Souza, R. F.; Suarez, P. A., Ionic liquid (molten salt) phase organometallic catalysis. *Chemical Reviews* **2002,** *102* (10), 3667-3692.

(73). Oldham, K. B., A Gouy–Chapman–Stern model of the double layer at a (metal)/(ionic liquid) interface. *Journal of Electroanalytical Chemistry* **2008,** *613* (2), 131-138.
(74). Islam, M. M.; Alam, M. T.; Ohsaka, T., Electrical double-layer structure in ionic liquids: a corroboration of the theoretical model by experimental results. *The Journal of Physical Chemistry C* **2008,** *112* (42), 16568-16574.
(75). Bohinc, K.; Kralj-Iglič, V.; Iglič, A., Thickness of electrical double layer. Effect of ion size. *Electrochimica Acta* **2001,** *46* (19), 3033-3040.
(76). Henderson, D.; Lamperski, S., Simple Description of the Capacitance of the Double Layer of a High Concentration Electrolyte. *Journal of Chemical & Engineering Data* **2011,** *56* (4), 1204-1208.
(77). Sha, M.; Wu, G.; Dou, Q.; Tang, Z.; Fang, H., Double-layer formation of [BMIM][PF6] ionic liquid triggered by surface negative charge. *Langmuir* **2010,** *26* (15), 12667-12672.
(78). Min, Y.; Akbulut, M.; Sangoro, J. R.; Kremer, F.; Prud'homme, R. K.; Israelachvili, J., Measurement of forces across room temperature ionic liquids between mica surfaces. *The Journal of Physical Chemistry C* **2009,** *113* (37), 16445-16449.
(79). Fukushima, T.; Kosaka, A.; Ishimura, Y.; Yamamoto, T.; Takigawa, T.; Ishii, N.; Aida, T., Molecular ordering of organic molten salts triggered by single-walled carbon nanotubes. *Science* **2003,** *300* (5628), 2072-2074.
(80). Fukushima, T.; Aida, T., Ionic liquids for soft functional materials with carbon nanotubes. *Chemistry-A European Journal* **2007,** *13* (18), 5048-5058.
(81). Pinilla, C.; Del Pópolo, M. G.; Lynden-Bell, R. M.; Kohanoff, J., Structure and dynamics of a confined ionic liquid. Topics of relevance to dye-sensitized solar cells. *The Journal of Physical Chemistry B* **2005,** *109* (38), 17922-17927.
(82). Rivera-Rubero, S.; Baldelli, S., Surface spectroscopy of room-temperature ionic liquids on a platinum electrode: A sum frequency generation study. *The Journal of Physical Chemistry B* **2004,** *108* (39), 15133-15140.
(83). Aliaga, C.; Baldelli, S., Sum frequency generation spectroscopy and double-layer capacitance studies of the 1-butyl-3-methylimidazolium dicyanamide-platinum interface. *The Journal of Physical Chemistry B* **2006,** *110* (37), 18481-18491.
(84). Perkin, S., Ionic liquids in confined geometries. *Physical Chemistry Chemical Physics* **2012,** *14*, 5052–5062.
(85). Kowsari, M.; Alavi, S.; Ashrafizaadeh, M.; Najafi, B., Molecular dynamics simulation of imidazolium-based ionic liquids. I. Dynamics and diffusion coefficient. *The Journal of chemical physics* **2008,** *129*, 224508.
(86). Gao, L.; McCarthy, T. J., Ionic liquids are useful contact angle probe fluids. *Journal of the American Chemical Society* **2007,** *129* (13), 3804-3805.
(87). Krumpfer, J. W.; Bian, P.; Zheng, P.; Gao, L.; McCarthy, T. J., Contact angle hysteresis on superhydrophobic surfaces: an ionic liquid probe fluid offers mechanistic insight. *Langmuir* **2011,** *27* (6), 2166-2169.
(88). Millefiorini, S.; Tkaczyk, A. H.; Sedev, R.; Efthimiadis, J.; Ralston, J., Electrowetting of ionic liquids. *Journal of the American Chemical Society* **2006,** *128* (9), 3098-3101.
(89). Paneru, M.; Priest, C.; Sedev, R.; Ralston, J., Static and dynamic electrowetting of an ionic liquid in a solid/liquid/liquid system. *Journal of the American Chemical Society* **2010,** *132* (24), 8301-8308.
(90). Restolho, J.; Mata, J. L.; Saramago, B., Electrowetting of ionic liquids: Contact angle saturation and irreversibility. *The Journal of Physical Chemistry C* **2009,** *113* (21), 9321-9327.
(91). Li, H.; Paneru, M.; Sedev, R.; Ralston, J., Dynamic Electrowetting and Dewetting of Ionic Liquids at a Hydrophobic Solid–Liquid Interface. *Langmuir* **2013,** *29* (8), 2631-2639.

(92). Paneru, M.; Priest, C.; Sedev, R.; Ralston, J., Electrowetting of aqueous solutions of ionic liquid in solid– liquid– liquid systems. *The Journal of Physical Chemistry C* **2010,** *114* (18), 8383-8388.
(93). Dubois, P.; Marchand, G.; Fouillet, Y.; Berthier, J.; Douki, T.; Hassine, F.; Gmouh, S.; Vaultier, M., Ionic liquid droplet as e-microreactor. *Analytical chemistry* **2006,** *78* (14), 4909-4917.
(94). Batchelor, T.; Cunder, J.; Fadeev, A. Y., Wetting study of imidazolium ionic liquids. *Journal of colloid and interface science* **2009,** *330* (2), 415-420.
(95). Cione, A. M.; Mazyar, O. A.; Booth, B. D.; McCabe, C.; Jennings, G. K., Deposition and Wettability of [BMIM][triflate] on Self-Assembled Monolayers. *The Journal of Physical Chemistry C* **2009,** *113* (6), 2384-2392.

6. Asymmetric Wetting Behavior of an Ionic Liquid on Electrically Charged Graphene Surfaces

6.1. Introduction

One way to change the wetting properties of a surface is by using electrowetting (EW), where an external electrical potential is applied between the solid and the liquid.[1-2] Presence of charged molecules (cations and anions) in the ILs make them a very good candidate to be used as the EW agents.[3-4] Even there have been extensive research focused on the different aspects of EW phenomenon, many questions are still open especially in the micro- and the nanoscales in this field. Ability to control different properties of the ILs by changing the size of the ions, distribution of the charges on the ions and chemical structure of the ions makes the ILs a very good candidate to study different aspects of EW at the molecular level. However, studying the wetting properties at the nanoscale by using experimental techniques is very challenging, and molecular dynamics (MD) simulations can be used as a powerful tool to overcome the experimental limitation at small scales. The decrease in the contact angle by applying an external voltage in the EW experiments has been mainly explained by the adsorption of the opposite charges of the liquid to the surface of the solid (formation of the electric double layer (EDL) at the interface). The change of the contact angle with the external voltage can be expressed by the Young-Lippmann equation as following:

$$\cos\theta_e = \cos\theta_0 + \frac{1}{2\gamma_{lv}}\overline{C}V^2$$

where θ_e and θ_0 are the contact angle at V and zero voltages, respectively, $\overline{C}$ is the overall interfacial capacitance per unit area and γ_{lv} is the liquid-vapor surface tension. In the case of EW on a dielectric where an insulating film is placed between the liquid and the electrode, $\overline{C}$ is mainly defined by the capacitance of the insulating layer, and the effect of the EDL capacitance is usually neglected. However, experimental results of electrolyte solutions and ILs have shown that specific ion adsorption on the surface at zero voltage leads to asymmetric change of the

contact angle with the surface polarity. Therefore, the EDL at the solid-liquid interface can influence the change of the contact angle by applying an external voltage.

By using MD simulations, several authors[5-7] have reported an asymmetric behavior for the contact angle of water with the electric field direction. The dependence of the contact angle of water to the polarity of the electric field was explained by the different orientations and the average number of hydrogen bonds of the molecules at the interfaces, which lead to difference in the interfacial tensions of the liquid.[5] Simulation results showed that in the case of parallel electric fields with the surface the trailing and leading contact angles would be different depending on the field strength. With an increase in the field strength from zero, the difference between the leading and the trailing contact angles increases and then start to decrease, and it disappears at high field strength.[7]

Raj et al.[8] have investigated experimentally the effect of the ions size on dielectric failure (charge penetration) which frequently occurs in EW of aqueous salt solutions. Results indicated that, making the ions larger prevent them to penetrate into the dielectric and therefore increase the performance of the EW setup. In the case of ILs, since the size of cations and anions are different, one could expect asymmetry in different interfacial properties of the liquid with the polarity of the surface. MD simulations have already shown asymmetric changes of the number and the volume charge density of the ions, the electric potential drop and the capacitance of EDL with the surface polarity.[9-11] It is very interesting to see how these asymmetries are reflected in the change in the contact angle in EW.

Although, a lot of researches have been done on the interfacial properties of ILs at the molecular level, the wetting properties of ILs have not been discussed so much to date. Cione et al. reported so far the only MD simulation on the wetting of ILs, where they have looked at the equilibrium contact angle of [BMIM][triflate] droplet consisting of 100 ion pairs on a CH_3- and OH-terminated silica. Simulation results showed more spreading of the droplet on the hydrophilic substrate.

Paneru et al.[12] reported an experimental EW study for a droplet of [BMIM][BF_4] IL at different DC voltages (±50, ±100, ±150 and ±200 V). Results showed that at low voltages (±50 and ±100 V) the base area of the droplet is independent of the sign of the voltage, while an asymmetry was observed at high voltages (±150 and ±200 V): the droplet spreads more (larger base area) for negative DC voltages where the cations are adsorbed on the surface.[12]

In this chapter, we study the change in the contact angle of [BMIM][BF_4] IL on graphene with positive and negative surface charges by MD simulations, and main sources for possible asymmetric behavior of the contact angle in EW of ILs are discussed.

6.2. Morphology and Methods

Force field parameters for atomistic simulation of [BMIM][BF_4] are taken from work of Chaban and co-workers[13] where the total charge on the cation and the anion has been chosen to be 0.78e and −0.78e, respectively, to account for the polarization of the ions and accurately describe the dynamic properties of the IL. The cutoff radius for the non-bonded interactions in the atomistic simulations is 1.4 nm. Since long simulations are needed to reach the equilibrium state for the contact angle measurement, the simple coarse-grained (CG) model developed by Merlet et al.[22] is used for the wetting simulations. This allows us to perform MD simulation of bigger systems and for longer time, while keeping all different properties of the IL as close as possible to the experimental data.

A schematic view of the correspondence between atoms and the CG beads for [BMIM][BF_4] is given in Figure 6.1a and b. The bead A is representing the anion (BF_4), while the cation is split into three beads: the methyl group of the imidazolium ring (bead H), the imidazolium ring (bead R) and the alkyl tail (bead T). Our mapping scheme for graphene surface is taking three carbon atoms as one bead (bead C3). The center of the bead is located at the center of the rings, as indicated in Figure 6.1c.

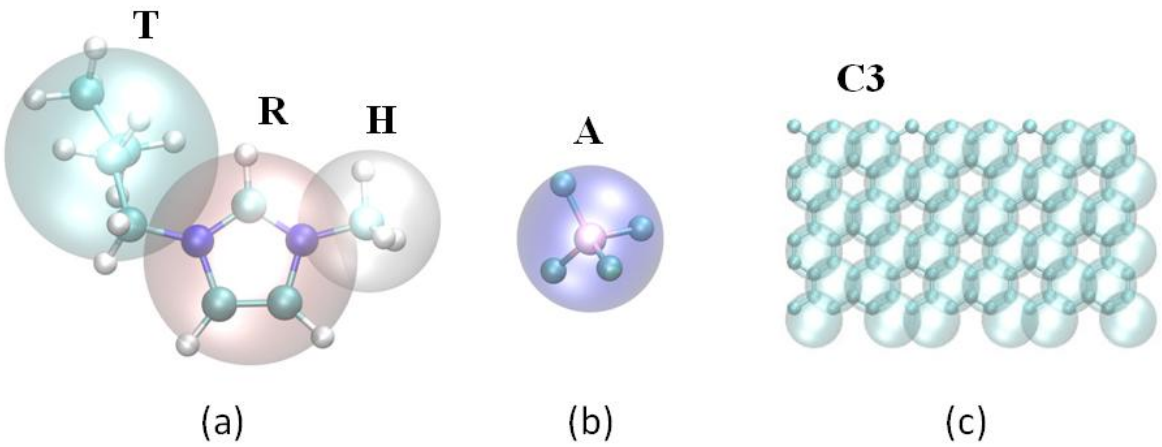

Figure 6.1. . Schematic CG mapping scheme of (a) cation, (b) anion and (c) graphene.

In the CG model of Merlet et al.[22] the intramolecular degrees of freedom in the cation are frozen (H-R and R-T bonds are set to 0.27 nm and 0.38 nm respectively, and the H-R-T angle is fixed at 116°). The distributions of H-R and R-T bonds and H-R-T angle calculated from the atomistic

simulation shown in Figure 6.2 indicate a wide distribution especially for the R-T bond and the H-R-T angle. To better reproduce the atomistic structure of the IL at the CG level the interaction parameters of Merlet et al.[22] are refined here to have a flexible model for the cation. The interaction potentials are obtained by the iterative Boltzmann inversion[24] method. In this method the CG potentials are iteratively corrected to reproduce the atomistic bond and angle distributions. The iterative procedure is done using VOTCA package.[25] In Figure 6.2, the intramolecular distributions from atomistic simulations (solid line) are compared with those obtained from the CG model (filled circles). Results show that the atomistic and the CG model have same intramolecular distribution for the cation.

The Lennard-Jones parameter ε for the beads A and T are refined manually to obtain the best agreement of density and diffusion coefficient with the corresponding experimental data. All the non-bonded interaction parameters of the CG model are reported in Table 6.1.

Table 6.1. Force-field parameters for the CG model of [BMIM][BF_4] and graphite.

interaction site	M (g/mol)	σ (nm)	ε (kJ/mol)	q (e)
A	86.81	0.451	3.44	-0.78
H	15.04	0.341	0.36	0.1578
R	67.07	0.438	2.56	0.4374
T	57.12	0.504	2.33	0.1848
C3	36.00	0.4788	0.4937	-

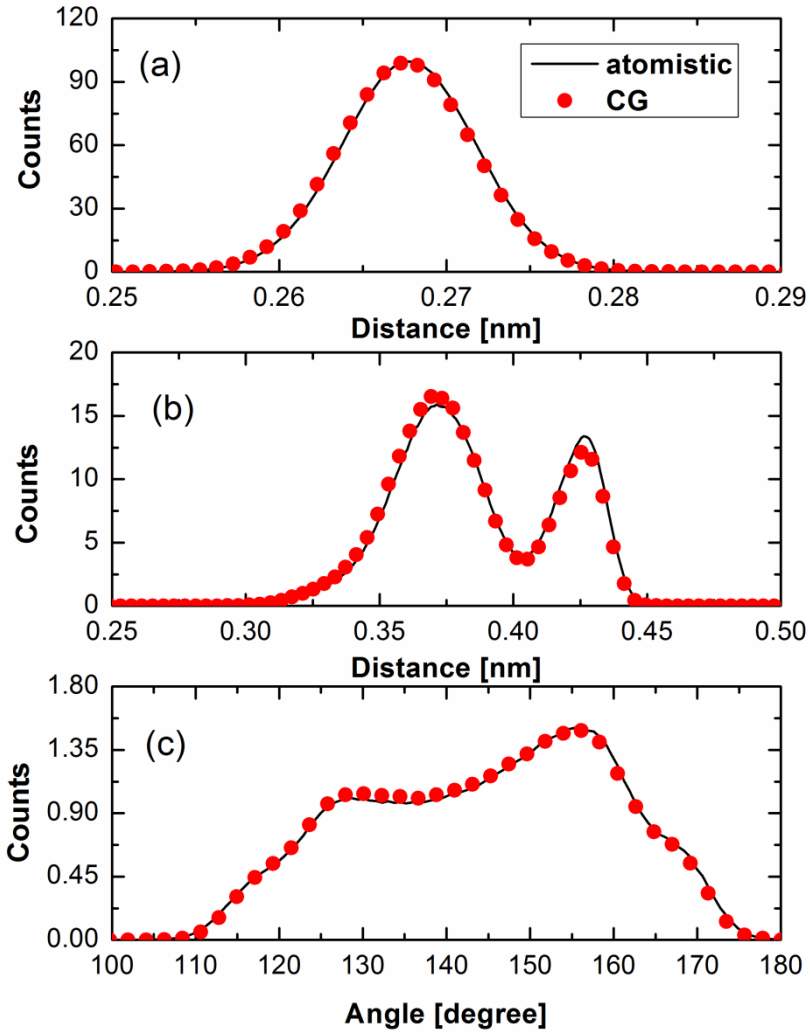

Figure 6.2. Distribution of (a) H-R, (b) R-T bond lengths and (c) H-R-T angle obtained from atomistic and CG simulations at 350 K.

Since the cutoff for the non-bonded interaction in the CG simulations is 1.6 nm, five graphene layers are used here to model the graphite surface. Same approach, as we used recently for water-graphene system, is used here to develop the interaction parameters between the IL and the graphite surface.[26] The LJ parameters for C3 are determined as ε_{C3} = 0.4937 kJ mol^{-1} and σ_{C3} = 0.4788 nm to match the experimental contact angle for [BMIM][BF_4] on graphite (49°).[27] In the rest of the paper, all the simulations are done on a single graphene layer with the same interaction parameters as graphite.

To measure the macroscopic contact angle of [BMIM][BF_4] on graphene a cylindrical droplet consist of 2000 ion pairs (with a diameter of *ca.* 13.5 nm) is placed on the surface. Periodic boundary conditions are applied such that the droplet is infinite in x-direction. The dimensions

of the simulation box are 5.16 nm × 54.95 nm × 45 nm. The advantage of simulating a cylindrical droplet is that it mimics the situation where the droplet radius is infinite, thus there is no contribution of line tension to the contact angle. The droplet spreads on the uncharged surface with the initial contact angle of 180°, and reaches the equilibrium state during 150 ns. Then the simulation is extended for 50 ns to calculate the average contact angle. To test how the size of the system influencing the contact angle, a droplet of 6000 ion pairs (with a diameter of *ca.* 21 nm) is simulated on graphene and no change in the contact angle is observed compared to the droplet with 2000 ions pairs.

For the simulation of droplet on charged surfaces, we construct eight independent systems, and the surface charge densities are set to ±6.5, ±5.0, ±3.5 and ±1.5 μc/cm^2, respectively. Corresponding charges for C3 bead are ±0.0319, ±0.0245, ±0.0172 and ±0.0073 *e*, respectively. To make the system neutral in each case, an oppositely charged graphene layer is used at distance 10 nm below the surface, where the droplet is spreading. The final configuration of the droplet on the uncharged surface is used for the simulation of different charged surfaces. Simulations at different surface charge densities are performed for 350 ns, where the last 200 ns are used to calculate the average contact angle.

To compute the diffusion coefficient and the density, a NPT simulation, at T=350 K and P=1.0 bar, with a box consisting of 1331 ion pairs is performed for 30 ns to equilibrate the system, and then the equilibrated box is used for NPT simulation of 20 ns for production run. The final dimensions of the box for the bulk simulation are 7.53 nm × 7.53 nm × 7.53 nm. The temperature and the pressure are kept constant with the Nose-Hoover thermostat[14-15] and the Parrinello-Rahman barostat,[16] respectively. The timestep is 2 fs.

In order to calculate the liquid-vapor surface tension using MD, a simulation of a liquid-vapor interface is carried out at T=350 K. The box size in the *z*-direction is set to 50 nm,[18] and the simulation under NVT conditions is run for 100 ns. As it mentioned in Chapter 2, the surface tension can be calculated using the pressure components as following:[19]

$$\gamma_{lv} = \frac{L_z}{4}(2P_{zz} - (P_{xx} + P_{yy})) \qquad (6\text{-}1)$$

where L_z is the box size perpendicular to the interface. Since the Lennard-Jones interactions are truncated at the cutoff radius a tail correction is needed to include the effect of the long-range interactions. To calculate the tail correction, the density profile of the liquid-vapor interface along z ($\rho(z)$) is fitted to a hyperbolic tangent function defined as following:

$$\rho(z) = \frac{1}{2}(\rho_l + \rho_v) - \frac{1}{2}(\rho_l - \rho_v)\tanh[(z - z_0)/d] \quad (6\text{-}2)$$

where ρ_l, ρ_v, z_0 and d are the fitting parameters. The fitting has been done on both interfaces and the average value is taken. Then, using the fitting parameters obtained from eq. (6-2) the correction term to the surface tension can be calculated by:[20-21]

$$\gamma_{tail} = \int_0^1 \int_{r_c}^{\infty} 12\pi(\rho_l - \rho_v)^2 \coth(\frac{2rs}{d})(\frac{3s^2 - s}{r^3})drds \quad (6\text{-}3)$$

An excellent agreement between the simulation results (sum of the surface tension calculated with eq. (6-1) and the tail correction using eq. (6-3)) with different models (atomistic and CG) and the experimental data is shown in Table 6.2.

Table 6.2. Atomistic, CG and experimental values of density, diffusion coefficient (cations and anions) and surface tension at T=350K.

	Density ($kg.m^{-3}$)	**D_- ($\times 10^{-11}$ $m^2.s^{-1}$)**	**D_+ ($\times 10^{-11}$ $m^2.s^{-1}$)**	**Surface tension (mN/m)**
Atomistic	1158.5 (±0.2)	9.9 (± 0.8)	10.3 (± 0.9)	36.9 (± 1.8)
CG (Merlet et al.) [a]	1175	10.1	11.3	33.8 (T=400 K)
CG (refined force fields)	1166.7 (± 0.1)	8.3 (± 0.3)	12.9 (± 0.3)	40.4 (± 0.7)
Experiment [b]	1167	9.5	9.2	41.6 (T=341 K)

[a] T=348 K, Ref. 22.

[b] T=348 K, Ref. 23.

6.3. Results and Discussion

Since no atomistic details on the wetting of ILs on graphene have been reported so far, before discussing the simulation results for the charged surfaces, structure properties of an equilibrated droplet on the uncharged grapheme surface are presented in the following section.

6.3.1. Droplet on uncharged surface

The interaction parameters between all the beads of the IL and bead C3 of the surface are optimized at the same time to reproduce the experimental contact angles of 49.4°. Since the graphite surface we use in our simulations is fixed, instead of tuning several ε_{C3X}, Lennard-Jones

parameter where X is any bead of the IL, we tune just one parameter, namely the ε_{C3C3} (which will be in the following named ε_{C3}). We are of course aware that this procedure holds just in the case of rigid surfaces. By using the Lorentz-Berthelot mixing rules all different ε_{C3X}, that describe the interaction of the IL and the surface, are generated. A cylindrical drop of 2000 ions pairs is simulated on the graphite with different ε_{C3} and a linear interpolation is used to find the parameter for which the contact angle matches the experimental value. Simulating a droplet on a single graphene layer with the same interaction parameters leads to equilibrium contact angle of 74.7°, which is 25.3° higher than graphite.

Number densities: It has been already shown by experiment and MD simulations that ILs at the solid-liquid interface displays a layered structure.[29-35] To investigate the cation and the anion structure in the droplet and at the interface with graphene, the ions density profile perpendicular to the surface are calculated in a cube with a base area of 5.16 nm × 1.5 nm along the centerline of the droplet with a resolution in the z-direction (perpendicular to the surface) of 0.005 nm. Figure 6.3 shows the density profiles perpendicular to the surface for the different beads of the cation (bead H, R and T) and bead A of the anion. As it is shown in the figure, layering of the IL at the centerline of the droplet can observed up to distances around 2.0 nm from the surface, which is similar to the previous simulation of ILs on graphite.[30, 34-36] At distances beyond 2.0 nm the number densities are converged to the bulk values. At the liquid-vacuum interface also a slightly higher density of the ions compared to the bulk value was observed. The separation of the peaks at liquid-vapor interface shows that surface of the droplet is covered by the alkyl chains of the cations.

Figure 6.3 shows that the bead H is at the closest distance to the graphene surface compared to the other beads, while the imidazolium rings and the alkyl tail are standing at the same distance to the surface (or in other word no separation of polar and nonpolar domains at IL-solid interface), which distinguishes the IL-solid interface from the IL-vapor interface.[37-38] The results show that the R-T bond lie rather parallel to the graphene surface at the IL-solid interface. The orientation of R-T bonds will be discussed in the next section.

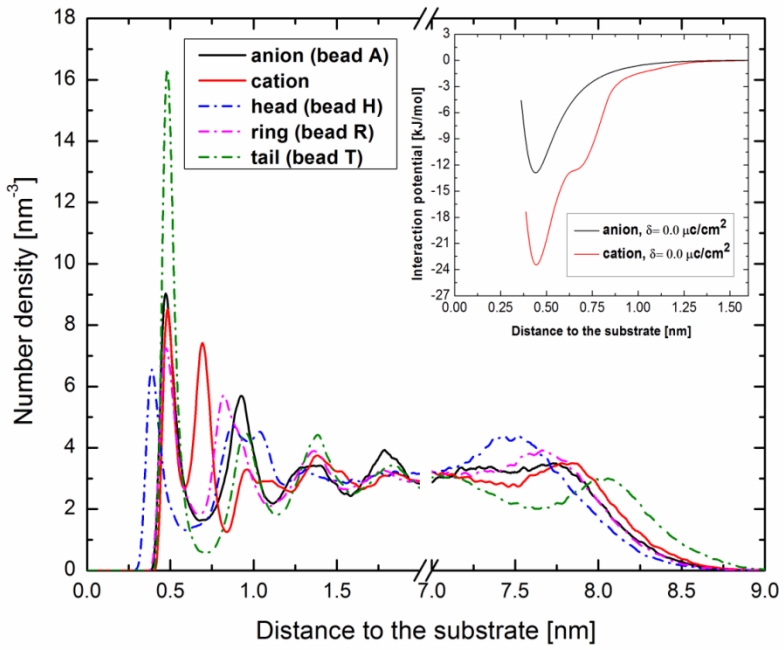

Figure 6.3. The number density profiles of the anions (bead A), center of mass of the cations, imidazolium ring (bead R), alkyl tail (bead T) and head group (bead H) of the cations. The inset shows the averaged interaction potential per ions with the graphene surface as a function of distance to the surface.

IL-surface interaction potential: As it can be seen in Figure 6.3, there is a high tendency for the cations to be adsorbed to the surface. To understand the reason for dominant adsorption of cations on graphene, the averaged interaction potential per ions (cation and anion) along the centerline of the droplet up to the range of the IL-surface interaction are calculated in the inset of Figure 6.3. The results show that the interaction potential for the cation and the anion has a minimum around 0.43 nm (corresponds to the first maximum in the ions number density), and the value of the interaction potential for the cations at the minimum is almost twice the corresponding value for the anions. Therefore, the higher number density of the cations than the anions at the interfacial region is due to the stronger van der Waals interaction with the surface. The interaction potential of the cation shows a small shoulder around 0.7 nm, since as we will discuss in the next section there are two favourable orientations for the cations near to graphene.

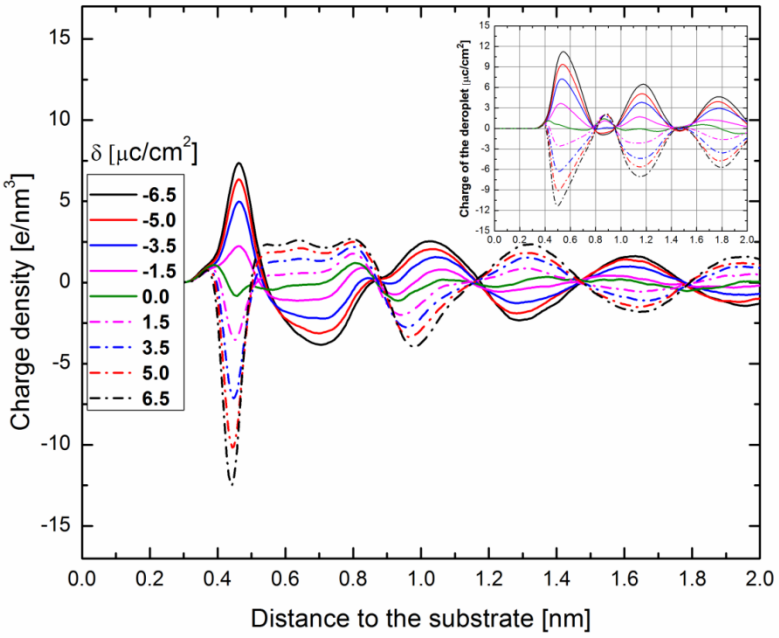

Figure 6.4. Volume charge density of the [BMIM][BF_4] droplet along its centerline on graphene with different surface charge densities (δ). Inset shows the integral of the charge density (accumulated charge on the surface) versus distance from the surface.

Charge density: The charge density of the droplet on the uncharged surface along the centerline and at the solid-liquid interface is shown in Figure 6.4 (black line). The oscillation in the volume charge density is extended over *ca.* 1.5 nm from the surface. Due to the layering of the cations and anions at the interface the charge density shows an oscillatory behaviour.

Orientational ordering: To understand more the interfacial structure of [BMIM][BF_4] droplet on graphene, the orientations of the R-T bonds in the center of the droplet along the normal to the surface is investigated. The order parameter of the cations can be defined by using the second Legendre polynomial function as following:

$$\langle P_2(\theta)\rangle = \left\langle \frac{1}{2}\left(3\cos^2\theta - 1\right)\right\rangle \qquad (6\text{-}4)$$

where θ is the angle between bond R-T and the surface normal z. $P_2(\theta)$ changes between 1 and −0.5. For the parallel vectors $P_2(\theta)$ value is equal to 1, while a value of −0.5 representing two vectors which are perpendicular . The average values $<P_2(\theta)>$ at the solid-liquid and the

liquid-vapor interfaces are shown in Figure 6.5a and b, respectively. Results show that the cations next the graphene surface are oriented such that the corresponding R-T bond is parallel to the surface. At slightly larger distances from the surface, the bond R-T stands perpendicular to the surface. Since the number density of bead T in the first layer is higher than bead R, one could conclude that some of the cations are standing such that their tail belong to the first layer of bead T, while their ring are in the second layer for bead R. For these cations, R-T bonds are perpendicular to the surface. At the IL-vapor interface, R-T bonds are tilted with the angle of around 50° relative to the liquid-vapor interface, with rings pointed into the droplet.

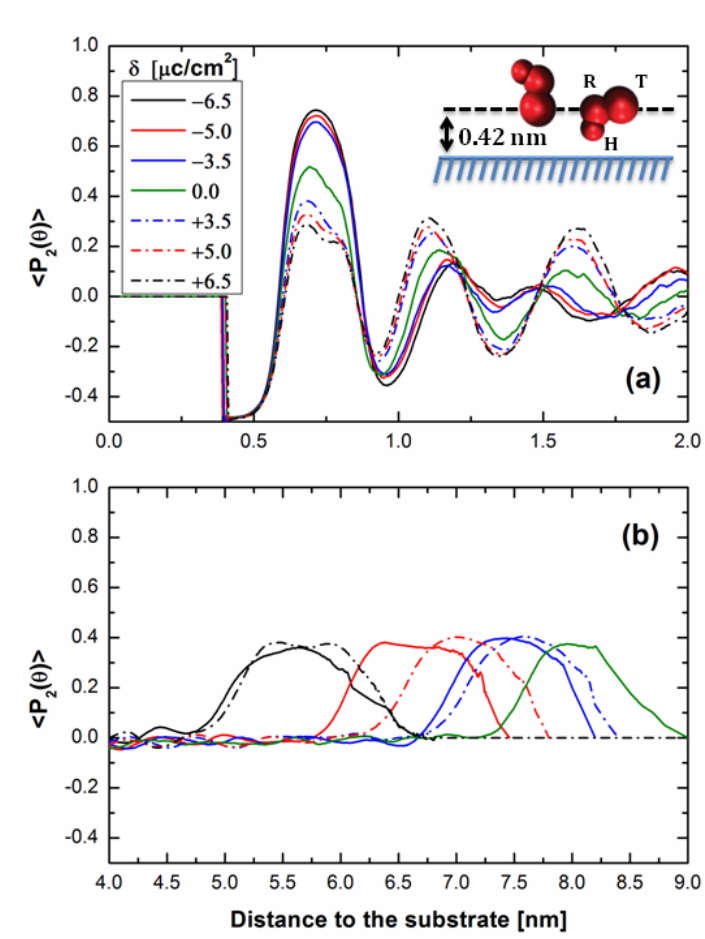

Figure 6.5. Orientational ordering of R-T bond along the normal to the graphene surface with different charge densities (δ) at the center of the droplet and at the solid-liquid (a) and the liquid-vapor (b) interfaces. The center of the R-T bond is used to define its distance to the substrate.

6.3.2. Droplet on charged surface

After equilibrating the droplet on the uncharged surface, the surface is charged with eight different charge densities from -6.5 μc/cm^2 to +6.5 μc/cm^2, and the simulations are continued for 350 ns for further equilibration. Different wetting properties of the IL on the charged surfaces are discussed in the following.

Contact angle: The average contact angle over last 200 ns for different charge densities are reported in Table 6.3 and also plotted in Figure 6.6. Simulation results indicate that, with increasing the surface charge density (positive or negative) the contact angle decreases compared to the uncharged surface. The decrease in the contact angle can be understood through analysing the Young equation in terms of surface energy by taking a film in contact with the surface and measuring the solid-liquid interaction energies. The interaction energy is calculated by summing the value over all the molecules in the range of the potential. Evaluation of the total interaction energies for different charged surfaces, as they are reported in Table 6.3 and plotted in Figure 6.7, shows that by increasing the charge density of the surface the electrostatic interaction between the solid and the liquid increases, which leads to gaining the energy by system with spreading. Therefore, the droplet spreads more by enhancing surface charge density.

For the positively charged surfaces the anions will have a strong attractive Coulomb interaction with the surface, while for the negatively charged surfaces cations are the favourable ions to interact with the surface. Even the size of the cations and anions are quite different, the total IL-graphene interaction is same for the positively and the negatively charged surfaces, irrespective of the sign of surface charge density.

Table 6.3. The surface charge densities, the corresponding contact angle and the total (LJ+Coulomb) IL-graphene interaction energy.

surface charge density (μc/cm^2)	θ (degree)	LJ+ Coulomb [BMIM][BF_4]-graphene (kJ/mol/nm^2)
-6.5	37.4 (± 1.0)	-78.02 (± 2.26)
-5	50.6 (± 0.7)	-64.75 (± 2.16)
-3.5	62.5 (± 1.0)	-54.41 (± 1.59)
-1.5	70.1 (± 0.7)	-46.48 (± 0.98)
0	74.7 (± 0.7)	-44.99 (± 0.71)
1.5	72.9 (± 0.8)	-47.42 (± 0.99)
3.5	67.1 (± 0.7)	-55.93 (± 1.51)
5	57.6 (± 0.9)	-66.24 (± 2.01)
6.5	37.3 (± 1.0)	-79.86 (± 2.55)

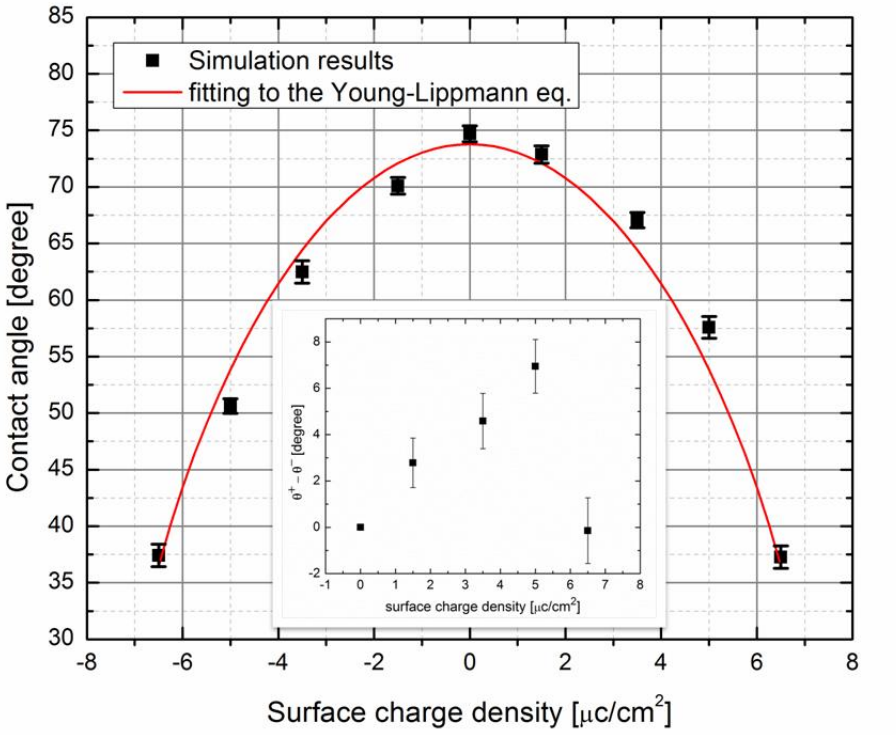

Figure 6.6. Contact angle of a cylindrical droplet with 2000 ions pairs on graphene with different charge densities. The solid line is the fit to the equation $\cos(\theta) = \cos(\theta_0) + b\delta^2$ ($\cos(\theta_0)$ and b are the fitting parameters, and equal to 0.28 and 0.0124 $(\mu c/cm^2)^{-2}$, respectively. The inset shows the difference in the contact angle on positive and negative charged surfaces.

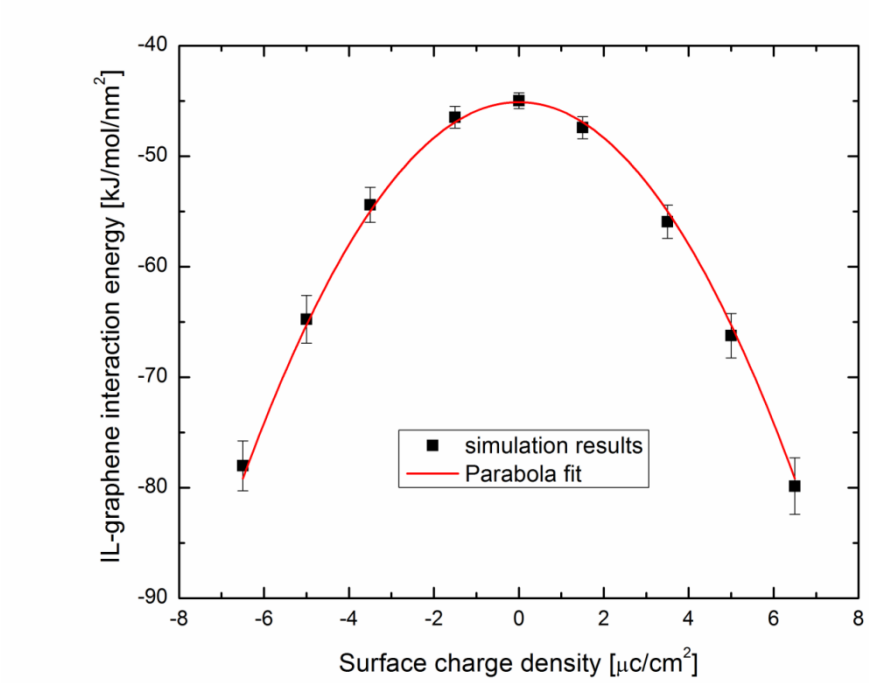

Figure 6.7. The total (LJ+Coulomb) [BMIM][BF_4]-graphene interaction energy at different charged densities. The solid line shows a parabola fit to the data.

The inset of Figure 6.6 shows the deference between the contact angle on the positively and the negatively charged surfaces. As it is shown in the figure, with increasing the surface charge density a difference appear in the contact angle and it reaches 6.9° ± 1.1° on the surfaces with +5.0 and -5.0 μc/cm^2 charges. Then, the difference drops very fast back to zero on the surfaces with +6.5 and -6.5 μc/cm^2 charges.

The total solid-liquid interaction energy (sum of the Coulomb and the van der Waals interaction of all the ions in the range of the potential), as it is shown in Figure 6.7, has a symmetric behaviour (within the error bars) with charge of the surface, and cannot explain the asymmetric behaviour of the contact angle.

The Young-Lippmann equation: To estimate the values of the contact angles at different surface charge densities by the using the Young-Lippmann equation 3993 ions pairs are confined between two grapehene layers with a wall distance of 19.54 nm. The wall distance is chosen somehow to reproduce the bulk density of the IL at the center of the confinement. The size of simulation box in z direction is set to 100 nm to exclude the effect of the periodic images. The dimensions of the box in x and y directions are 8.118 and 8.094 nm, respectively. The lower graphene layer is charged negatively, while the upper one carries the opposite charge. The electrical potential distribution ($\phi(z)$) across the channel is calculated by determining the volume charge density of the IL as a function of distance to the wall ($\rho(z)$) and using the Poisson equation:

$$\varphi(z) = -\frac{\sigma}{\varepsilon_0} z - \frac{1}{\varepsilon_0} \int_0^z dz' \int_0^{z'} \rho_e(z'') dz'' \qquad (6\text{-}5)$$

The position of the zero potential is chosen to be on the lower graphene surface. Figure 6.8 shows the distribution of the electrical potential across the channel at the different surface charge densities. Due to the oscillations of the volume charge density at the interface, the electrical potential shows also the same behaviour. By subtracting the potential on the walls at different surface charge densities from the corresponding value at the middle of the channel, the potential drop at the EDL is calculated. The results for the different surface charge densities are reported in Table 6.4. As it is shown in the table, a positive value of 0.12 V is found for the surface at the zero charge (potential of zero charge (PZC)), in agreement with the previous simulations. The non-zero value for the potential drop at the zero charge is due to the higher adsorption of the cations at the interface compared to the anions, as discussed in the previous section.

With increasing the surface charge density to the positive or negative values the electrical potential drop at the interface also increases. To calculate the effective capacitance of the EDL, the potential drop at the different charge densities is subtracted from PZC. Then by using the following equation the capacitance at different charge densities is calculated:

$$C_{eff} = \frac{\sigma}{\varphi_{EDL}(\sigma) - \mathrm{PZC}} \qquad (6\text{-}6)$$

Results for the positively and the negatively charged surfaces are reported in Table 6.4. As it can be seen, C_{eff} at low surface charge densities ($\leq$3.5 μc/cm^2) are the same on positively and negatively charged surfaces, but at higher surface charges the EDL capacitance on the positively charged surfaces are bigger. Such behavior of the EDL capacitance has been also observed previously in the atomistic simulation of several ILs.. Feng et al. have developed a theoretical model to describe the change in the structure of the cations and the anions at the interface upon charging the surface. They have shown that the higher value of the EDL capacitance on the positively charged surfaces is due to the fact that on these surfaces the adsorption of the anions (counter-ions) is the dominant factor to form the EDL, while on the negatively charged surfaces the deduction of the anions (co-ions) is the leading factor. The different mechanism of EDL formation according to Feng's model leads to different EDL capacitances.

By substituting the values of the EDL capacitance and the electrical potential drop at the interface in the Young-Lippmann equation given by:

$$\cos\theta = \cos\theta_0 + \frac{1}{2\gamma_{lv}} C_{eff} (\varphi_{EDL} - PZC)^2 \qquad (6\text{-}7)$$

one can calculate the contact angle at the different surface charge densities. The contact angle values predicted by eq. (6-7) and from the droplet simulations are reported in Table 6.4. Results show that according to the Young-Lippmann equation the change in the contact angle is symmetric on the positively and the negatively charged surfaces up to ±3.5 μc/cm^2, and at the higher surface charges the complete wetting of the IL on graphene is happening. Such behavior is not consistence with the droplet simulations, where a non-zero value for the contact angle is found even at the surface charges equal to ±6.5 μc/cm^2, and a difference in the contact angle of around 6 degrees is observed at ±5.0 μc/cm^2. The deviation of the Young-Lippmann predictions from the droplet simulations is due to not taking into account the contribution of the contact-line on the equilibrium contact angle, which will be discussed in the next sections.

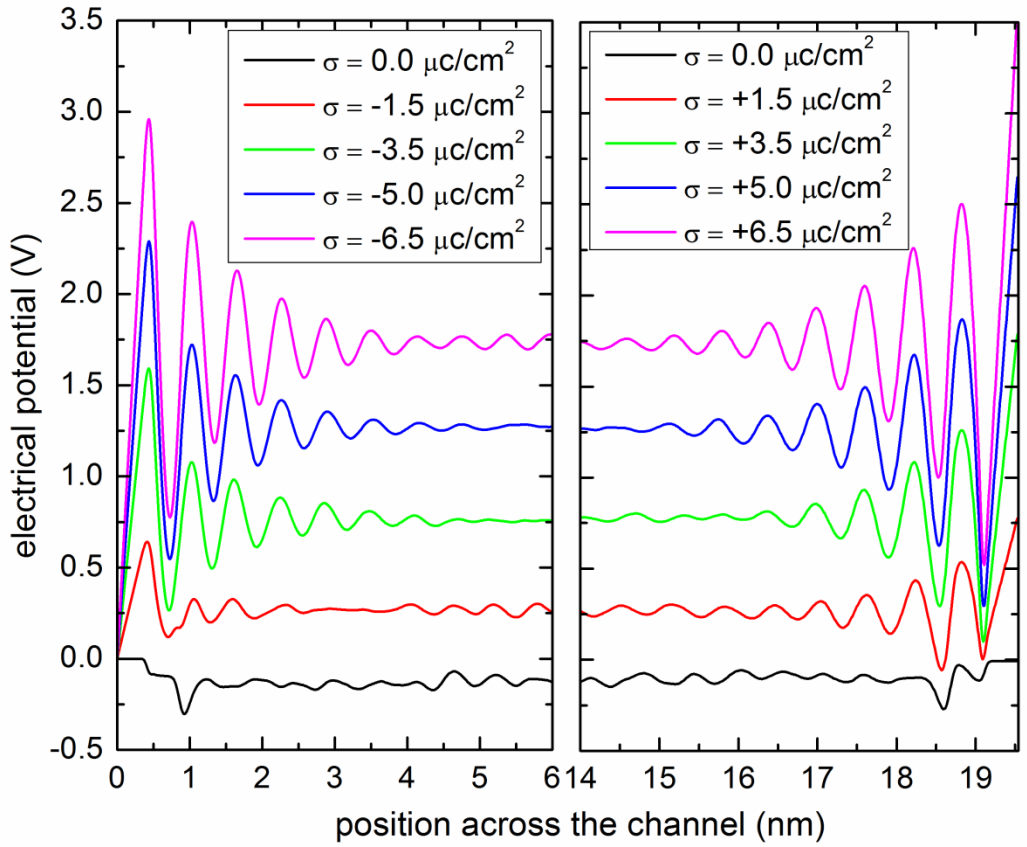

Figure 6.8. Distribution of the electrical potential across the channel at different surface charge densities.

Table 6.4. The electrical potential and the effective capacitance of the electrical double layer at different surface charge densities, corresponding prediction of the contact angle using the Young-Lippmann equation and the results from the droplet simulations.

δ (μc/cm²)	ϕ_{EDL} (V)	(ϕ_{EDL} -PZC) (V)	C_{eff} (μF/cm²)	Θ (Young-Lippmann)	θ (droplet Simulation)
-6.5	-1.73	-1.85	3.51 (0.04)	-	37.42
-5.0	-1.25	-1.36	3.65 (0.08)	-	50.62
-3.5	-0.77	-0.89	3.91 (0.09)	49.31	62.48
-1.5	-0.24	-0.36	4.13 (0.25)	70.66	70.09
0.0	0.12	0.0	0.0	74.70	74.70
1.5	0.50	0.38	3.96 (0.25)	70.48	72.87
3.5	1.00	0.88	3.95 (0.09)	49.69	67.07
5.0	1.40	1.28	3.91 (0.07)	-	57.57
6.5	1.81	1.69	3.85 (0.05)	-	37.27

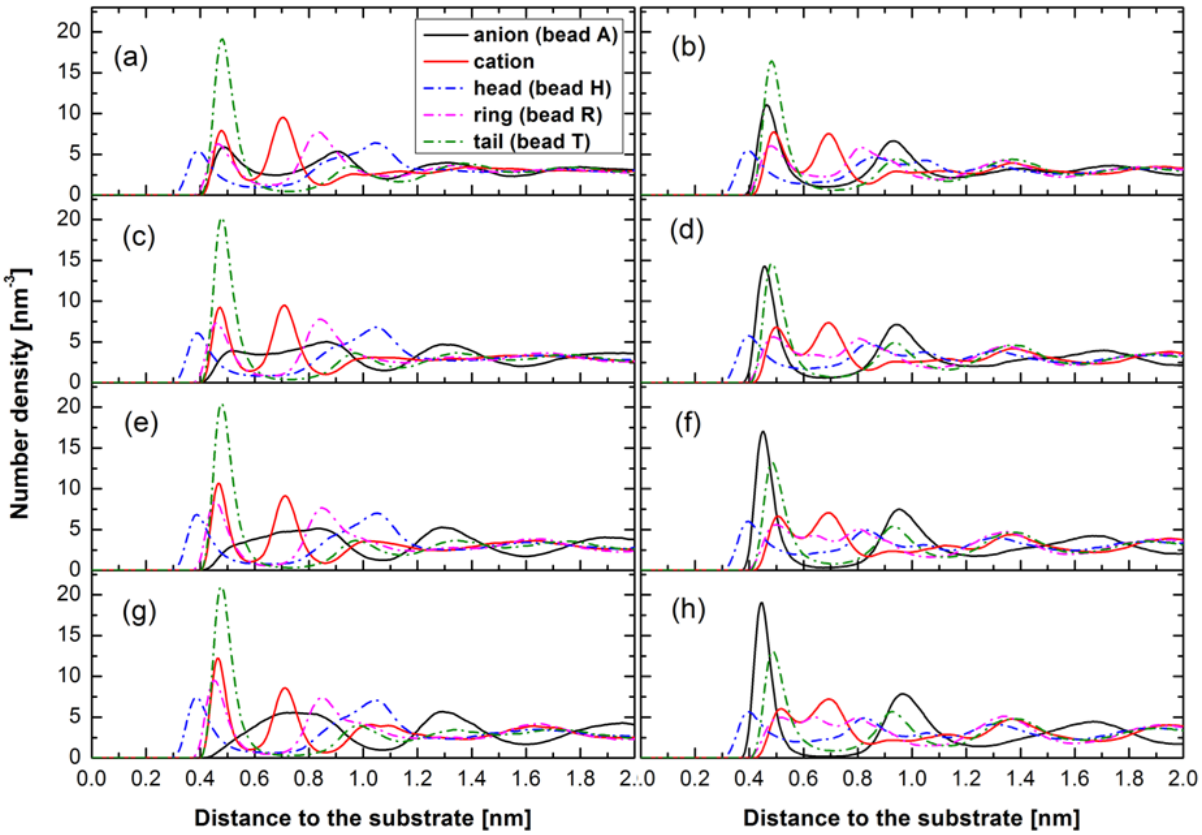

Figure 6.9. Number density of anions (bead A), cations (center of mass), head (bead H), ring (bead R) and tail (bead T) of cations on graphene with (a) -1.5 μc/cm², (b) +1.5 μc/cm², (c) -3.5 μc/cm², (d) +3.5 μc/cm², (e) -5.0 μc/cm², (f) +5.0 μc/cm² (g) -6.5 μc/cm², (f) +6.5 μc/cm²charge densities.

To understand the source of the asymmetry in the contact angle, several structure properties of the cations and the anions at the solid-liquid, liquid-vapor and the three phase contact-line are investigated.

Number density: The number density of different CG beads along the centerline of the droplet on graphene with different surface charge densities are shown in Figure 6.9. As it is shown in the figure, at low surface charge densities due to the strong Coulombic interaction between the cations and the anions, the both ions are present next to the graphene surface, but with increasing the surface charge density alternative layers of the ions formed at the interface. Comparison of the structure of the ions on the surfaces with different charge densities shows an asymmetric behavior of the ions with the charge of the surface: as the surface is charged more negatively the anions are expelled from the surface, and more cations are adsorbed on the

surface, while in the case of positively charged surfaces due to the strong van der Waals interaction between the cations and the surface they are present at the first layer of the ions even at high surface charge densities. Same asymmetric change of the structure of ILs with the charge of the surface at the solid-liquid interface where also reported for [BMIM][PF_6][11] and [BMIM][CL][39] using the atomistic simulations.

Volume charge density: The asymmetry found in the number density profiles is also reflected in the volume charge density of the IL at the solid-liquid interface in Figure 6.4. As it is shown, the local charge of the droplet at the interface for the positively charged surfaces is higher than the negatively charged surfaces.

As it is show in the inset of Figure 6.6, the asymmetry in the contact angle disappears at high surface charge densities. One assumption to explain this behavior could be that the droplet at +6.5 μc/cm^2 charge density spreads more than one expected. To test the assumption and look for an unexpected change (discontinuity) in the behavior of the ions going from surface charge density +5 to +6.5 μc/cm^2, the number density profile of the ions at the three phase contact-line are calculated in Figures 6.10 and 6.11 for the positively and the negatively charged surfaces, respectively. There are several interesting points that can be extracted from the figures. On the positively charged surfaces, a maximum in the number density profiles of the cations is found close to the contact-line (light blue/green spots) for the surface charges $\leq$ 5 μc/cm^2, and it disappears at 6.5 μc/cm^2. There is also such maximum in the number density of anions at low negative surface charge densities (0 and -1.5 μc/cm^2). At higher surface charge densities, the anions are expelled more from the surface and a transition from the first to the second layer is happening. That is why the anions distributions become fuzzier at the surface charge density -3.5 μc/cm^2. At 0 and -1.5 μc/cm^2 surface charge densities, the cations also show a maximum in the number density close to the contact line. It seems that it gradually looses intensity when the surface charge is enhanced. Note that this maximum goes along with a quite structured liquid-vacuum interfaces at z > 0.8 nm. It seems that presence of the local maximum density of the cations on the positively charged surfaces defines as “gating mechanism” that restricts the spreading, and as soon as it disappears the droplet spreads out more. To understand the source of the local maximum density, the orientation of R-T bonds with respect to the surface normal along the centerline of the droplet (Figure 6.5) and near to the three phase contact-line (Figure 6.12) are calculated.

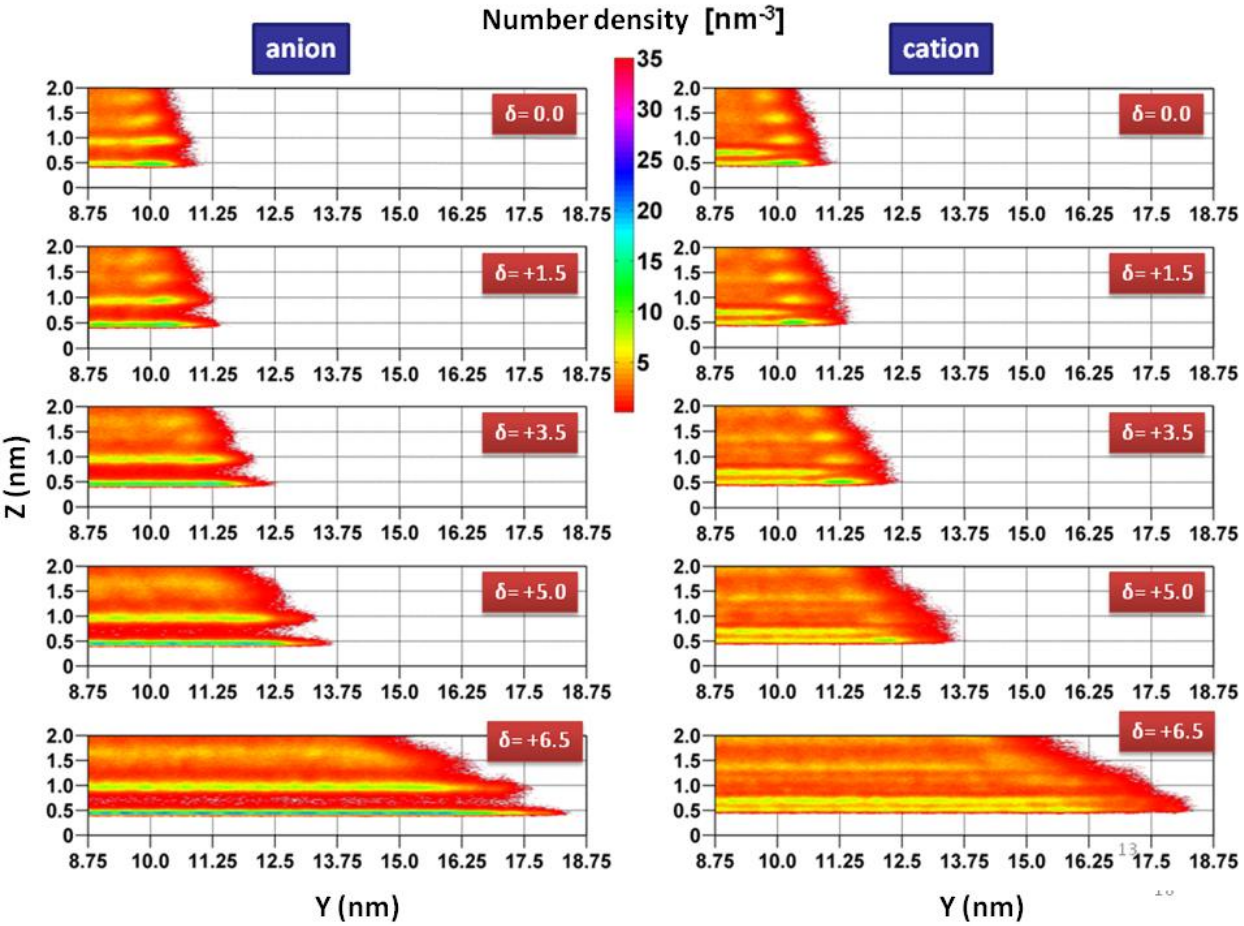

Figure 6.10. The cations and the anions distribution on the positively charged surfaces.

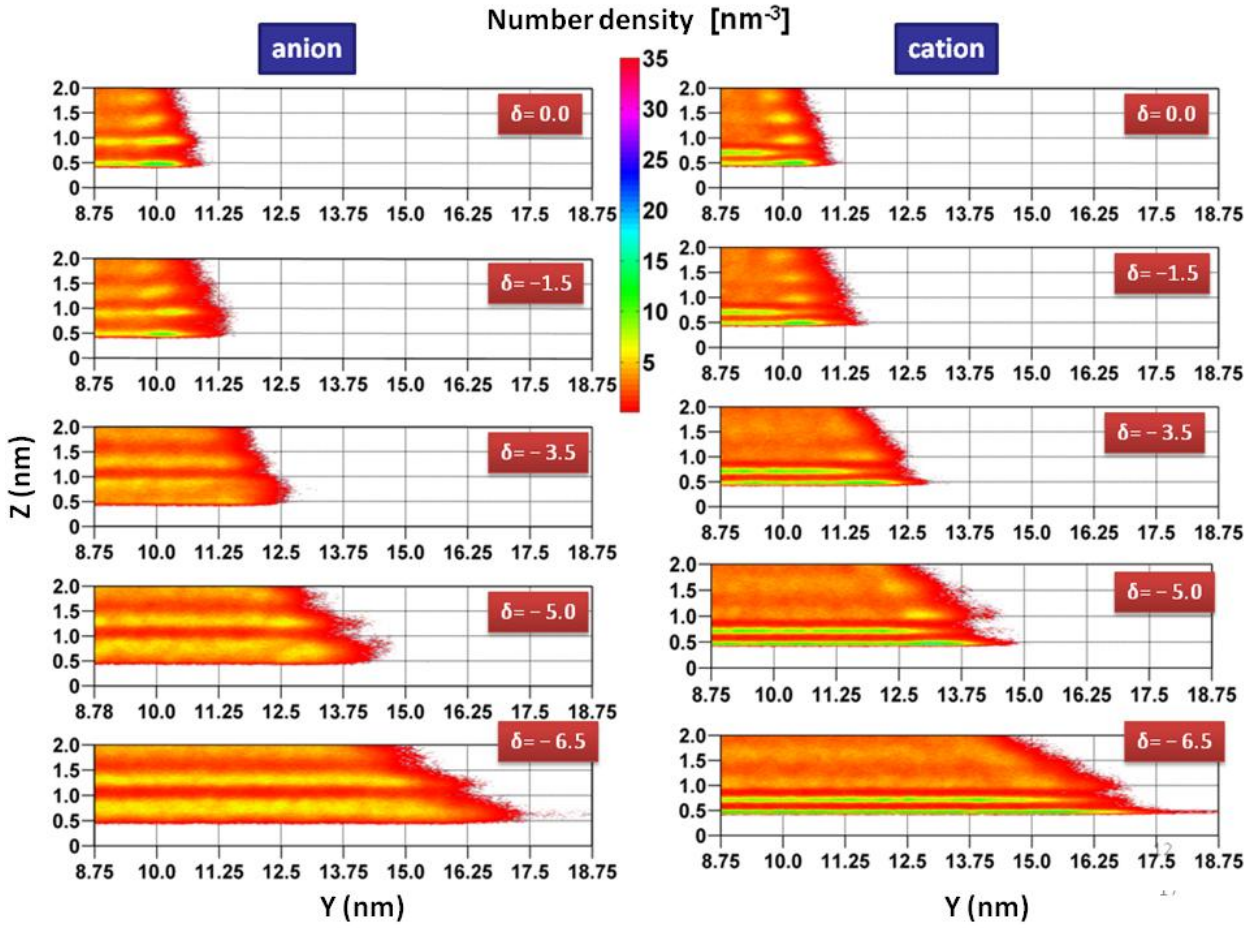

Figure 6.11. The cations and the anions distribution on the negatively charged surfaces.

As it is shown in Figure 6.5a, the two favourable orientations of the cations close to the uncharged surface are also present at different surface charge densities. The R-T bonds of the cations in the first layer are standing parallel to the surface, and this orientation does not change with the charge of the surface. In the second favourable orientation, the R-T bonds are more perpendicular to the surface. This tendency increases on the negatively charged surfaces, while for the surfaces with the higher positive charge densities the orientation of these cations become more random because of their high repulsive interaction with the surface. At the liquid-vapor interface (Figure 6.5b) R-T bond is more perpendicular to the surface, with rings point into the droplet. Since the figure shows the orientation at the top of the droplet far from the surface, there is no change in the height of the peak at the liquid-vapor interface with the charge of the surface.

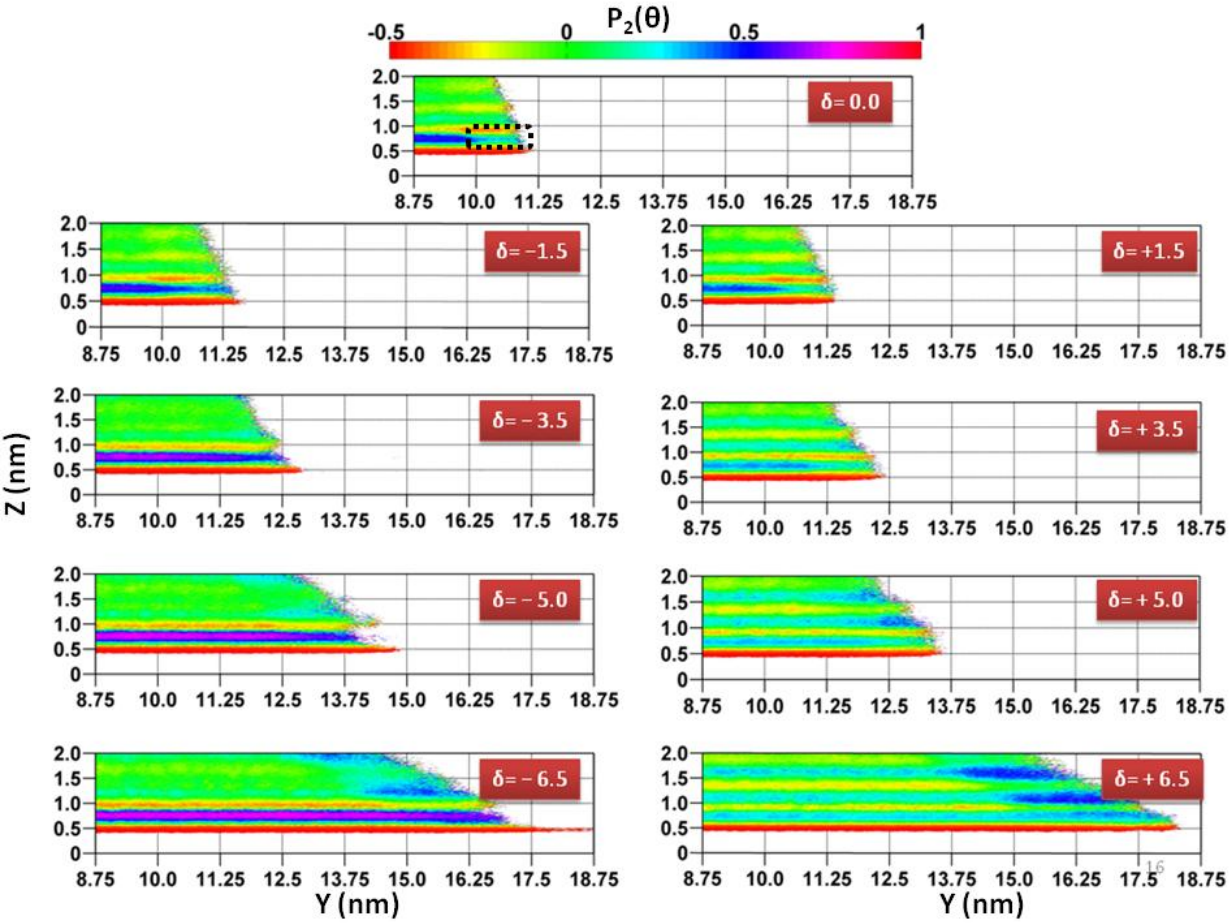

Figure 6.12. Orientational ordering of R-T bond at different surface charge densities. The area where there is competition between the solid-liquid and the liquid-vapor interface are marked with a dotted square for uncharged surface. The center of R-T bond is used to define its coordinates.

Figure 6.12 compares the orientation of the cations close to the contact-line for different surface charges. Results show that the cations in the second layer, on the one hand, try to be more perpendicular to the graphene surface due to the solid-liquid interaction, and on the other hand, the liquid-vacuum interface wants the cations to be more parallel to the surface. The competition between these two orientations at the contact-line leads to a random orientation of the cations in the second layer (as indicated with a dotted square for the uncharged surface in Figure 6.12), and apparently to the accumulation of the cations close to the contact-line (Figure 6.10).

On the positively charged surfaces, by enhancing the surface charge density the tendency of the cation to be more parallel to the surface in the second layer decreases (Figure 6.4), and with decreasing the contact angle the liquid-vapor interface is tilted more to the solid-liquid interface. Then at a critical surface charge density, the cations at the contact-line and in the second layer

are reordered more perpendicular, and the local maximum density disappears. At this point the droplet spreads more than one expected.

By comparing the positive and the negative surface densities based on the orientation maps, it seems that on the negatively charged surfaces the orientation of the cations in the second layer are more or less the same all the way toward the contact-line. It seems on the negatively charged surfaces the liquid-vapor interface does not significantly disturb the orientation of the cations with respect to the solid-liquid interface by getting closer to the contact-line. In this case, the contact angle changes "continuously" with the charge of the surface.

In conclusion, the asymmetry seems to be related to the conflicting packing effect of the cations at the three phase contact-line on the positively charge surface, where the cations do not have a proper orientation with respect to the solid-liquid and liquid-vacuum interfaces and cause a mixture orientation of the cations at this region. This leads to more rigid structure of cations at the contact line, and explains why the droplet spread less on positively charged surfaces than the negative ones. Because of the fixed arrangement, the frustration in the orientation of the cations stays up to the surface charge density of +5.0 $\mu c/cm^2$. As it has been mentioned in the discussion of the orientation profiles all of sudden at the high charge densities there is jump in the contact angle where the contact angle immediately becomes smaller.

6.4. Conclusions

In summary, our results show an asymmetry in the wetting behavior of [BMIM][BF_4] at the nanoscales, which cannot be explained by the macroscopic surface energy used in Young equation and the work of adhesion. In such description the surface energies are sum of the interaction energy of all molecules affected by interface. Therefore, the energies that enter in the Young equation are always the energies based on the two bulk phases (solid-liquid, liquid-vapor and solid-vapor) with infinitely extend interfaces, without any influence of having three phase contact line.

As it has been shown by the number density plots, for the positively charged surfaces, the cations are the closest ions to the surface. In the first layer, they are always flat, while in the second layer they like to be tilted with respect to the solid-liquid interface. They also would like to be tilted at the liquid-vacuum interface. This means that by moving from the bulk of the droplet toward the contact-line, the cation start to introduce frustration, because they cannot be tilted with respect to the both interfaces. Since both interfaces are not parallel to each other, they start to introduce

frustration in terms of the packing of the cations in the contact line. Therefore, this make the wetting less favorable on the positively charged surfaces compared to the negatively charged ones. Having some frustration in the contact-line means that the contact-line probably has some higher energy contribution, which suppresses the wetting, and that one could only overcome by applying sufficient voltage.

6.5. References

(1). Mugele, F., Fundamental challenges in electrowetting: from equilibrium shapes to contact angle saturation and drop dynamics. *Soft Matter* **2009,** *5* (18), 3377-3384.
(2). Mugele, F.; Baret, J.-C., Electrowetting: from basics to applications. *Journal of Physics: Condensed Matter* **2005,** *17* (28), R705.
(3). Dubois, P.; Marchand, G.; Fouillet, Y.; Berthier, J.; Douki, T.; Hassine, F.; Gmouh, S.; Vaultier, M., Ionic liquid droplet as e-microreactor. *Analytical chemistry* **2006,** *78* (14), 4909-4917.
(4). Galiński, M.; Lewandowski, A.; Stępniak, I., Ionic liquids as electrolytes. *Electrochimica Acta* **2006,** *51* (26), 5567-5580.
(5). Daub, C. D.; Bratko, D.; Leung, K.; Luzar, A., Electrowetting at the nanoscale. *The Journal of Physical Chemistry C* **2007,** *111* (2), 505-509.
(6). Daub, C. D.; Bratko, D.; Luzar, A., Nanoscale wetting under electric field from molecular simulations. In *Multiscale Molecular Methods in Applied Chemistry*, Springer: 2012; pp 155-179.
(7). Song, F. H.; Li, B. Q.; Liu, C., Molecular Dynamics Simulation of Nanosized Water Droplet Spreading in an Electric Field. *Langmuir* **2013,** *29* (13), 4266-4274.
(8). Raj, B.; Dhindsa, M.; Smith, N. R.; Laughlin, R.; Heikenfeld, J., Ion and liquid dependent dielectric failure in electrowetting systems. *Langmuir* **2009,** *25* (20), 12387-12392.
(9). Feng, G.; Qiao, R.; Huang, J.; Dai, S.; Sumpter, B. G.; Meunier, V., The importance of ion size and electrode curvature on electrical double layers in ionic liquids. *Physical Chemistry Chemical Physics* **2011,** *13*, 1152–1161.
(10). Feng, G.; Zhang, J.; Qiao, R., Microstructure and capacitance of the electrical double layers at the interface of ionic liquids and planar electrodes. *The Journal of Physical Chemistry C* **2009,** *113* (11), 4549-4559.
(11). Kislenko, S. A.; Samoylov, I. S.; Amirov, R. H., Molecular dynamics simulation of the electrochemical interface between a graphite surface and the ionic liquid [BMIM][PF6]. *Physical Chemistry Chemical Physics* **2009,** *11* (27), 5584-5590.
(12). Paneru, M.; Priest, C.; Sedev, R.; Ralston, J., Static and dynamic electrowetting of an ionic liquid in a solid/liquid/liquid system. *Journal of the American Chemical Society* **2010,** *132* (24), 8301-8308.
(13). Chaban, V. V.; Voroshylova, I. V.; Kalugin, O. N., *Phys. Chem. Chem. Phys.* **2011,** *13*, 7910–7920.
(14). Nose, S., A molecular dynamics method for simulations in the canonical ensemble. *Mol. Phys.* **1984,** *52*, 255-268.
(15). Hoover, W. G., Canonical dynamics: equilibrium phase-space distributions. *Phys. Rev. A* **1985,** *31*, 1695-1697.
(16). Parrinello, M.; Rahman, A., *J. Appl. Phys.* **1981,** *52*, 7182.
(17). Berendsen, H. J. C.; van der Spoel, D.; Lindahl, E.; Hess, B.; Groenhof, G.; Mark, A. E., GROMACS: Fast, Flexible, and Free. *J. Comput. Chem.* **2005,** *26*, 1701–1718.
(18). Merlet, C.; Salanne, M.; Rotenberg, B.; A. Madden, P., Imidazolium Ionic Liquid Interfaces with Vapor and Graphite: Interfacial Tension and Capacitance from Coarse-Grained Molecular Simulations. *The Journal of Physical Chemistry C* **2011,** *115*, 16613–16618.
(19). Vega, C.; Miguel, E. d., Surface tension of the most popular models of water by using the test-area simulation method. . *J. Chem. Phys.* **2007,** *126*, 154707–154710.
(20). Alejandre, J.; Tildesley, D.; Chapela, G. A., Molecular dynamics simulation of the orthobaric densities and surface tension of water. *J. Chem. Phys.* **1995,** *102*, 4574-4583.
(21). Blokhuisab, E. M.; Bedeauxb, D.; Holcombc, C. D.; Zollwegd, J. A., *Molecular Physics* **1995,** *85*, 665.

(22). Merlet, C.; Salanne, M.; Rotenberg, B., New coarse-grained models of imidazolium ionic liquids for bulk and interfacial molecular simulations. *J. Phys. Chem. C* **2012,** *116*, 7687-7693
(23). Tokuda, H.; Hayamizu, K.; Ishii, K.; Susan, M. A. B. H.; Watanabe, M., *J. Phys. Chem. B* **2004,** *108*, 16593–16600.
(24). Reith, D.; Pütz, M.; Müller-Plathe, F., *J. Comput. Chem.* **2003,** *24*, 1624.
(25). Rühle, V.; Junghans, C.; Lukyanov, A.; Kremer, K.; Andrienko, D., Versatile object-oriented toolkit for coarse-graining applications. . *J. Chem. Theory Comput.* **2009,** *5*, 3211-3223.
(26). Taherian, F.; Marcon, V.; van der Vegt, N. F. A.; Leroy, F., What is the Contact Angle of Water on Graphene? *Langmuir* **2013,** *29*, 1457-1465.
(27). Allen, M. P.; Tildesley, D. J., *Computer Simulation of Liquids*. Clarendon: Oxford, 1987.
(28). Cole, M. W.; Klein, J. R., *Surf. Sci.* **1983,** *124*, 547–554.
(29). Sha, M.; Wu, G.; Dou, Q.; Tang, Z.; Fang, H., Double-layer formation of [BMIM][PF6] ionic liquid triggered by surface negative charge. *Langmuir* **2010,** *26*, 12667-12672.
(30). Maolin, S.; Fuchun, Z.; Guozhong, W.; Haiping, F.; Chunlei, W.; Shimou, C.; Yi, Z.; Jun, H., Ordering layers of [BMIM][PF] ionic liquid on graphite surfaces: Molecular dynamics simulation. *J. Chem. Phys.* **2008,** *128*, 134504-134507.
(31). Mezger, M.; Schröder, H.; Reichert, H.; Schramm, S.; Okasinski, J. S.; Schröder, S.; Honkimäki, V.; Deutsch, M.; Ocko, B. M.; Ralston, J.; Rohwerder, M.; Stratmann, M.; Dosch, H., Molecular layering of fluorinated ionic liquids at a charged sapphire(0001) surface. *Science* **2008,** *322*, 424–428.
(32). Atkin, R.; Warr, G. G., Structure in confined room-temperature ionic liquids. *J. Phys. Chem. C* **2007,** *111*, 5162-5168.
(33). Kislenko, S. A.; Samoylov, I. S.; Amirov, R. H., Molecular dynamics simulation of the electrochemical interface between a graphite surface and the ionic liquid [BMIM][PF6]. *Phys. Chem. Chem. Phys.* **2009,** *11*, 5584-5590.
(34). Wang, S.; Li, S.; Cao, Z.; Yan., T., Molecular dynamic simulations of ionic liquids at graphite surface. *J. Phys. Chem. C* **2009,** *114*, 990-995.
(35). Dou, Q.; Sha, M. L.; Fu, H. Y.; Wu., G. Z., Molecular dynamics simulation of the interfacial structure of [Cnmim][PF6] adsorbed on a graphite surface: effects of temperature and alkyl chain length. *J. Phys.: Condens. Matter* **2011,** *23*, 175001-175008.
(36). Chen, S.; Wu, G.; Sha, M.; Huang, S., Transition of ionic liquid [BMIM][PF6] from liquid to high-melting-point crystal when confined in multiwalled carbon nanotubes. *J. Am. Chem. Soc.* **2007,** *129*, 2416-2417.
(37). Yan, T.; Li, S.; Jiang, W.; Gao, X.; Xiang, B.; Voth, G. A., Structure of the liquid-vacuum interface of room-temperature ionic liquids: a molecular dynamics study. *J. Phys. Chem. B* **2006,** *110*, 1800-1806.
(38). Bhargava, B. L.; Balasubramanian, S., Layering at an ionic liquid-vapor interface: A molecular dynamics simulation study of [BMIM][PF6]. *J. Am. Chem. Soc.* **2006,** *128*, 10073-10078.
(39). Lynden-Bell, R. M.; Frolov, A.; Fedorov, M. V., Electrode screening by ionic liquids. *Physical Chemistry Chemical Physics* **2012,** *14* (8), 2693-2701.

7. Conclusion and Outlook

In order to extract molecular level insights of several wetting phenomena and to overcome experimental limitations in the nanoscale regime, molecular dynamics (MD) simulations was used in this dissertation. In the following, conclusion of the different topics discussed in this dissertation is given, and some ideas to extend the current work are introduced.

7.1. Conclusion

Contact angle of water on graphene: In Chapter 3, we addressed the unresolved question of the contact angle of water on a graphene monolayer. In particular, we have addressed the question of whether the value of 127° recently suggested in the literature is compatible with the accepted value of approximately 90-95° on graphite. To do so, first we interpreted the work of adhesion as arising from the strength of the water-substrate interaction and from the fluctuations of this interaction. Then, we have shown that the water-substrate interaction energy is the main contribution to the work of adhesion of water. Results indicated that a change in θ from 90° on graphite to 127° on graphene yields a change in the work of adhesion, which is incompatible with the short-range nature of the interaction potentials between water and these carbon materials. We anticipated that the contact angle of water on a monolayer of graphene is of the order of 95-100°.

Interfacial entropy of water on rigid hydrophobic surfaces: To obtain a quantitative description of the work of adhesion the entropy contribution cannot be neglected. In Chapter 4, a theoretical model was developed to estimate the interfacial entropy of hydrophobic surfaces. Results showed that contribution of the interfacial entropy to the work of adhesion for water on hydrophobic surfaces like graphite, graphene and diamond is ~30%. The liquid molecules win some liquid-solid interaction energy and lose some entropy upon wetting the substrate. One important remark to make about the interfacial entropy, is that even significant water structuring occurs on the solid surfaces with corresponding changes in water entropy, these changes in entropy is compensated exactly with the enthalpy part and are therefore not affecting the equilibrium contact angle. The most interesting results of this work is that the contribution

of the interfacial entropy of the liquid to the work of liquid-solid adhesion can be described in terms of fluctuations of the attractive liquid-substrate interaction energy. In the mean field approximation, where the fluctuation in the interaction energy is ignored, entropy has no contribution to the work of adhesion, and we will only have the contribution of the solid-liquid interaction. In this approximation, interaction of a liquid molecule with the surface is not dependent on distance to the surface, and it is always equal to the average value.

Interfacial properties of ionic liquids at the solid-liquid interface: In the last part of this PhD thesis, the interfacial properties of ionic liquids (ILs) and their aspect of wetting and electrowetting were discussed. The interfacial properties of ILs at the solid surfaces were shown to be dependent on the characteristic of the surface, the type of the IL and on the thermodynamic conditions of the interface. The characteristic of the surface includes the chemical nature of the surface, the surface curvature, the surface charge density, and for the confined geometries the size of the confinement and the number of the ions in the confinement. Regarding the properties of the IL, the size of the cations and the anions and the thickness of the IL film are needed to be taken into account. It was shown that depending of the temperature the structure and the dynamic properties of the liquid at the interface changes.

Asymmetry in wetting properties of ILs with the surface polarity: In the case of ILs, since the size of cations and anions are different, one could expect asymmetry in different interfacial properties of the liquid with the polarity of the surface in the electrowetting setup. By using MD simulations it has already been shown that the different properties of the liquid at the interface like the number and the volume charge density of the ions and the electrical potential drop and the capacitance of the electrical double layer show an asymmetric behavior with the polarity of the surface.[1-3] It is very interesting to see how these asymmetries influence the contact angle. In Chapter 6 by using the coarse-grained MD simulations, we have investigated the change in the contact angle of [BMIM][BF_4] IL on graphene with positive and negative surface charges. Simulation results revealed an asymmetric change of the contact angle with the surface polarity, which increases with the charge of the surface. The surface with negative charges showed more spreading (lower contact angle) of the droplet compared to positively charged surfaces. These results are in agreement with the experimental observation of Paneru et al.[4]. The simulation however showed that this asymmetry disappears at high surface charge densities before a complete wetting of the droplet happens. Results indicated that the effect of frustrated cation

orientations in the three-phase contact line, which prevents further spreading, is overcome at a threshold value of the surface charge density. This leads to more spreading of the droplet on the positive surface charge densities.

7.2. Outlook

Interfacial entropy: In this work, we have established a connection between the work of adhesion and the enthalpy and entropy changes of water at the solid surfaces. A simple theoretical model was proposed for computing the interfacial entropy of water at rigid hydrophobic surfaces. The interfacial entropy, which is not considered in existing mean field models of the work of adhesion, was evaluated from the fluctuations of the water-surface dispersion energy at the single particle level and represents the configurational bias imposed on the fluid molecules by the attractive external potential of the surface. A natural extension of this work is modifying the existing model or developing a new model to estimate the interfacial entropy of water on hydrophilic surfaces.

Dynamic wetting: In this dissertation, we addressed several questions in the static wetting, where the three-phase contact-line is at stationary state. Another interesting field of wetting is the dynamic wetting. In this case the three phase contact-line is not at the stationary state any more, and the contact angle is changing during the time. There are two main parameters that one could use to quantify the dynamic wetting, which are the velocity of the contact-line relative to the solid and the dynamic contact angle. Even extensive studies have been done and great progress has been made in this field, still there are still many open questions especially in the nanoscales which needed to be answered in order to understand the wetting at the molecular scales.

The evaluation of the contact angle during the spreading the droplet is mainly described by the hydrodynamic (HD) [5-6] or the molecular kinetic (MK) models.[7] The main difference between two models are the main source of the energy dissipation during the spreading the droplet. In the HD model the main source of the energy dissipation is considered to be the bulk viscous dissipation, while the dissipation of the energy at the contact-line is ignored. In contrast to the HD model, in MK model the energy dissipation at the contact-line is considered to be the main source for the dissipation and it assumes that the liquid molecules are jumping on the potential energy of the solid surface during the spreading. MD simulations using simple Lennard-Jones liquid[8-12] have

been used to investigate the range of the application of the HD and MK models. A natural extension of these works is considering the real liquid models like water to study the wetting dynamics, where for example hydrogen bond interactions are influencing the spreading of the liquid. In some of the applications of wetting like coating or printing, it is required to wet a solid surface fast and completely uniform. Different techniques have been used to attain such spreading and one way to do that, is by decreasing the surface tension of the liquid with different additives. This will leads to more efficient spreading of the liquid on the surface. One could use MD simulation to understand the effects of the additives on the wetting dynamics at the molecular scales.

In the following some open questions regarding the interfacial properties of ILs and their aspect of wetting and electrowetting are given.

Influencing factors on the phase transition of ILs at the solid-liquid interface: As it is mentioned in 5.2.1.4, Sha et al.[13-14] have shown that by confining [DMIM][Cl] between the graphite walls the IL may transfer to solid state and form mono- or bi-layer at 425 K depending on the distance between the walls. However, there are several remaining questions that would require further detailed investigations, e.g.: How the structure of the ions (molecular size and symmetry) affects the transition from the liquid to the solid state? What is the contribution of the surface chemistry and possible surface defects on the transition? What are the influencing factors on the time evaluation of the phase transition?

ILs at the interface in non-equilibrium condition: Due to the special properties of the ILs like low vapor pressure or high thermal stability they can be used as lubricates in different applications, where the liquid is sheared on a solid surface. All the MD simulations have been looking at the interfacial properties of the ILs at the solid surfaces in the equilibrium state. Therefore, simulating the ionic liquids under non-equilibrium conditions would be very interesting to understand the rearrangement of the ions during the shearing of the liquid.

Influence of the solid-liquid force field parameters: The solid-liquid interaction parameters have a direct influence on the structure and dynamic properties of ILs at the interface. Although, a lot of research have been done on the interfacial properties of ILs, as it is reviewed in Chapter 5, to the best of our knowledge only one of them[15] used quantum calculation to develop the interaction parameters between the solid and the liquid. The rest were using common mixing rule to derive

the parameters for the interaction between solids and ILs. Our simulation results for the contact angle calculation of several ILs ([Bmim][PF_6], [Bmim][BF_4] and [Bmim][Tf_2N]) on graphite using the force field parameters already employed to study the interface properties showed a complete wetting of the ILs, while experimental results indicated the partial wetting. Therefore, developing the force field parameters specially to study wetting problems remains a challenge.[16] However, a detailed analysis to investigate the effect of different type of the force fields (polar and non-polar) available for ILs on the interfacial properties is straightforward.

Influence of water on the interfacial properties of ILs: By exchanging the cations with the longer or shorter ones, or choosing anions with different chemistry, one could change the surface tension and consequently the hydrophilicity of the liquid. Therefore, depending on the type of the IL, the liquid can dissolve water or may form two phases for the IL and water. The dissolved water can influence strongly different properties of the liquid. [18] Thus, it is important to investigate the effect of added water on the IL interactions with surface and the wetting parameters.

Line tension: For droplets with macroscopic size the Young's equation is used to describe the equilibrium contact angle. However, at the smaller scales, where the number of the liquid molecules at the contact-line is comparable to the molecules in the bulk or at the liquid-vapor interface, the equilibrium contact angle changes depending on the curvature of the contact-line ($\kappa = 1/r_B$, where r_B is the droplet contact-line radius). The first order correction of the contact-line with κ is called line tension (τ). The source of the line tension is consider to be the difference in the interaction energy of the molecules at the contact-line and the molecules which are far from the contact line. Since ILs have a very unique future like strong Coulombic interaction or capability to control the size of the ions, they can be used to study the effect of molecular structure of the liquid on the magnitude and the sign of line tension.

Asymmetry in dynamic electrowetting: A few experimental studies have investigated the dynamic behavior of IL droplets (contact angle versus the contact-line velocity) under electrowetting condition.[4, 20] By studying the dynamic behavior and fitting the results to theoretical models (hydrodynamic [5-6] or molecular-kinetic models[7]) one could understand how the energy is dissipated during the spreading of the droplet. Very recently Li et al.[20] studied the dynamic electrowetting and dewetting of several imidazolium-based ILs experimentally. Results showed that the electrowetting and the retraction process are following different wetting mechanisms.

By comparison of the electrowetting dynamics of [BMIM][BF_4] IL on positive and negative DC voltages reported by Paneru et al.[4], one could see a faster spreading of the droplet for DC voltages, therefore size of the ions influences the dynamic of the electrowetting. As an outlook for future work, it is also very interesting to investigate in detail the influence of the difference in cations and anions geometries on the dynamics of wetting on the surfaces with different polarities.

Contact angle saturation in electrowetting: Experimental results of electrowetting at different voltages showed that the Young–Lippmann equation is only able to explain the wetting behavior at low voltages. At high voltages, the contact angle saturation is happening, and the Lippmann–Young equation is not valid any longer. Several hypothesis like charging of the dielectric due to a failure,[21] charging of the insulating fluid around the droplet,[22] separation of the small droplets[23] or the zero solid-liquid interfacial tension at the saturation[24] are proposed in the literature to explain the saturation, but none of them are confirmed to be the main reason for the saturation. MD simulations can be used as a powerful tool in order to understand the molecular sources of the saturation.

7.3. References

(1). Feng, G.; Qiao, R.; Huang, J.; Dai, S.; Sumpter, B. G.; Meunier, V., The importance of ion size and electrode curvature on electrical double layers in ionic liquids. *Physical Chemistry Chemical Physics* **2011,** *13*, 1152–1161.

(2). Feng, G.; Zhang, J.; Qiao, R., Microstructure and capacitance of the electrical double layers at the interface of ionic liquids and planar electrodes. *The Journal of Physical Chemistry C* **2009,** *113* (11), 4549-4559.

(3). Kislenko, S. A.; Samoylov, I. S.; Amirov, R. H., Molecular dynamics simulation of the electrochemical interface between a graphite surface and the ionic liquid [BMIM][PF6]. *Physical Chemistry Chemical Physics* **2009,** *11* (27), 5584-5590.

(4). Paneru, M.; Priest, C.; Sedev, R.; Ralston, J., Static and dynamic electrowetting of an ionic liquid in a solid/liquid/liquid system. *Journal of the American Chemical Society* **2010,** *132* (24), 8301-8308.

(5). Voinov, O., Hydrodynamics of wetting. *Fluid Dynamics* **1976,** *11* (5), 714-721.

(6). Cox, R., The dynamics of the spreading of liquids on a solid surface. Part 2. Surfactants. *Journal of Fluid Mechanics* **1986,** *168* (1), 195-220.

(7). Blake, T. D.; Haynes, J. M., Kinetics of liquid/liquid displacement. *Journal of Colloid and Interface Science* **1969,** *30* (3), 421–423.

(8). Ruijter, M. J. d.; Blake, T. D.; Coninck, J. D., Dynamic Wetting Studied by Molecular Modeling Simulations of Droplet Spreading. *Langmuir* **1999,** *15*, 7836-7847.

(9). Seveno, D.; Dinter, N.; De Coninck, J., Wetting dynamics of drop spreading. New evidence for the microscopic validity of the molecular-kinetic theory. *Langmuir* **2010,** *26* (18), 14642-14647.

(10). Benhassine, M.; Saiz, E.; Tomsia, A.; De Coninck, J., Nonreactive Spreading at High-Temperature Revisited for Metal Systems via Molecular Dynamics. *Langmuir* **2009,** *25* (19), 11450-11458.

(11). Bertrand, E.; Blake, T. D.; De Coninck, J., Influence of solid–liquid interactions on dynamic wetting: a molecular dynamics study. *Journal of Physics: Condensed Matter* **2009,** *21* (46), 464124.

(12). De Coninck, J.; Blake, T., Wetting and molecular dynamics simulations of simple liquids. *Annu. Rev. Mater. Res.* **2008,** *38*, 1-22.

(13). Sha, M.; Wu, G.; Fang, H.; Zhu, G.; Liu, Y., Liquid-to-solid phase transition of a 1, 3-dimethylimidazolium chloride ionic liquid monolayer confined between graphite walls. *The Journal of Physical Chemistry C* **2008,** *112* (47), 18584-18587.

(14). Sha, M.; Wu, G.; Liu, Y.; Tang, Z.; Fang, H., Drastic phase transition in ionic liquid [Dmim][Cl] confined between graphite walls: new phase formation. *The Journal of Physical Chemistry C* **2009,** *113* (11), 4618-4622.

(15). Mendonça, A. C.; Malfreyt, P.; Pádua, A. A., Interactions and Ordering of Ionic Liquids at a Metal Surface. *Journal of Chemical Theory and Computation* **2012,** *8* (9), 3348-3355.

(16). Herbers, C. R.; Li, C.; van der Vegt, N. F., Grand challenges in quantum-classical modeling of molecule–surface interactions. *Journal of computational chemistry* **2013,** *34*, 1177-1188.

(17). Kohno, Y.; Ohno, H., Temperature-responsive ionic liquid/water interfaces: relation between hydrophilicity of ions and dynamic phase change. *Physical Chemistry Chemical Physics* **2012,** *14* (15), 5063-5070.

(18). Peter Wasserscheid, T. W., *Ionic Liquids in Synthesis*. Wiley-VCH Verlag GmbH & Co. KGaA: 2008.

(19). Drelich, J., The significance and magnitude of the line tension in three-phase (solid-liquid-fluid) systems. *Colloids and Surfaces A: Physicochemical and Engineering Aspects* **1996,** *116* (1), 43-54.
(20). Li, H.; Paneru, M.; Sedev, R.; Ralston, J., Dynamic Electrowetting and Dewetting of Ionic Liquids at a Hydrophobic Solid–Liquid Interface. *Langmuir* **2013,** *29* (8), 2631-2639.
(21). Drygiannakis, A. I.; Papathanasiou, A. G.; Boudouvis, A. G., On the connection between dielectric breakdown strength, trapping of charge, and contact angle saturation in electrowetting. *Langmuir* **2008,** *25* (1), 147-152.
(22). Zhang, J.; Van Meter, D.; Hou, L.; Smith, N.; Yang, J.; Stalcup, A.; Laughlin, R.; Heikenfeld, J., Preparation and analysis of 1-chloronaphthalene for highly refractive electrowetting optics. *Langmuir* **2009,** *25* (17), 10413-10416.
(23). Vallet, M.; Vallade, M.; Berge, B., Limiting phenomena for the spreading of water on polymer films by electrowetting. *The European Physical Journal B-Condensed Matter and Complex Systems* **1999,** *11* (4), 583-591.
(24). Quinn, A.; Sedev, R.; Ralston, J., Influence of the electrical double layer in electrowetting. *The Journal of Physical Chemistry B* **2003,** *107* (5), 1163-1169.
(25). Liu, J.; Wang, M.; Chen, S.; Robbins, M. O., Uncovering Molecular Mechanisms of Electrowetting and Saturation with Simulations. *Physical Review Letter* **2012,** *108*, 216101-216105.

Curriculum Vitae

Name: Fereshte Taherian

Nationality: Iranian

Education:

2013 – 2014: Research Assistance
Center of Smart Interfaces, Darmstadt University of Technology

2010 – 2013: Doctoral Studies
Center of Smart Interfaces, Darmstadt University of Technology

2007 – 2009: Master of Science (Physics)
Zanjan university, Zanjan, Iran.

2001 – 2005: Bachelor of Science (Physics)
Tehran, Iran.

_____

(Fereshte Taherian)

Fereshte Taherian
Center of Smart Interfaces
Alarich-Weiss-Straße 10
64287 Darmstadt

Tel.: 06151 16 4478
E-mail: tabasi@csi.tu-darmstadt.de

Darmstadt, den 12. December 2013

Erklärung

Ich erkläre hiermit, noch keinen Promotionsversuch unternommen zu haben.

_____

(Fereshte Taherian)

Fereshte Taherian
Center of Smart Interfaces
Alarich-Weiss-Straße 10
64287 Darmstadt

Tel.: 06151 16 4478
E-mail: tabasi@csi.tu-darmstadt.de

Darmstadt, den 12. December 2013

Eidesstattliche Erklärung

Ich erkläre mich hiermit an Eides Statt, dass ich meine Dissertation selbständig und nur mit den angegebenen Hilfen angefertigt habe.

_____

(Fereshte Taherian)